# Wave loads on vertical walls

## Validation of design methods for non-breaking waves of bimodal spectra

B. E. van Maris

TU Delft

ARCADIS

Cover photo: https://wallpaperscraft.com/download/sea_ocean_waves_surface_110859/1600x1200

# Wave loads on vertical walls

## Validation of design methods for non-breaking waves of bimodal spectra

by

B. E. van Maris

in partial fulfilment of the requirements for the degree of

**Master of Science**
in Civil Engineering

at the Delft University of Technology,
to be defended publicly on Wednesday June 13th, 2018 at 10:30 AM.

| | | |
|---|---|---|
| Student number: | 4143450 | |
| Project duration: | September 4th, 2017 – June 13th, 2018 | |
| Thesis committee: | Prof. dr. ir. S. N. Jonkman, | TU Delft |
| | Dr. ir. B. Hofland, | TU Delft |
| | Dr. ir. G. Ph. van Vledder, | TU Delft \| Van Vledder Consulting |
| | Ir. H. G. Tuin, | Arcadis |

An electronic version of this thesis is available at `http://repository.tudelft.nl/`.

TU Delft Delft University of Technology

ARCADIS Design & Consultancy for natural and built assets

# Summary

Hydraulic stuctures with a vertical wall such as locks and storm surge barriers can be loaded by waves. The load of non-breaking waves on vertical walls can be estimated by means of different design methods. Design guidelines such as Leidraad Kunstwerken (TAW, 2003) prescribe the formulae of Sainflou (1928) and Goda (1974) to derive a design load. These design formulae are based on the input of geometric parameters, a design wave height and a design wave period. The design wave height is found by extrapolation of the significant wave height with a design factor assuming a Rayleigh distribution of wave heights. Throughout different design guidelines this design factor as well as the design wave period vary. Furthermore, different versions of design formulae appear and the accounted design probability is not explicitly given. This results in ambiguity when determining the horizontal wave force.

A second problem emerged during the design process on the new sea lock in IJmuiden by Tuin et al. (2018). A spectral calculation was applied which translates the incident wave spectrum to a force spectrum using a response function based on the linear wave theory (LWT). The wave spectrum under consideration consisted of a familiar shaped wind sea component in combination with a low frequency component, shaping together a bimodal wave spectrum. The low frequency component, which is referred to as swell component, resulted in a relatively large peak in the force spectrum. From here, the question rises if the horizontal wave force from uni-modal wave spectra is different compared to bimodal spectra and if design methods account for this.

Besides the formulae of Sainflou, Goda and the spectral calculation, the LWT with design wave parameters was added as an additional design method. The design methods were verified with the numerical model SWASH, which was able to verify the force estimations for individual and characteristic waves, as well as the distribution of wave heights and force peaks. The performance of SWASH was limited to the lower frequency range (< 0.3 Hz) and unable to simulate steep waves in irregular wave fields. Validation with measurement data showed a small but consistent underestimation of SWASH for a range in wave steepness.

The geometry was a simplification of the IJmuiden case where a vertical wall was present on a flat sea bed with 20 m water depth. Numerical simulations in the two dimensional plane (x, z) were carried out for waves approaching a rigid, highly reflective vertical wall, yielding the surface elevation and pressure distribution in the vertical space and time domain. Incoming wave conditions were classified as gentle waves in intermediate to deep water. The simulated waves included regular waves and irregular waves based on uni-modal and bimodal wave spectra where the wind sea component was dominant over the swell component. To quantify the swell component within a bimodal spectrum, the relative swell variance $M_{Sw}$ and relative swell peak frequency $\Phi_{Sw}$ were introduced.

In the analysis of the individual wave force due to regular waves, the Sainflou formula resulted in an overestimation of approximately a factor 2 for intermediate and deep water. The LWT and Goda showed a better approximation of the SWASH results, although Goda underestimated the force in intermediate depths with approximately 10%. For irregular waves of uni-modal spectra, the estimations of the characteristic wave force resulted in a similar comparison as for regular waves. In addition, the spectral calculation method provided here an accurate calculation of the SWASH results.

After the additions of a swell component to the uni-modal spectrum, it was seen that the wave force by the SWASH model increased considerably (50% increase in force after adding 15% swell), while the increase of the force estimation by Sainflou, Goda and the LWT was negligible. Linear superposition of the swell and wind sea component resulted in an overestimation of the horizontal wave force. The relative increase in the horizontal wave force due to swell showed to be dependent on the relative depth and independent of wave steepness. The spectral calculation method showed somewhat conservative results in deep water and small underestimations in shallow water for wave fields where swell was included.

For a simulation duration of 12 hours the wave height and force peaks were analysed in the probability domain. In a spectrum with large relative swell parameters ($M_{Sw}$ = 0.27, $\Phi_{Sw}$ = 0.76) the force peaks showed an unfavourable deviation of 9% from the Rayleigh distribution at the 0.1% design level. However, the remainder bimodal wave spectra from the range under consideration did not show a substantial deviation under the influence of swell.

Apart from the force calculation, a deviation in mean water level was observed in both regular and irregular wave fields, depending on the location of nodes and anti-nodes. The expression of the local increase in mean water level $h_0$ by Sainflou showed an overestimation of a factor of 2 in regular wave fields.

It is concluded that in case of wave loads from a uni-modal wave spectrum Sainflou is too conservative. The horizontal wave force can be estimated accurately by Goda by taking note of a 10% underestimation in intermediate water depth. As an alternative, the LWT with design wave parameters is suggested. If a low frequency component is present in the wave spectrum, the use of Sainflou, Goda and the LWT may underestimate the force. The spectral calculation method is preferred as a robust alternative design method in an irregular wave field for both uni-modal and bimodal spectra. Extrapolation to a design force can be done accurately by a design factor based on the Rayleigh distribution.

It is recommended to perform physical experiments as additional validation and extension to deeper water and steeper waves. These experiments should validate the individual wave load and characteristic wave loads of uni-modal and bimodal spectra. In addition, it is recommended to carry out (numerical) simulations on the influence of a bimodal wave spectrum in geometries that include a sloped bottom or berm.

# Preface

This Master thesis with the subject *Wave loads on vertical walls* is the final part of my Master degree Hydraulic Engineering at the Delft University of Technology. I had the opportunity to conduct this research at Arcadis Nederland for which I am very thankful. The initiation of the interesting subject, good facilities at the offices and above all the great support and expertise of my colleagues definitely contributed to the process.

Completing this thesis would not have been possible without my supervising committee. First of all, I would like to thank Bas Jonkman for chairing the committee and his overview during the meetings. Also I want to show my recognition to Bas Hofland for the great guidance from the start and always coming up with new ideas. I am very lucky and thankful for the expertise of Gerbrant van Vledder in my committee. The support in SWASH was always usefull and I gained a lot more insight on wave studies in general. And of course, my gratitude goes out to Henry Tuin for his endless enthusiasm from begin to end and the problem solved thinking during our meetings.

Besides my committee, additional acknowledgement goes out to Matthijs Benit from Arcadis for all the support in SWASH and willingness to help me in the process. In addition, I would like to thank Marcel Zijlema for some essential advise on the numerical scheme of SWASH. Also, I thank Hessel Voortman from Arcadis for his pivotal role in the origin of this interesting topic and for his critical comments on my work.

I wish you a pleasant read.

*Bob van Maris,*
*Rotterdam, April 2018*

# Contents

# List of Figures

# List of Tables

# List of Symbols

**Greek symbols**

| *Symbol* | *Description* | *Unit* |
|---|---|---|
| $\gamma$ | Peak enhancement factor | [-] |
| $\gamma_d$ | Design factor | [-] |
| $\gamma_{SWASH}$ | Design value of a SWASH realisation | [-] |
| $\Delta f$ | Frequency interval | [Hz] |
| $\Delta Ray$ | Relative deviation from the Rayleigh distribution | [-] |
| $\Delta t$ | Sampling interval | [s] |
| $\zeta$ | Surface elevation in numerical grid | [m] |
| $\overline{\eta}$ | Time averaged surface elevation | [m] |
| $\eta$ | Elevation of the water surface | [m] |
| $\overline{\eta^2}$ | Wave variance based on time domain analysis | [$m^2$] |
| $\eta_{crest}$ | Height of a wave crest | [m] |
| $\eta_{trough}$ | Height of a wave trough | [m] |
| $\theta$ | Wave phase | [-] |
| $\rho$ | = Density of the water | [kg / $m^3$] |
| $\Phi_{Sw}$ | Relative swell peak frequency | [-] |
| $\chi$ | Reflection coefficient | [-] |
| $\omega$ | Radial frequency (= $2\pi/T$) | [$s^{-1}$] |

**Latin symbols**

| *Symbol* | *Description* | *Unit* |
|---|---|---|
| $a$ | Amplitude | [m] |
| $a_{inc}$ | Amplitude of incoming or incident wave | [m] |
| $a_{refl}$ | Amplitude of reflected wave | [m] |
| $B$ | Rayleigh parameter | [-] |
| $d$ | Water depth | [m] |
| $D$ | Duration of design storm | [hr] |
| $f$ | Wave frequency | [Hz] |
| $f_{max}$ | Maximum frequency in wave spectrum | [Hz] |
| $f_{min}$ | Minimum frequency in wave spectrum | [Hz] |
| $f_N$ | Nyquist frequency in wave spectrum | [Hz] |
| $f_p$ | Peak frequency in uni-modal wave spectrum | [Hz] |
| $f_{p1}$ | Peak frequency of swell component in bimodal wave spectrum | [Hz] |
| $f_{p2}$ | Peak frequency of wind wave component in bimodal wave spectrum | [Hz] |
| $\underline{F}$ | Stochastic value of a force peak (in SWASH) | [kN/m] |
| $F_{1/3}$ | Average of highest $1/3^{rd}$ of force peaks | [kN/m] |
| $F_d$ | Design wave force | [kN/m] |
| $F_h$ | Horizontal wave induced force | [kN/m] |
| $F_{max}$ | Maximum force peak in a storm | [m] |
| $F_s$ | Significant wave force (= $F_{1/3}$) | [kN/m] |
| $g$ | Acceleration of gravity | [$m/s^2$] |

| | | |
|---|---|---|
| $h$ | Total water depth ($d + \zeta$) | [m] |
| $h_0$ | Increase in mean water level | [m] |
| $h_h$ | Vertical layer thickness in SWASH | [m] |
| $h_p$ | Maximum height to which wave pressure exerts on the wall | [m] |
| $H$ | Local wave heigth in regular wave field | [m] |
| $\overline{H}$ | Time averaged wave height | [m] |
| $\underline{H}$ | Stochastic value of wave height (in SWASH) | [m] |
| $H_{1/3}$ | Average of the highest $1/3^{\text{rd}}$ of wave heights | [m] |
| $H_{1/10}$ | Average of the highest $1/10^{\text{th}}$ of wave heights | [m] |
| $H_d$ | Design wave height | [m] |
| $H_{inc}$ | Incoming or incident wave height | [m] |
| $H_{m0}$ | Significant wave height, based on spectral analysis | [m] |
| $H_{max}$ | Maximum wave height in a storm | [m] |
| $H_{refl}$ | Reflected wave height | [m] |
| $H_s$ | Significant wave height (defined as $H_{m0}$ or $H_{1/3}$) | [m] |
| $k$ | Wave number | [$m^{-1}$] |
| $K$ | Amount of vertical layers in SWASH | [-] |
| $L$ | Local wave length (in irregular wave field based on $T_{1/3}$) | [m] |
| $L_{basin}$ | Length of basin | [m] |
| $m_{-1}$ | Spectral wave variance accounting for momentum | [s $m^2$] |
| $m_0$ | Spectral wave variance | [$m^2$] |
| $m_{0,f}$ | Spectral wave force variance | [$m^2$] |
| $M_{Sw}$ | Relative swell variance | [-] |
| $N$ | Amount of waves in design storm | [-] |
| $p_0$ | Wave pressure at bottom of structure | [kN/$m^2$] |
| $p_1$ | Wave pressure at still water level | [kN/$m^2$] |
| $p_{sub}$ | Wave pressure below SWL | [kN/$m^2$] |
| Pr $\{\underline{H} < H\}$ | Design probability of wave height (= 1 - Probability of exceedance) | [-] |
| Pr $\{\underline{F} < F\}$ | Design probability of wave force (= 1 - Probability of exceedance) | [-] |
| $q$ | Non-hydrostatic wave pressure | [N/$mm^2$] |
| $R(f)$ | Response function | [$kN^2/m^4$] |
| $R_{sub}(f)$ | Response function for section below SWL | [kN/$m^2$] |
| $R_{top}$ | Response function for section above SWL | [kN/$m^2$] |
| $S_{var}(f)$ | Wave variance spectrum | [$m^2$/Hz] |
| $S_F(f)$ | Wave force spectrum | [($kN^2/m^2$)/ Hz] |
| $t$ | Time | [s] |
| $T_{1/3}$ | Significant wave period (associated with $H_{1/3}$) | [s] |
| $T_{avg}$ | Average wave period | [s] |
| $T_d$ | Design wave period | [s] |
| $T_{loc}$ | Local wave period | [s] |
| $T_{m-1,0}$ | Spectral wave period | [s] |
| $T_p$ | Peak period | [s] |
| $u$ | Flow velocity | [m/s] |
| $x$ | Horizontal coordinate | [m] |
| $z$ | Vertical coordinate | [m] |

# Abbreviations

| *Abbreviation* | *Description* |
|---|---|
| b.c. | Boundary Condition |
| CEM | Coastal Engineering Manual |
| CERC | Coastal Engineering Research Center |
| FFT | Fast Fourier Transform |
| JONSWAP | JOint North Sea WAve Project |
| LWT | Linear Wave Theory |
| MWL | Mean Water Level |
| NEN | NEderlandse Norm |
| PIANC | Permanent International Association of Navigation Congresses |
| SLS | Servicability Limit State |
| SPM | Shore Protection Manual |
| SWASH | Simulating WAves till SHore |
| SWL | Still Water Level |
| TAW | Techinische Adviescommissie voor de Waterkeringen |
| ULS | Ultimate Limit State |
| USACE | United States Army Corps of Engineers |

# 1 Introduction

Coastal structures can appear in different forms and shapes, among which structures with a vertical wall subjected to hydraulic loads. These coastal structures are also classified as vertical breakwaters and frequently appear in seawalls within port areas, but can also be found in movable structures like sea locks or storm surge barriers. With the growth of the port sector and vessel draught there is a rising demand for these vertical structures. In addition, the water depths in which these structures are desired to be constructed increases.

According to the Shore Protection Manual, (USACE, 1984, p.7-1): "Wind-generated waves produce the most powerful forces to which coastal structures are subjected (except for seismic sea waves)". It is therefore most likely that wave loads have a big influence on the design of coastal structures. A current example of a structure with a vertical wall is the new sea lock in IJmuiden, see Figure 1.1. With the dimensions of the lock chamber of 500 m by 70 m by 18 m (L x W x D) it will become the largest sea lock in the world. The lock door has the dimensions of 72 m by 12 m by 24 m (L x W x D) and will become part of the primary sea defence of the Netherlands. Due to the presence of a small bay in front of the lock and the location near the sea, the lock door is subjected to waves from sea.

Figure 1.1: Artist impression of the new IJmuiden sea lock. Copyright: ZUS (2016)

## 1.1. Motivation

In the design of coastal structures with a vertical retaining wall, a distinction is made between three types of wave loads: non-breaking, breaking, and broken wave loads. In deep water conditions, the wave load is likely to be classified as non-breaking and possibly a standing wave occurs. Non-breaking wave load is treated as quasi-stationary, hence it can be approached by static force calculation (Oumeraci et al., 1999). For non-breaking wave loads, the formulae of Sainflou (1928) and Goda (1974) are frequently found in literature and design guidelines, such as Leidraad Kunstwerken (TAW, 2003) in the Netherlands and the Coastal Engineering Manual (USACE, 2002) in the USA.

The formula of Sainflou is originating from the time before the introduction of the significant wave height and the wave spectrum. The formula has proven its value, though there are still some uncertainties about the use of the formula in a probabilistic approach. A clear substantiation of the input parameters to utilize is lacking. The formula of Goda is partly based on empirical laboratory results and is nowadays widely used as design tool. The advantage of Goda is the broad applicability for different geometries of vertical breakwaters as well as its validity for both non-breaking and depth induced breaking waves (in the presence of a sloped bottom or berm).

The way in which the formulae are presented varies throughout literature and design manuals, from which Table 1.1 presents a brief overview. There is an ambiguous use of design factors applied on the wave height, which relates a representative load (e.g. the significant load) to the design load. Design guidelines derive this factor from the assumption of a Rayleigh distribution of the wave heights. The validity of a Rayleigh distribution is therefore critical for design guidelines in the determination of a design load.

Table 1.1: Overview of the most relevant design guidelines for wave loads on vertical walls. The Sainflou formula appears in three different versions, as described in Appendix B.4.

| Design guideline | Formula | Input parameters | Probability within design storm |
|---|---|---|---|
| Leidraad kunstwerken, 2003 | Sainflou (v1) | 2.2 $H_s$ and $T_p$ | $\Pr\{\underline{H} > H\} = 0.0001$ |
| | Goda | 2.2 $H_s$ and $T_p$ | $\Pr\{\underline{H} > H\} = 0.0001$ |
| CEM, 2002; PIANC, 2003 | Sainflou (v2) | $H_{1/3}$ in Japan, $H_{1/10}$ in other countries and $T_{loc}$ | unknown |
| | Goda | 1.8 $H_s$ and 1.1 $T_{avg}$ | $\Pr\{\underline{H} > H\} = 0.0015$ |
| SPM, 1984 | Sainflou (v3) | $H_{inc}$ and $T_{loc}$ | unknown |
| | Miche-Rundgren | $H_{inc}$ and $T_{loc}$ | unknown |

New methods make it possible to approximate the design load on a vertical wall in a different way than the formulae encountered in the design guidelines. These methods take into account the complete wave spectrum, which is widely recognized as a valuable tool for design purposes (Holthuijsen, 2007; Ochi, 1998). One of these methods is an analytical method, based on the linear wave theory in combination with the response function (Holthuijsen, 2007). This so-called spectral calculation method translates the complete wave spectrum to a wave force spectrum which represents the characteristic wave force. If the wave induced force peaks are Rayleigh distributed, the statistical properties of the forces are fully described by the characteristics of the wave force spectrum. With the spectral calculation method, more insight is obtained in the origin of wave force over the frequency domain.

A spectral calculation was used by Tuin et al. (2018) for the serviceability limit state (SLS) design load on the roller mechanism in the lock gate of IJmuiden. It turned out that a small low frequency peak (located at 0.08 Hz) within a bimodal wave spectrum led to a big peak in the force spectrum, as can be seen in Figure 1.2 [1]. This can be explained by the fact that the response function (based on the linear wave theory) is sensitive for low frequencies. A greater penetration depth of low frequency waves in the water column seems to deliver a considerable contribution to the force spectrum.

[1] In the continuation of the report a low frequency peak is described with the term "swell peak". However, the origin of the low frequency peak is not necessarily the similar to the origin of swell waves. The origin of a bimodal spectrum is further elaborated in Section 2.1.

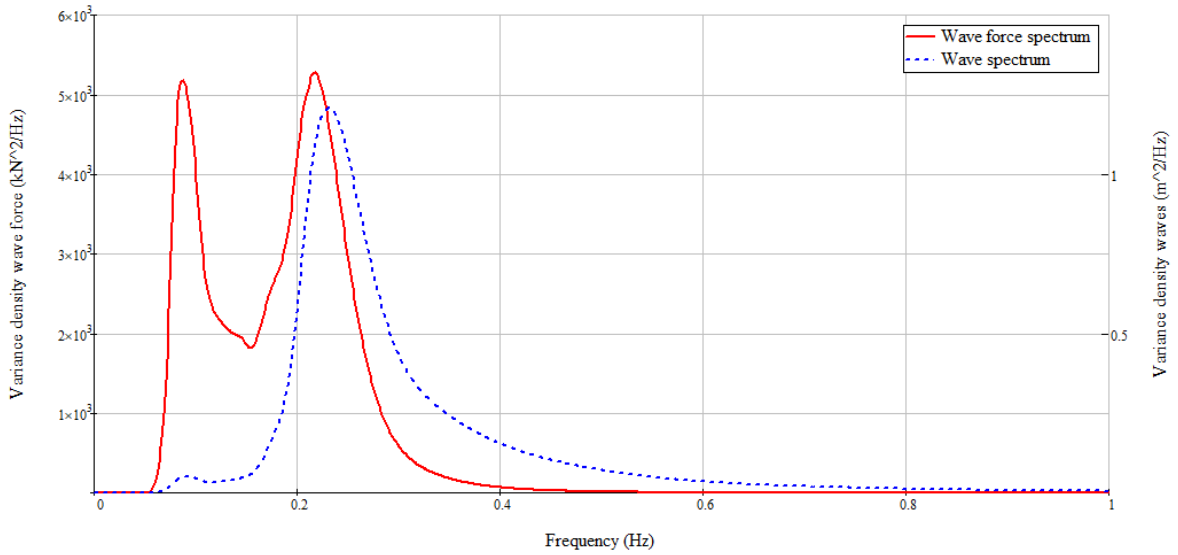


Figure 1.2: Incoming wave spectrum and wave force spectrum for the IJmuiden project. The wave force spectrum is obtained with the spectral calculation method. Based on: Tuin et al. (2018)

## 1.2. Problem statement

From the described motivation two problems are identified. First, Table 1.1 shows that the design guidelines concerning non-breaking wave load on vertical walls present ambiguity: there is inconsistency with respect to input parameters to be used, different versions of formulae appear and the represented safety level of the horizontal wave force is unclear. Secondly, Figure 1.2 from the case study in IJmuiden shows that a small swell component in the wave spectrum leads to a large component in the force spectrum. The question rises till what extend this influences the total horizontal wave force and if different design methods account for this. In summary, the two folded problem is as follows:

1. Design guidelines present inconsistency in input parameters, different versions of design formulae and an unclear probability of the estimated horizontal wave force.
2. It is unknown till what extend a swell component within a bimodal spectrum is influencing the horizontal wave force and if design methods take this into account.

## 1.3. Research questions and objective

The two folded problem can be decomposed in three research questions:

- Are the currently used design guidelines accurate for wave conditions from uni-modal wave spectra?
- Are the currently used design guidelines accurate for wave conditions from bimodal wave spectra?
- Is the spectral calculation method a good alternative for the estimation of the horizontal wave force of irregular waves?

By answering these questions, sufficient substantiation is obtained for achieving the research objective, which reads:

*Validation and improvement of the currently used design guidelines for non-breaking wave loads on vertical walls considering both uni-modal and bimodal spectra.*

## 1.4. Scope

The formulated problem could be applied to a wide range of scenarios with respect to geometries and boundary conditions. This study is focusses on the comparison of the force estimation of different design methods for different wave fields. Therefore, most other variables concerning the geometry and boundary conditions are simplified.

**Geometry**
The geometry is a two dimensional (x-axis, z-axis) simplification of the IJmuiden case with a water depth of 20 m in front of a vertical wall. This vertical wall is a rigid structure, tended to be fully reflective and has a height that is sufficient to assume no wave overtopping. The slope of the sea bed is zero, since for sloping sea beds or breakwaters on mound structures depth-induced breaking may occur. These type of loads are described by different physical phenomena and laborious to compare with non-breaking waves. The water depth (= 20 m) is classified as intermediate to deep water, depending on the wave conditions. Relative deep water is of interest since swell has a bigger penetration depth than wind waves. As a structure is located in deeper water, the influence of swell on the horizontal wave force is expected to be better noticeable.

**Boundary conditions**
The generated boundary conditions that are considered are regular waves, irregular waves from a uni-modal wave spectrum and irregular waves from a bimodal wave spectrum. The starting point for the wave conditions is the incoming wave spectrum obtained in the IJmuiden project and concerns gentle waves in relatively deep water. From here, input parameters such as the peak frequencies and total variance are varied to create both uni-modal and bimodal wave spectra. These input parameters are chosen in such a way that the influence of the swell component can be quantified. With respect to wave incidence the most unfavourable scenario is assumed: a perpendicular wave incidence on the structure. The bimodal spectrum consists of a dominant wind sea component and a small swell component (swell peak is lower than wind sea peak) . The wave spectrum is assumed to be uni-directional: swell and wind waves are originated from the same direction.

The measurement data used in this study is limited. It includes experimental data from literature for the model validation and measurement data from the IJmuiden project which functions as a starting point of the simulated wave conditions. The assessment on the probability of occurrence of the simulated scenarios is left outside the scope. The extent of the research is limited to the output of the horizontal force $F_h$. The effect of wave loads on the stability of the structure and structural impact is not treated in this study.

## 1.5. Approach

The approach is aimed at answering the three research questions and thereby obtaining enough insight in the research problem to fulfil the research objective.

First, a literature study is carried out on various design guidelines, manuals and handbooks. In addition to Sainflou and Goda, which appear in the design guidelines, the linear wave theory (LWT) with input parameters $H_d$ and $T_d$ is considered as a design formula. After this, additional calculations are made to verify the design formulae and the spectral calculation method. This verification is done with the numerical model SWASH (Zijlema et al., 2011). SWASH is a phase resolved numerical model, based on the non-linear shallow water equations with an extension in the vertical axis. Table 1.2 presents an overview of the considered design methods.

Table 1.2: Overview of the different design methods included in this research to determine wave load on vertical walls. *Wave field refers to the type of wave field on which the design method is based.

| Design method | Type of method | Wave field* | Wave theory | b.c. input | Output |
|---|---|---|---|---|---|
| Linear wave theory | Analytical | Regular | Linear theory | $H_d$ and $T_d$ | $F_h$ |
| Sainflou | Analytical | Regular | $2^{\text{nd}}$ order stokes | $H_d$ and $T_d$ | $F_h$ |
| Goda | Analytical/empirical | Irregular | Empirical | $H_d$ and $T_d$ | $F_h$ |
| Spectral calculation | Analytical | Irregular | Linear theory | $S_{var}(f)$ | $\Pr\{\underline{F} > F\}$ |
| SWASH | Numerical | Irregular | Non-linear | $S_{var}(f)$ | $F$ realizations |

Three types of design methods are covered: the design formulae, the spectral calculation method and the numerical simulation by SWASH. Figure 1.3 gives a schematisation of the design steps of the three types of design methods. The input of geometrical parameters such as the depth are omitted in this overview. The scope of this research is limited to the design process from wave spectrum to horizontal wave force $F_h$.

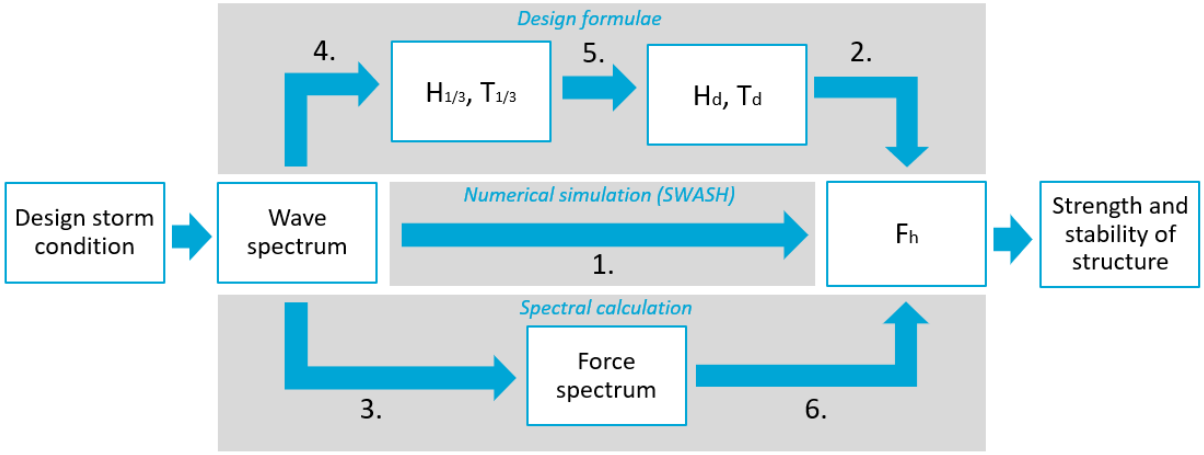


Figure 1.3: The application of three categories of design methods, determining a horizontal design force, based on a wave spectrum. The arrows indicate the design steps that are taken under consideration.

The numbers in the figure indicate the design steps that will be considered in this study. The actions that will be carried out in the design steps include the following:

1. **Validation of the SWASH model**
   Since SWASH functions as a validation tool of the other design methods, SWASH is considered as one design step: a direct numerical simulation. To get insight in the quality of the validation, the SWASH model is validated as well.
2. **Estimation of the individual wave force**
   This step concerns the application of the design formulae Sainflou, Goda and the LWT.
3. **Determination of the force spectrum**
   In the spectral calculation, the force spectrum (which represents the characteristic wave force) is determined by means of a response function, based on the linear wave theory.
4. **Simplification of the wave spectrum**
   Since design formulae use design parameters as input instead of a wave spectrum, the first step to undertake is the representation of the wave spectrum by the wave characteristics[2].
5. **Extrapolation to design values**
   This step determines the design wave height and design wave period utilized in the design formulae. Determination of design wave is based on the Rayleigh distribution. For the design wave period, different options are possible.
6. **Extrapolation to design force**
   This step considers the determination of a design force, performed with extrapolation, based on the Rayleigh distribution.

By analysing the results for each of these steps, the origin of potential deviations in horizontal force can be examined with precision.

## 1.6. Outline

In this chapter, the subject was introduced and the motivation of the problem was given. From here, three research questions and a research objective were defined. The limitations of the study were given by the scope. Furthermore, an approach was formulated that made a distinction of design steps.

Chapter 2 presents fundamental theoretical background. This includes the description of waves by wave characteristics and the wave spectrum. Then, the linear wave theory is presented, which is applied in many applications throughout the report. Subsequently, some statistical properties of waves in storm conditions are explained. Lastly, the design formulae of Sainflou and Goda are presented.

[2]Logically, a wave spectrum would be represented by $H_{m_0}$ and $T_p$, since these parameters can directly be derived from the spectrum. The choice for $H_{1/3}$ and $T_{1/3}$ is explained in Section 3.4.

The modelling by means of the different design methods is elaborated in Chapter 3. First, the geometry and simulated wave conditions are presented. After that, the model set-up in SWASH is treated. This is followed by the substantiation of the performed simulations in SWASH. Hereby a division is made between regular waves, a uni-modal spectrum, a bimodal spectrum and the probability distribution. Ultimately, an elaboration is made on the application of the design methods.

In the same structure as the performed simulations were introduced, the results are presented in Chapter 4.

Chapter 5 discusses the limitations of the approach, scope and models used throughout the study. In addition, several new insights are discussed.

Finally, Chapter 6 covers the conclusions and recommendations of this study. It reviews the design steps that were determined in the approach. The three research questions are answered and some remarks are given as a validation and improvement of the design guidelines. The recommendations consider suggestions for further research that should validate and extent the scope of this study.

A complete elaboration of the spectral calculation method can be found in Appendix A. Appendix B gives more background in the design formulae and design guidelines. SWASH is elaborated in more detail Appendix C. It discusses the model set-up, validation and an overview of all the input parameters. Appendix D and E present additional results and derivations respectively.

In Figure 1.4, the outline of the report is visualized. The chapters are indicated by the white boxes. The black arrows on the right indicate the relation between three aspects from the introduction with three topics in the conclusion. The order of the performed simulations in during the modelling is equal to the presentation of the results.

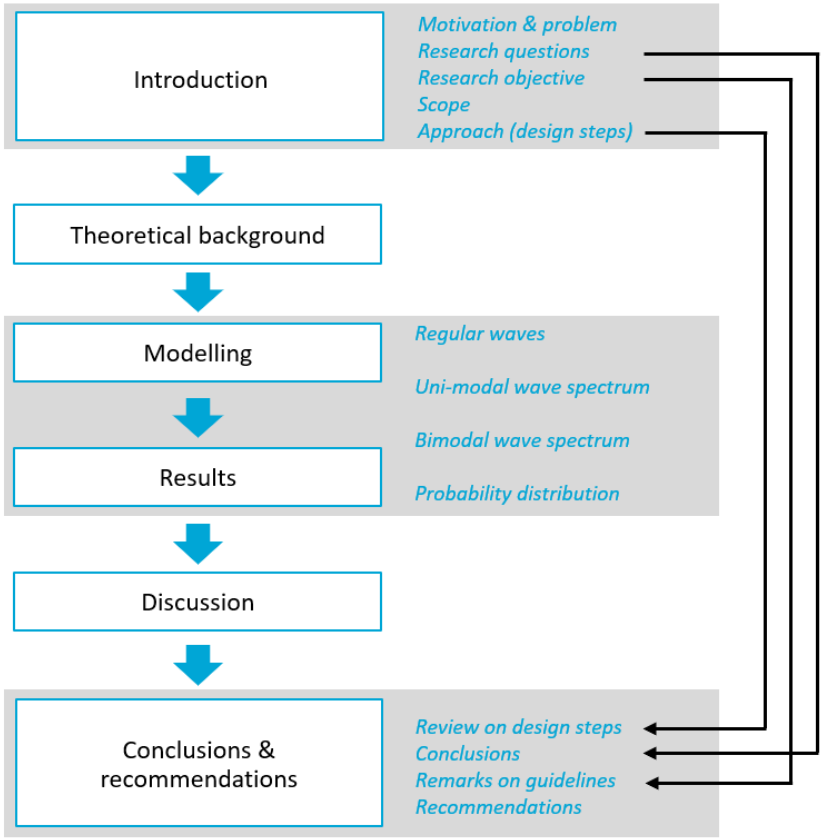


Figure 1.4: Schematisation of the outline of the report.

# 2

# Theoretical background

This chapter starts by treating the description of waves in Section 2.1. Subsequently, Section 2.2 explains shortly the physics and kinematics of a harmonic wave according to the linear wave theory. Also the spectral calculation method is briefly discussed. Since waves on open seas show most often a random character, statistical properties are used to say something useful about it. The statistical approach that is used within a design storm is addressed in Section 2.3. Ultimately, the design formulae of Sainflou and Goda are presented in Section 2.4.

## 2.1. Wave description

In storm conditions, waves on open seas show an irregular wave pattern that is classified as a stochastic process. In the design process of a coastal structure, this irregular wave field is measured close to the considered coastal structure. This is most often done by measuring the surface elevation over time $\eta(t)$, which results in a so called wave record. In most processing methods of the wave record, the surface elevation is assumed to be Gaussian distributed, with the average sea water level as $\eta = 0$. Also, the waves are assumed to be independent and not influencing one another. An other condition needed for processing methods is the condition of a stationary sea state. Wave records that are processed are therefore constricted by a duration of approximately 20 to 30 minutes, which is assumed to approximate a stationary condition. Such a wave record is also called a time series. From a time series two types of wave analysis can be performed:

1. Wave-by-wave analysis.
2. Spectral analysis in combination with the random-phase/amplitude model.

The wave-by-wave analysis is carried out in the time domain and identifies each wave by two successive zero-up or two successive zero-down crossings. Each wave has a wave height defined by the difference between its maximum and minimum surface elevation. From the collection of waves with wave height, a significant wave height $H_{1/3}$ can be obtained, which is equal to the average of the highest $1/3^{\text{rd}}$ of all waves. This significant wave height is a widely used tool for engineering purposes and was introduced by Sverdrup and Munk (1946). The significant wave period $T_{1/3}$ is the average wave period of the highest $1/3^{\text{rd}}$ of all waves. The average of the squared surface elevation of the time series, $\overline{\eta(t)^2}$, is equal to the variance of the surface elevation. This variance is proportional to the significant wave height and therefore a useful parameter to describe the sea state.

The random-phase/amplitude model is based on an analysis on the time series with the auto covariance function, as explained in Bendat and Piersol (2010). This procedure can nowadays be carried out more efficient with the Fast Fourier Transform (FFT). The model describes the surface elevation as a sum of sinuses (Fourier series):

$$\eta(t) = \sum_{i=1}^{N} a_i \cos(2\pi f_i t + \theta_i) \tag{2.1}$$

where $N$ is the number of discretised frequencies and the subscript $i$ refers to the number of the frequency. $a_i$ and $\theta_i$ are the amplitude and phase respectively for each frequency $f_i$. The duration of the time series

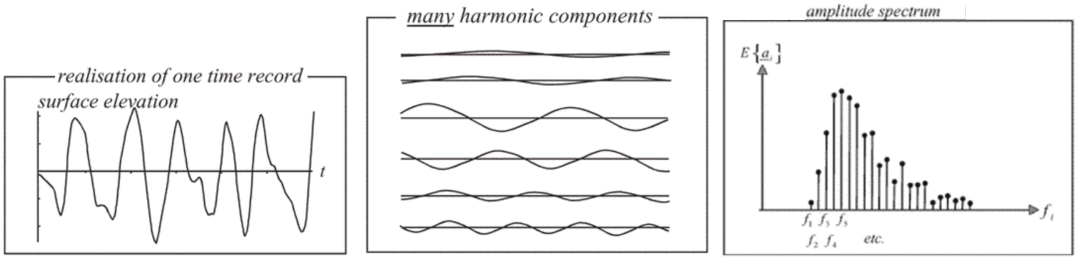


(a) One realisation of a wave record (b) Harmonic components (c) Amplitude spectrum

Figure 2.1: Explanation of the random phase-amplitude model to obtain the amplitude spectrum. Based on: Holthuijsen (2007)

is indicated by $D$. The frequency interval of two successive $f_i$ is given as $\Delta f$ and is equal to $1/D$. Figure 2.1 shows the principle of obtaining an amplitude spectrum from a time series by means of the random-phase/amplitude model. By plotting the values of amplitudes and phases over each of the corresponding frequencies, the amplitude spectrum $S_a(f)$ and phase spectrum $S_\theta(f)$ can be created.
In the random-phase/amplitude model, the values of the phases $\theta_i$ are uniform distributed over the probability domain:

$$p(\theta_i) = \frac{1}{2\pi} \qquad \text{for} \qquad 0 < \theta_i \leq 2\pi \tag{2.2}$$

Due to the uniform distribution of the phases in the frequency and probability domain, the phase spectrum is for most applications of minor interest. More interesting is the amplitude spectrum and amplitude distribution. With the assumption of a stationary and Gaussian distributed surface elevation, the random-phase/amplitude model distributes the value of the amplitude $a_i$ according a Rayleigh distribution (Rayleigh, 1880), given by:

$$p(a_i) = \frac{\pi}{2}\frac{a_i}{\mu_i^2}\exp\left(-\frac{\pi a_i^2}{4\mu_i^2}\right) \qquad \text{for} \qquad a_i \geq 0 \tag{2.3}$$

where $\mu_i$ is the expected value of $a_i$. The subscript $i$ refers to the number of the discretised frequency.

The Rayleigh distribution is a one-parameter distribution, where the only parameter is the scale parameter $B$ (the Rayleigh distribution is equal to a Weibull distribution with a shape parameter of 2). In Equation 2.3, the scale parameter $B_i$ is given by $\mu_i\sqrt{2/\pi}$.

With processing one time series, only one amplitude $a_i$ is taken for each frequency $f_i$. This leads to a 100% error of the value of $a_i$, since the amplitude is distributed according the Rayleigh distribution. Therefore, often an average is taken over multiple time series, leading to $\overline{a}_i$. Additionally, instead of the amplitude, it is more useful to describe the variance $\frac{1}{2}\overline{a}_i^2$ of a spectrum. Formally, this can be denoted as the expected value of the variance as a stochastic value $E\{\frac{1}{2}\underline{a}^2\}$.

By dividing the variance for each frequency over its frequency interval $\Delta f$, the so called variance density is obtained. To go from a discontinuous to a continuous spectrum, the limit of the $\Delta f$ to 0 is taken. Now, a complete statistical description of the ocean waves is obtained and given by the variance density spectrum (also called "wave spectrum" or "power spectrum") (Holthuijsen, 2007, p. 36):

$$S_{var}(f) = \lim_{\Delta f \to 0} \frac{1}{\Delta f} E\left\{\frac{1}{2}\underline{a}^2\right\} \tag{2.4}$$

In case a sea-surface elevation is following a Gaussian process and the sea state is stationary, all statistic characteristics are determined by the variance density spectrum $S_{var}(f)$. The tools to describe these statistical characteristics are the moments of the spectrum, defined by (Holthuijsen, 2007, p. 57):

$$m_n = \int_0^\infty f^n S(f)\mathrm{d}f \qquad \text{for} \qquad n = \ldots,-3,-2,-1,0,1,2,3,\ldots \tag{2.5}$$

in which $m_n$ is called the $n$th-order moment of the spectrum $S(f)$. The zero'th moment of the spectrum $m_0$ is by definition equal to the total variance of the surface elevation: $m_0 = \overline{\eta^2}$ (Goda, 2000). The higher the order

moment, the more errors the value will contain due the exponential influence of deviations in especially the higher frequencies. The significant wave height can be expressed in terms of the variance of the spectrum by:

$$H_{m_0} \approx 4\sqrt{m_0} \tag{2.6}$$

The frequency at which the wave variance is maximum is defined as the peak frequency $f_p$. The corresponding wave period, the peak period, is found by $1 / f_p = T_p$. The peak period and the previously introduced significant wave period $T_{1/3}$ are frequently used in many coastal processes assuming standard spectral shapes and deep water conditions (Hofland et al., 2017).

An alternative wave period used in approximations of coastal processes between sea waves and coastal structures is the spectral wave period $T_{m-1,0}$. This wave period is equivalent to calculate the energy flux and defined as:

$$T_{m-1,0} = \frac{m_{-1}}{m_0} \tag{2.7}$$

Compared to $T_p$ and $T_{1/3}$, the spectral wave period is more sensitive for the variance associated with lower frequencies in the wave spectrum. Recommendations by van Gent on the application of $T_{m-1,0}$ are found in wave run-up and overtopping process for uni-modal and bimodal spectra (van Gent, 1999, 2001).

**Bimodal wave spectra**

The shape of wave spectra observed in oceanic water can vary considerably (Ochi and Hubble, 1976). In some cases, a spectrum can emerge where two (or more) peaks can be distinguished. For example, when besides the locally generated wind waves an additional swell component is identified. According to Ochi (1998), swell is defined as waves which have travelled out of their generating area and are not any more under influence of wind. Due to frequency dispersion and directional dispersion a fairly regular and uni-directional swell peak is generated in the frequency domain (Bosboom and Stive, 2015, p. 105). Figure 2.2 presents an example of the generation of a multi-directional bimodal wave spectrum as the sum of swell waves originated from a remote location and a locally generated wind storm.

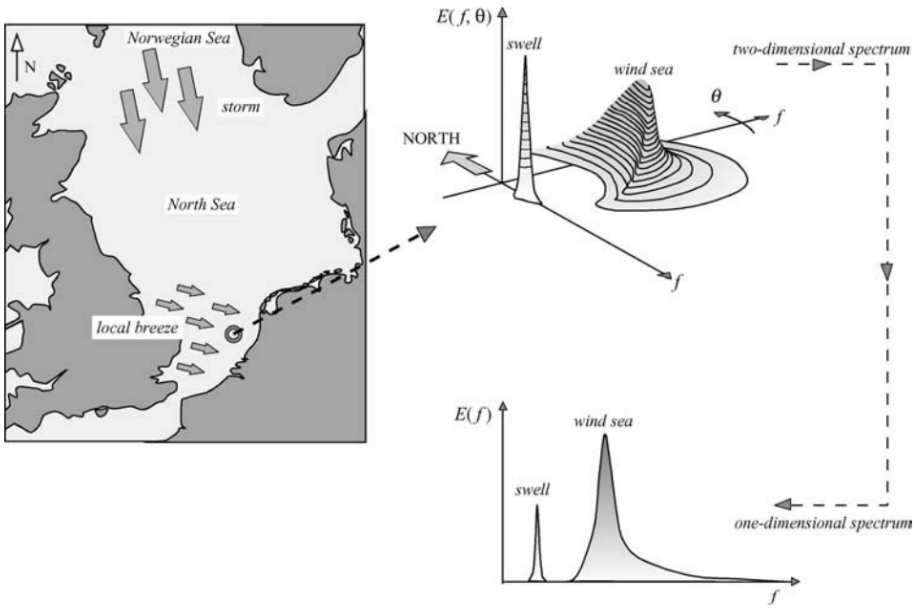


Figure 2.2: Origin of a multi-directional bimodal wave spectrum in front of the coast of the Netherlands. Based on: Holthuijsen (2007)

A bimodal wave spectrum can also be generated locally. This could occur in partly sheltered areas such as large harbor basins. An example of a locally generated bimodal wave spectrum occured in the IJmuiden project, see Figure 2.3. Here, under design conditions wind sea waves from the North Sea penetrate partially through the breakwaters into the harbor basin. In addition to this, a locally generated wind sea causes a higher frequency peak, shaping together a bimodal spectrum (Van Vledder and Enet, 2014).


Figure 2.3: Situation sketch of new sealock IJmuiden (yellow) and primary sea defences (red). Based on: Van Vledder and Enet (2014)

In the literature review of Lucas and Guedes Soares (2015) different models to describe bimodal spectra are addressed. Strekalov and Massel (1971) was one of the first who proposed a model and consisted of a high frequency wind spectrum and a Gaussian shaped swell system. Ochi and Hubble (1976) gives a description on how such a bimodal spectra can be modelled by a sum of two Γ-spectra, arriving at a six-parameter spectrum. It turned out that the six-parameter wave spectra were able to represent almost all stages of a sea during storm. A combination of two JONSWAP (Hasselmann et al., 1973, see also Section 3.3) spectra with different peak frequencies was used by Guedes Soares (1984). A similar approach was applied by Torsethaugen and Haver (2004) and added varying peak enhancement factors to obtain an appropriate fit.

## 2.2. Linear wave theory

The linear wave theory (also Airy wave theory (Airy, 1845)) is based on the mass balance and momentum balance equations and some boundary conditions that describe the kinematic and dynamic aspects of waves. The most relevant requirement is the small amplitude approximation, i.e. a small amplitude compared to the wave length $L$ and water depth $d$. For a derivation of the linear wave theory is referred to Holthuijsen (2007).

The linear wave theory implies that the only force on the waves is the gravitational force. Waves do not affect one another (statistical independent waves) and the water is assumed to be an ideal fluid. This means an incompressible fluid, with a constant density (in time and space) and no viscosity. Water particles are irrotational, i.e. vorticity is neglected. Also, the water body is continuous. The later is not the case when waves break (e.g. in steep waves or shallow water), so the theory only applies to non-breaking waves. Concerning the geometry, the sea bottom is assumed as impermeable and bottom friction is neglected. All these assumptions are in agreement with the random-phase/amplitude model. One of the analytical results of the linear wave theory is a harmonic function:

$$\eta(x,t) = a\sin(\omega t - kx) \tag{2.8}$$

where $\omega$ is the radial frequency of the incoming wave ($= 2\pi/T$) and $k$ is the wave number of the incoming wave ($= 2\pi/L$). Figure 2.4 presents the propagating sine wave.

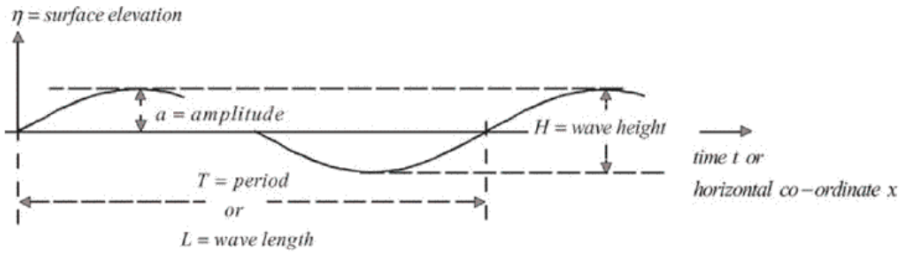


Figure 2.4: The sine wave. Based on: Holthuijsen (2007)

When this harmonic wave profile is substituted in the boundary condition of zero pressure at the surface elevation, the dispersion formula is obtained. This implicit function presents the relationship between the wave period $T$ (or frequency) and the wave length $L$, and is given by:

$$L = \frac{gT^2}{2\pi}\tanh\left(\frac{2\pi d}{L}\right) \tag{2.9}$$

where $g$ is the gravitational acceleration. The harmonic motions in terms of the velocity potential function can be combined with the Bernoulli equation to come to the wave-induced pressure. It leads to the following harmonic function of a progressive wave, which will be used as the basis for the linear theory for wave loads on vertical walls (Holthuijsen, 2007, p.128):

$$p_{wave} = \hat{p}_{wave}\sin(\omega t - kx) \qquad \text{with} \qquad \hat{p}_{wave} = \rho g a\frac{\cosh(k(d+z))}{\cosh(kd)} \tag{2.10}$$

where:

| | | |
|---|---|---|
| $p_{wave}$ | = Wave pressure as a function of time and horizontal and vertical location | [N/mm$^2$] |
| $\hat{p}_{wave}$ | = Amplitude of the wave pressure as a function of the vertical location | [N/mm$^2$] |
| $d$ | = Water depth (measured positive downward from SWL) | [m] |
| $\rho$ | = Density of the water | [kg/m$^3$] |

In coastal areas, where waves approach a highly reflective boundary condition, a standing wave could occur. With the assumption of a one dimensional long-crested wave at normal incidence, the wave profile can be described by a summation of an incident wave and a reflected wave. If there is no phase shift at reflection, the surface elevation is described by:

$$\eta(x,t) = (a_{inc} - a_{refl})\sin(\omega t - kx) + 2a_{refl}\cos(kx)\sin(\omega t) \tag{2.11}$$

where $a_{inc}$ and $a_{refl}$ are the amplitudes of the incident and reflected wave respectively.

For a fully reflective wall, a wave field with nodes and anti-nodes is formed. In case of partial reflection these are limited to quasi-nodes and quasi-anti nodes, see Figure 2.5[1].

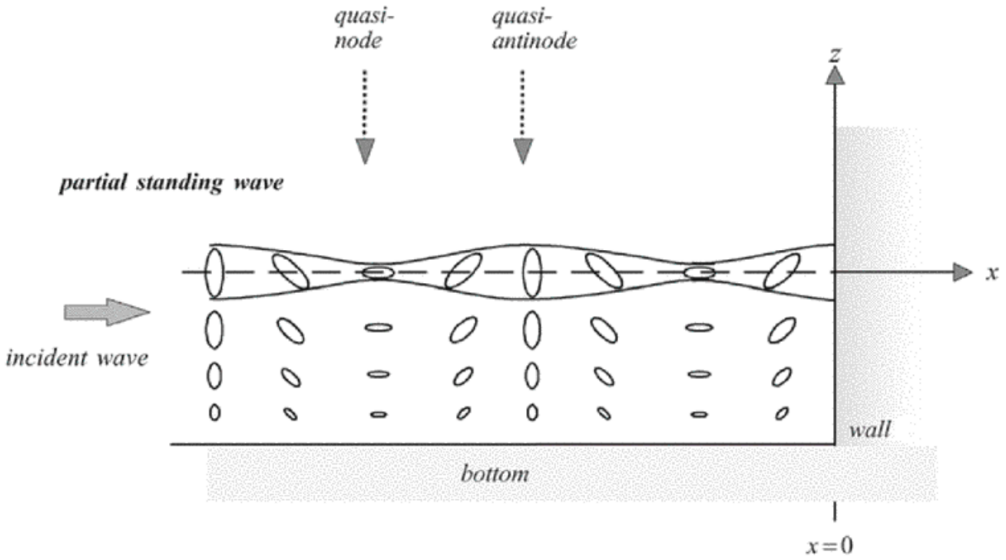


Figure 2.5: A partially standing wave due to the partial reflection of a vertical wall. The ellipses in the figure are the trajectories of water particles in the motion of one wave period. Based on: Holthuijsen (2007)

With the assumption that the wave height is equal to 2 times the amplitude, the minimum wave height $H_{min}$ is defined as 2 $(a_{inc} - a_{refl})$ and located at the nodes $(x = \frac{1}{4}L + (n/2)L)$. The maximum wave height $H_{max}$

[1] In the continuation of this report, a standing wave basin with partial reflection is regarded. For simplicity, the quasi-nodes and quasi-anti nodes that occur are referred to as nodes and anti nodes respectively.

is defined as $2(a_{inc} + a_{refl})$ and located at the anti-nodes ($x = (n/2)L$). After rewriting this expressions, the incoming and reflected wave height in a regular wave field can be determined by:

$$H_{inc} = \frac{H_{min} + H_{max}}{2} \tag{2.12}$$

$$H_{refl} = H_{max} - H_{min} \tag{2.13}$$

In the scenario of a standing wave against a vertical wall (x = 0) , the maximum pressure distribution ($\sin(\omega t)$ = 1) below still water level (SWL) is described by the amplitude of Equation 2.10. Above SWL, the linear theory describes the pressure as hydrostatic pressure, induced by the (reflected) amplitude. It results in the following pressure distribution formulae over the vertical z-axis:

$$p_{top}(z) = (1+\chi)\rho g a_{inc}\left(1 - \frac{z}{(1+\chi)a_{inc}}\right) \tag{2.14}$$

$$p_{sub}(z) = (1+\chi)\rho g a_{inc}\frac{\cosh(k(d+z))}{\cosh(kd)} \tag{2.15}$$

where $\chi$ is the reflection coefficient and is given by $\chi = H_{refl}/H_{inc}$. The pressure distribution for different wave lengths is showed Figure 2.6.

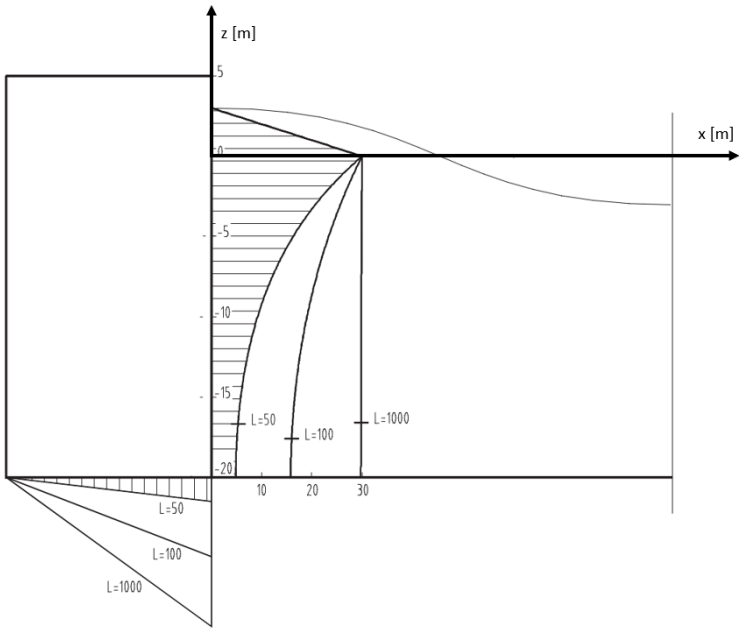


Figure 2.6: Wave pressure distribution in linear wave model for different wave lengths. Based on: Molenaar and Voorendt (2017)

**Spectral calculation**

With the representation of a irregular wave field by a wave spectrum, as a sum of harmonic components obtained. Every wave harmonic consist of an amplitude and a frequency, which can be used as the input for the linear wave theory. The wave spectrum is in this way translated to a force spectrum which is representation of the characteristic wave force. This concise description is the basis of the previously introduced spectral calculation by Tuin et al. (2018) and is elaborated in a more comprehensive way in Appendix A. It results in the force spectrum, which is obtained by multiplying the squared sum of two response functions with the wave variance spectrum:

$$S_F(f) = (R_{sub}(f) + R_{top})^2 S_{var}(f) \tag{2.16}$$

where:

| | | |
|---|---|---|
| $S_F(f)$ | = Wave force spectrum | [(kN/m)$^2$/ Hz] |
| $R_{sub}(f)$ | = Response function for section below SWL | [kN/m$^2$] |
| $R_{top}$ | = Response function for section above SWL | [kN/m$^2$] |

**Non-linear wave theories**
If waves are too steep or the water is too shallow, the small amplitude assumption of the linear wave theory is not valid. In this case, non-linear effects are involved and the wave components are not harmonic and independent. Therefore, also the spectral and probabilistic description mismatches the waves. The wave steepness can be expressed in $H/L$ and the relative depth in $d/L$. For progressive waves, the Ursell number combines these two characteristics (Dingemans, 1997a,b):

$$N_{Ursell} = \frac{\text{wave steepness}}{(\text{relative depth})^3} = \frac{HL^2}{d^3} \tag{2.17}$$

Novak et al. (2007) gives the validity of the linear wave theory for steepness of progressive waves in deep water by:

$$\frac{H}{L} \leq \frac{1}{6}\tanh(kd) \tag{2.18}$$

and in shallow water by:

$$\frac{HL^2}{d^3} \leq \frac{32\pi^2}{3} \tag{2.19}$$

When non-linear waves are considered on a local scale, non-linear theories such as Stokes (1847) for steep waves and cnoidal theory by Korteweg and De Vries (1895) for waves in shallow water can be used. Stokes adds extra harmonic waves to the basic harmonic as described in the linear theory. With one addition of a harmonic wave, the surface elevation of the second-order Stokes wave is presented by:

$$\eta(x,t) = a\cos(\omega t - kx) + ka^2 \frac{\cosh(kd)}{4\sinh^3(kd)}(2+\cosh(2kd))\cos(2(\omega t - kx)) \tag{2.20}$$

The second term on the right-hand side is the second-order Stokes correction and its phase speed is equal to the phase speed of the basic harmonic. This is not conform the dispersion relation and called a bound wave (the phase speed is bounded to the basic harmonic). The Stokes correction can be carried out for an continuing indefinite amount of harmonic components.

In deep water, Miche (1944) describes a maximum steepness, given by:

$$\frac{H}{L} = 0.142\tanh(kd) \tag{2.21}$$

This limit considers progressive waves. In a standing wave basin, where a progressive wave is reflected, steeper waves occur. Danel (1952) gave an expression for the limited steepness of standing waves by:

$$\frac{H}{L} = 0.218\tanh(kd) \tag{2.22}$$

Note that the limit of the steepness of standing waves is larger than for progressive waves, however not double. The breaking of waves in infinite depth is described by the process of white-capping. According to Holthuijsen (2007), this energy dissipation effect is a complicated phenomenon and locally highly non-linear. Averaged over a large number of waves it is however rather weak, and it can be represented as a source term in energy balance of a sea state of which Hasselmann (1974) gives the best-known expression.

Nagai (1969) gives classifications for the relative depths and wave steepness of standing waves in terms of the incoming wave. Relative depth $d/L < 0.135$ for very shallow water, $0.135 \geq d/L > 0.5$ for shallow water and $d/L \geq 0.5$ for deep water. Steep waves are indicated by waves $H_{inc}/L > 0.04$. With 100% reflection assumed, this corresponds with $H_{loc}/L > 0.08$. Waves with a lower steepness are classified as gentle waves.

## 2.3. Wave statistics

In the statistics that describe waves, a distinction is made between long term and short term statistics. The wave description presented in the Section 2.1 is an application to the short term statistics. In this case, the assumptions are made that the sea state is a stationary process and the surface elevation follows a Gaussian distribution. Practically, this may be assumed for a maximum of about half an hour (Holthuijsen, 2007) or

wave records with in the order of hundreds of waves.

On a longer time scale, these conditions do not apply. Long term statistics are aimed at determining an extreme sea state by the extreme-value theory. Often, data of numerous significant wave heights over a time span of 10 to 50 years are collected. Each $H_s$ value is obtained from short term statistic dataset. These values are subsequently distributed by the best suitable extreme value distribution function (may be a Weibull or log-normal exponential distribution). By means of inter- or extrapolation a significant wave height is determined which presents a design storm.

The determination of the design load in the ultimate limit state (ULS) or service limit state (SLS) is based on a design storm representable for a certain return period. Such a design storm is represented by a design wave spectrum or simplified by the wave characteristics $H_{m_0}$ and $T_p$. The design storm has a duration $D_{storm}$ and consist of an amount of $N_{storm}$ waves. Since in the design storm stationary conditions and a Gaussian distributed surface elevation are assumed, the amplitude is Rayleigh distributed. Holthuijsen (2007)[p. 68] proves that, based on the average of surface exceedance time intervals $T_\eta$ expressed in terms of spectral moments by Rice (1944), that for a narrow spectrum, and with the assumption of $H = 2\,\eta_{crest}$, wave heights are also Rayleigh distributed according to the probability density function:

$$p(H) = \frac{H}{4m_0}\exp\left(-\frac{H^2}{8m_0}\right) \tag{2.23}$$

and the cumulative distribution:

$$\Pr\{\underline{H} < H\} = 1 - \exp\left(-\frac{H^2}{8m_0}\right) \tag{2.24}$$

which is a Rayleigh distribution with scale parameter $B = \sqrt{4m_0}$. These equations are the probability distribution of an individual wave. If the wave height $H$ is normalized by the significant wave height $H_{1/3}$, the cumulative distribution for the relative wave height $H/H_{1/3}$ is given by (Holthuijsen, 2007, p. 72):

$$\Pr\{\underline{H} < H\} = 1 - \exp\left[-2\left(H/H_{1/3}\right)^2\right] \tag{2.25}$$

This gives an expression of the probability that a stochastic wave $\underline{H}$ is smaller than given wave height $H$. In design practices, the wave $H$ can be chosen as a design wave height $H_d$. This results in a ratio between the wave design wave height and significant wave height, here defined as the design factor:

$$\gamma_d = \frac{H_d}{H_{1/3}} \tag{2.26}$$

If the Rayleigh distribution of wave heights is valid and the significant wave height is known, this factor can directly relate any safety level to a design wave height, by:

$$H_d = \sqrt{-2m_0 \ln\left(1 - \Pr\{\underline{H} < H_d\}\right)} = \gamma_d H_{1/3} \tag{2.27}$$

Note that this safety level (and design factor) accounts for the expected wave height that occurs in the sea state. It includes no inherent safety.

The Rayleigh scale parameter for Equation 2.25 becomes $B = 0.5$. Since this scale parameter is not dependent on input parameters, the Rayleigh distribution as presented in this form can be plotted as a straight line in a probability plot, independent of the value of $H_{1/3}$.

The Rayleigh distribution is theoretical derived based on some assumptions and may not be valid for:

- Shallow water conditions (wave breaking and other non-linear processes. Battjes and Groenendijk (2000) splits the probability distribution and replaces the tail of the Rayleigh distribution by a Weibull distribution.)
- Steep waves (surface elevation not Gaussian distributed)
- A very irregular wave field (wide wave spectrum)

In contrast to the distribution of wave height in a storm condition, the wave periods do not follow a clear distribution. However, several studies are carried out amongst others by Longuet-Higgins (1975) about the joint probability of wave amplitudes and wave periods.

## 2.4. Design formulae

The first order (linear wave) theory, presented in Section 2.2, is important for a basic approach for the prediction of wave pressure on a vertical wall. A well known-second order theory is described by Sainflou (1928) and a third order theory by Tadjbaksh and Kelle (1960). Goda and Kakizai (1967) treats the fourth order theory for finite amplitude waves and compared the results for the pressure with experiments. Mallayachari and Sundar (1995) carried out experiments for regular and irregular waves. At various depths, the measured pressures of the regular waves are compared with the linear theory and the third-order solution. For irregular waves, different spectral parameters were compared. Gurhan and Unsalan (2005) compared first and second order theories and Goda's formula with experimental data. It turned out that first order theory underestimates and the second order term overestimates the pressure in case of increasing steepness. Goda's formula showed a good correlation for all cases.

In design applications, most used theories refer to Sainflou (1928) and Goda (1974). Theste two formulae are presented here according the notation of Leidraad Kunstwerken (TAW, 2003), since it is the most relevant Dutch standard. A more elaborated description of these two formulae and the different forms in which they appear can be found in Appendix B.

### 2.4.1. Sainflou

Sainflou (1928) introduced a pressure formula that could be used for standing waves. This formula was directly utilized by many port engineers throughout the world. The approach of Sainflou is based on Stokes' second order wave theory and is therefore applicable to somewhat steeper waves compared to the linear theory. It is assumed that there is complete reflection and waves are of the non-breaking type. The waves follow the trochoidal standing wave theory. Leidraad Kunstwerken presents a pressure distribution as in Figure 2.7 and describes the Sainflou formula in the following form:

$$p_1 = \rho g(a_{loc} + h_0) \tag{2.28}$$

$$p_0 = \frac{\rho g a_{loc}}{\cosh(kd')} \tag{2.29}$$

with:

$$h_0 = \frac{1}{2} k a_{loc}^2 \coth(kd) \tag{2.30}$$

where:

| | | |
|---|---|---|
| $p_1$ | = Maximum wave pressure at the level of $h_0$ | [N/m$^2$] |
| $p_0$ | = Wave pressure at sea bottom | [N/m$^2$] |
| $h_0$ | = Increase of mean water level | [m] |
| $d'$ | = The water depth directly in front of the structure | [m] |
| $d$ | = Water depth in front of the sill, 2 or 3 wave lengths away front the wall | [m] |
| $a_{loc}$ | = Amplitude of the wave directly in front of the wall (including relfection) | [m] |
| $k$ | = Wave number of the incoming wave | [m$^{-1}$] |

The pressure between $p_0$ and $p_1$ is linear distributed. Sainflou includes a $h_0$ factor, which represents the increase in water level underneath an anti-node in a regular wave field (Wiegel, 1964). Different definitions of $h_0$ are found in literature, amongst others by Penny and Price (1952) and Miche (1953).

According to the description of Leidraad Kunstwerken, the maximum pressure $p_1$ exerts at the water level of SWL + $h_0$. This is in contrast with the figure that is presented in Leidraad Kunstwerken (as can be seen as well in Figure 2.7) and all other appearances of the formula, where the pressure $p_1$ exerts at the SWL. For consistency with other design formulae, the latter will be applied. Since the introduction of the significant wave and the wave spectrum took place later in the century, it is unclear which wave characteristic should be used as input. Leidraad Kunstwerken proposes that the local amplitude $a_{loc}$ is defined as $H_{d,loc}/2$, where $H_{d,loc} = 2H_{d,inc}$ and that $H_{d,inc}$ should be chosen as 2.2 $H_s$. A specification of $H_s$ as $H_{1/3}$ or $H_{m0}$ is not made. As design wave period, the peak period $T_p$ is chosen.

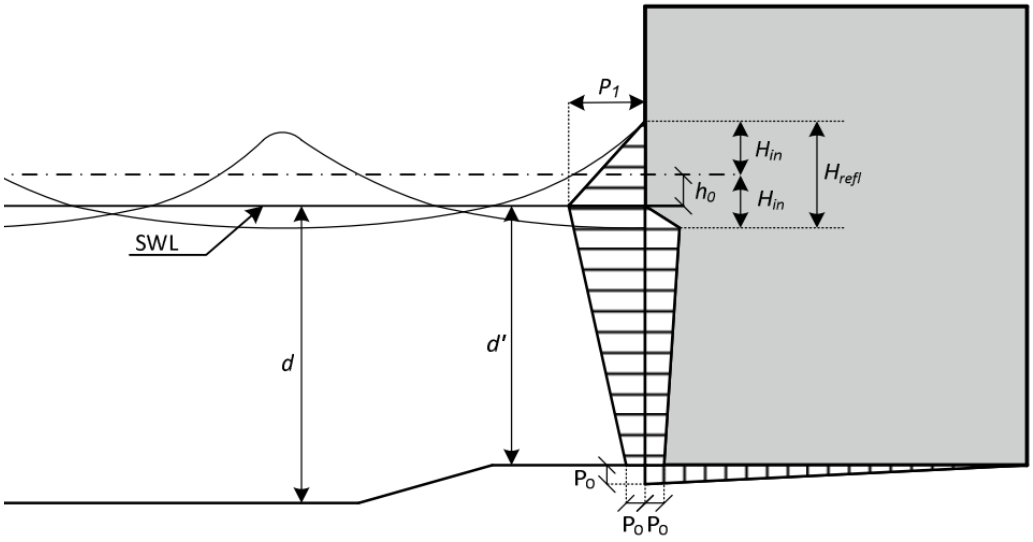


Figure 2.7: Wave pressure distribution according to Sainflou. Based on Leidraad Kunstwerken, TAW (2003)

### 2.4.2. Goda

Ito et al. (1966) proposed a formula for covering both breaking wave load and non-breaking wave load. After verification with much laboratory data and theoretical considerations in Goda and Kakizai (1967) and Goda and Fukumori (1972), Goda (1974) presented wave pressure formulae for the design of vertical breakwaters. Tanimoto et al. (1976) modified the formulae for oblique wave approach, after which they were widely employed as wave pressure formula in Japan. Extensions on the effect of a berm, sloping top, wave breaking and wave incident were made by Takahashi et al. (1993) and Takahashi and Hosoyamada (1994).

The parameters Goda uses are determined by a lot of laboratory data. Goda also carried out evaluations of constructed breakwaters and their performance to establish accurate empirical parameters. The structures on which Goda applied his formulae, concerned gravity based breakwaters with a low crest (overtopping takes place in storm conditions) and mostly the breakwaters were founded on a rubble ballast, to reduce the size of the breakwater (Verhagen and Van den Bos, 2017). In this way, the Goda formulae are widely applicable for different boundary conditions and geometry[2].

Regardless if the waves are breaking or non-breaking, the pressure distribution on the vertical section is trapezoidal shaped, as shown in Figure 2.8. The notation of the formulae differs throughout different sources. The form in which the formulae of Goda are presented by Leidraad Kunstwerken is the following:

$$\eta^* = 0.75(1+\cos\beta)\lambda_1 H_d, \tag{2.31}$$

$$p_1 = \frac{1}{2}(1+\cos\beta)(\lambda_1\alpha_1 + \lambda_2\alpha_*\cos^2\beta)\,\rho g H_d, \tag{2.32}$$

$$p_3 = \alpha_3 p_1, \tag{2.33}$$

$$p_4 = \alpha_4 p_1, \tag{2.34}$$

$$p_u = 0.5(1+\cos\beta)\lambda_3\alpha_1\alpha_3\rho g H_d \tag{2.35}$$

with:

$$\alpha_* = \alpha_2 \qquad \text{for non-breaking waves} \tag{2.36}$$

$$\alpha_1 = 0.6 + \frac{1}{2}\left[\frac{4\pi h/L_d}{\sinh(4\pi h/L_d)}\right]^2, \tag{2.37}$$

[2] Often is mentioned that Goda is valid for both breaking an non-breaking wave conditions. It should be noted that the formulae of Goda are formulated in such a way, that they only account for depth induced wave breaking. Breaking waves by severe wave conditions solely (white-capping) is not included in the formula.

$$\alpha_2 = \min\left\{\frac{h_b - d}{3h_b}\left(\frac{H_d}{d}\right)^2, \frac{2d}{H_d}\right\}, \tag{2.38}$$

$$\alpha_3 = 1 - \frac{h'}{h}\left[1 - \frac{1}{\cosh(2\pi h/L_d)}\right], \tag{2.39}$$

$$\alpha_4 = \left(1 - \frac{h_c}{\eta_*}\right) \quad \text{for} \quad \eta^* > h_c \qquad \text{and} \qquad \alpha_4 = 0 \quad \text{for} \quad \eta^* \leq h_c, \tag{2.40}$$

where:

| | | |
|---|---|---|
| $\eta^*$ | = Elevation to which the wave pressure is exerted | [m] |
| $\beta$ | = Angle between the direction of the wave approach and a line normal to the breakwater | [rad] |
| $H_d$ | = Unreflected design wave height (according to Goda 1.8 $H_{1/3}$) | [m] |
| $L_d$ | = Design wave length (according to Goda based on $T_{1/3}$) | [m] |
| $p_1$ | = Wave pressure at still water level | [N/m$^2$] |
| $p_3$ | = Wave pressure at sea bed level | [N/m$^2$] |
| $p_4$ | = Wave pressure at highest point on breakwater where load applies | [N/m$^2$] |
| $p_u$ | = Uplift pressure at front of structure | [N/m$^2$] |
| $\alpha_*$ | = Pressure coefficient that accounts for the wave impact | [-] |
| $\alpha_1$ | = Pressure coefficient that accounts for the wave length of design wave | [-] |
| $\alpha_2$ | = Pressure coefficient that accounts for the wave steepness | [-] |
| $\alpha_3$ | = Pressure coefficient that accounts for the decrease in wave pressure over depth | [-] |
| $\lambda_{1,2,3}$ | = Modification factors that account for the geometry of the structure | [-] |
| $h_b$ | = Water depth in front of the structure, 5 wave lengths away front the wall | [m] |
| $h_c$ | = Height between SWL and top of caisson | [m] |
| $h$ | = Depth in front of the rubble ballast | [m] |
| $h'$ | = Height of vertical breakwater | [m] |
| $d$ | = Depth directly in front of the structure | [m] |

In case of breaking waves, $\alpha_2$ is defined alternatively to account for the impact force.

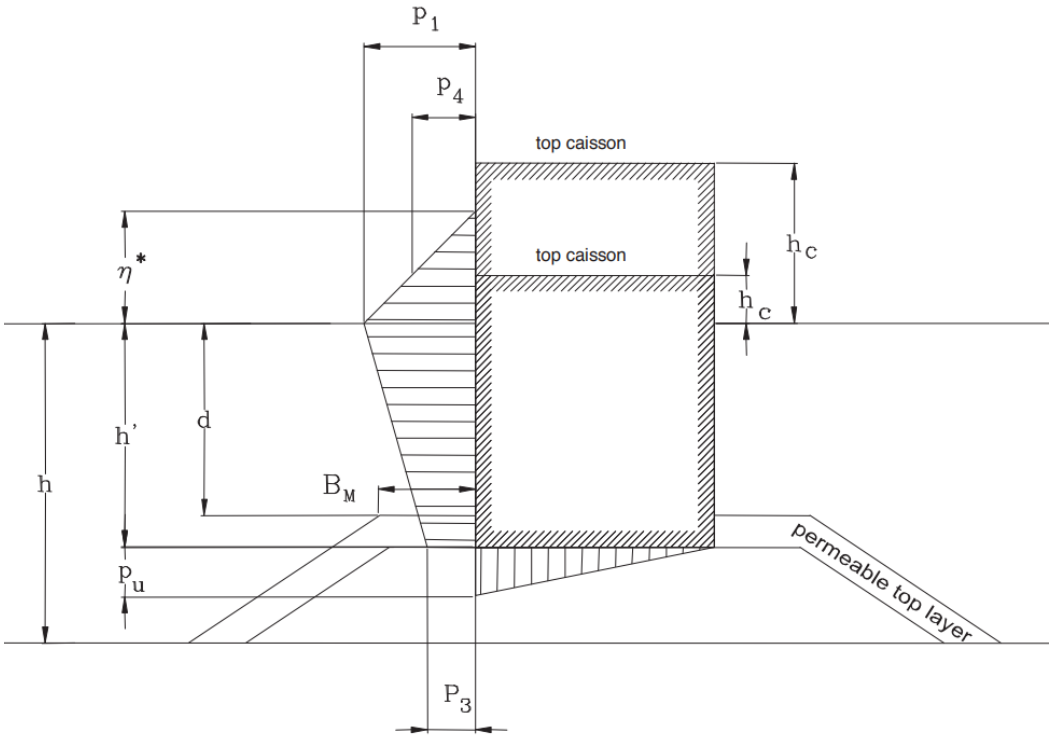


Figure 2.8: Wave pressure distribution according to Goda, based on: TAW (2003)

Goda (1974) states $H_d$ = 1.8 $H_{1/3,inc}$ in case of non-breaking waves at the structure and $T_d$ = $T_{1/3}$. The 100% wave reflectance at the wall is integrated in the formulae. With the input of design wave height $H_d$ = 1.8 $H_s$ and the assumption of the Rayleigh distribution, Goda theoretically assumes a design wave of $H_{1/250}$ or $H_{0.153\%}$. Laboratory data from a physical model test carried out by Van der Meer et al. (1992) and Juhl and Van der Meer (1992) showed an positive biased outcome on the horizontal force and momentum, as is discussed in Appendix B. Despite the recommendations of Goda concerning the input values, Leidraad Kunstwerken suggests $H_{d,inc} = 2.2 H_s$ and $T_d = T_p$ (similar as for the Sainflou formula).

### 2.4.3. Design guidelines

The safety factor of 2.2 applied to the significant wave height stated by Leidraad Kunstwerken is based on the assumption of the Rayleigh distribution of wave heights and the description: "The design height of a wave is such that this wave height may be exceeded by 10% of the waves during a storm peak." (TAW, 2003). With the assumption that a storm consist of 1000 waves, the following explanation is given to this definition. The expected maximum wave of this storm ($H_{0.1\%}$) may be exceeded by 10% of the time. The design wave according to Leidraad Kunstwerken becomes $H_{0.01\%}$ and has a probability of exceedance of 0.9999. With Equation 2.27, the following can be found:

$$H_{0.01\%}/H_{1/3} = \sqrt{\frac{\ln(-(\Pr\{\underline{H} < H_{0.01\%}\} - 1)}{-2}} = \sqrt{\frac{\ln(-(0.9999 - 1))}{-2}} = 2.146 \tag{2.41}$$

which is approximately a factor of 2.2. The actual probability of exceedence that is obtained can be calculated as well. For a safety factor of 2.2 the probability of exceedance of an individual wave becomes:

$$\Pr\{\underline{H} > H_D\} = \exp\left[-2\left(H_d/H_{1/3}\right)^2\right] = \exp\left[-2\left(2.2\right)^2\right] = 0.0000625 = 0.00625\% \tag{2.42}$$

Compared to the prescribed safety factor of Goda, the safety according Leidraad Kunstwerken is clearly higher. Table 2.1 presents a brief overview of the different design levels considered, their safety factor and according probability of exceedance.

Table 2.1: Overview of design probability that is related to design factors.

| Design level | Design factor | Design probability |
|---|---|---|
| Characteristic / Siginificant | - | 13.5 % |
| $H_d$ according Goda (2000) and USACE (2002) | 1.8 | 0.15 % |
| $H_d$ according Leidraad Kunstwerken | 2.2 | 0.00625 % ($\approx$ 10% exceedance of $H_{0.1\%}$) |

The design wave period is often prestented as $T_{1/3}$, $T_p$ or1.1 $T_{avg}$. Substantiation of the choice of a wave period is lacking.

# 3

# Modelling

This chapter discusses the design methods used to model the problem. In Chapter 2, already the linear wave theory, spectral calculation method and design guidelines were presented. Here, a third design method, the numerical modal SWASH, is introduced. This design method has the function as validation tool for the design formulae and spectral calculation method.

This chapter is structured as follows. First, Section 3.1 gives a general description of the geometry and the simulated wave field that is expected. Also, several symbols are (re)defined. The model set-up of SWASH is treated in Section 3.2. This contains a brief overview of the model equations, assumptions, discretisation, measurement set-up and the validation of SWASH. A more complete description of the SWASH model can be found in Appendix C. Subsequently, Section 3.3 elaborates on the simulations carried out in SWASH. The simulations are distinguished in four parts. The first three parts vary in the boundary conditions used and treat regular waves, irregular waves with uni-modal wave spectrum and irregular waves with bimodal spectrum. The last part covers both uni-modal and bimodal spectra, but with a focus on the probability distribution. Ultimately, Section 3.4 discusses the application of the various design methods to arrive at the horizontal force and the translation to the probability domain.

All the design methods are processed with the numerical software environment MATLAB R2017b. More background in the post processing is given in Appendix C.6.

# 3.1. General

## 3.1.1. Geometry

As explained in the introduction, the starting point for the geometry is based on the IJmuiden project (Tuin et al., 2018). The geometry is schematised in the 2-dimensional physical domain in Cartesian co-ordinates (x-axis, z-axis) and consists of a horizontal seabed with a vertical rigid structure located at x = 0 m (east boundary condition). The length of the water basin $L_{basin}$ in front of the vertical wall is 200 m. The downward measured water depth $d$ is 20 m. A wave generating boundary condition is present at x = -200 m (west boundary condition) and generates waves in the positive x direction. The surface elevation $\eta$ is positive in the z-direction. In Figure 3.1 the geometry is schematised. The list of symbols used is redefined, as different design formulae from Section 2.4 include ambiguous symbols.

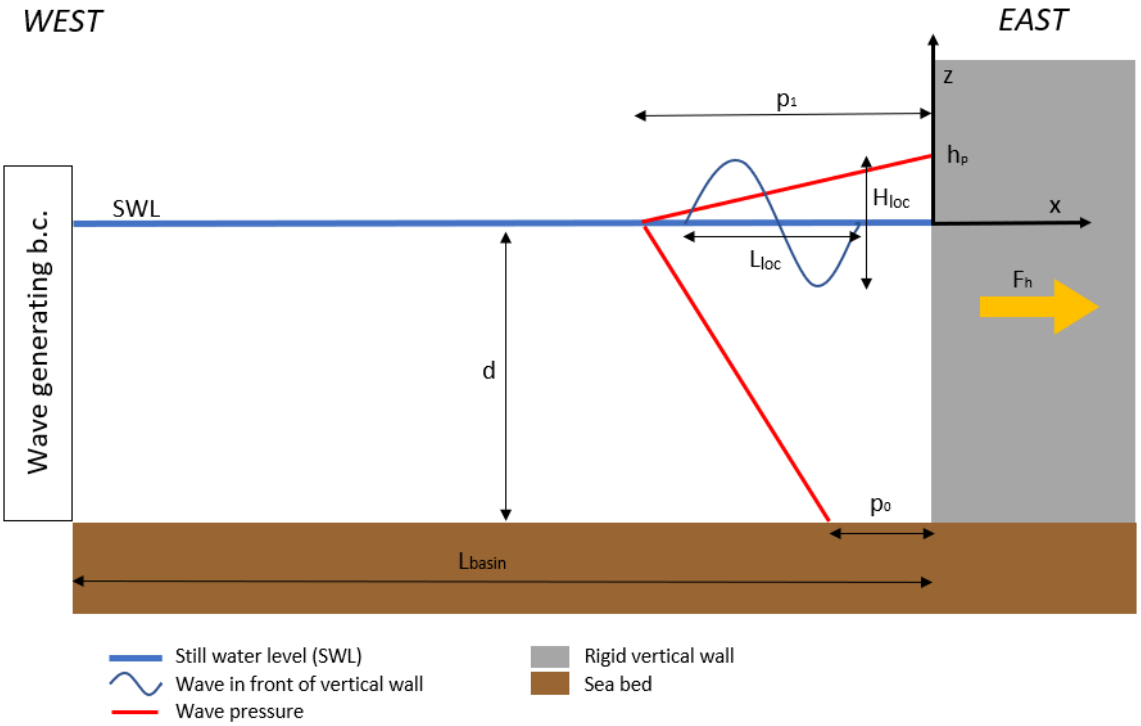


Figure 3.1: Schematisation of the geometry of the system. (Not on scale)

where:

| | | |
|---|---|---|
| $H_{loc}$ | = Wave height in front of the seawall (including reflection) | [m] |
| $L_{basin}$ | = Length between the wave generating b.c. and the vertical wall | [m] |
| $L_{loc}$ | = Wave length in front of the wall (= $2\pi$ / $k$) | [m] |
| $d$ | = Water depth at SWL (= constant over basin length) | [m] |
| $p_0$ | = Wave pressure at $z = -d$ | [kN/m$^2$] |
| $p_1$ | = Wave pressure at SWL | [kN/m$^2$] |
| $h_p$ | = Maximum height to which the wave pressure exerts on the wall | [m] |
| $F_h$ | = Horizontal wave force | [kN/m] |

The schematisation of the wave induced pressure is indicated with the solid red line. Different design methods give a different description for the wave pressure below SWL. Above SWL, the pressure distribution is approximated by assuming a hydrostatic pressure between SWL and $h_p$, possibly amplified with an empirical factor (Goda).

## 3.1.2. Wave field

The wave profile is a result of the sum of incoming and reflected waves. In a regular wave profile, these waves are in phase with each other leading to a surface profile in which nodes and anti-nodes are recognized, see Figure 3.2a. An irregular wave profile can be seen as a sum of regular wave profiles where wave phases are

randomly distributed over the horizontal axis. An exception of this random distribution is found near the vertical wall. Here, the incident irregular waves (sum of individual harmonic waves) are reflected and local features of the regular wave field occur (all individual waves have an anti-node at the wall). Further away from the boundary condition the wave phases are randomly distributed again, as was showed by Klopman and Van der Meer (1999). Figure 3.2b gives the concept of the summation of the time averaged wave heights $\overline{H}(x)$ of individual harmonic waves heights with different frequencies, leading to the time averaged wave height of an irregular wave field. The blue and red dashed line indicate the $H_{inc}$ and $H_{refl}$ respectively (for a scenario of a reflection coefficient lower than 1).

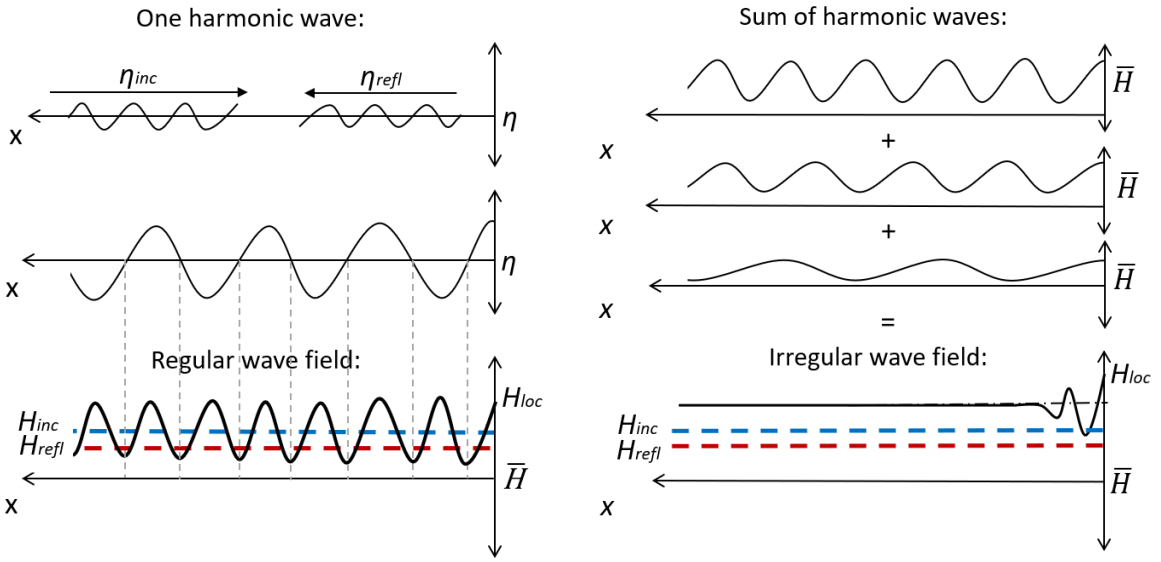


(a) A regular standing wave profile is created by the sum of an incoming and reflected wave. The vertical black dotted lines indicate the locations of nodes.

(b) The wave profile of an irregular wave field can be seen as a sum of regular standing wave profiles. A standing wave is recognized near the wall.

Figure 3.2: Sketch of the difference between a regular and irregular standing wave field.

In literature, the wave induced pressure or horizontal wave force is plotted as a function of the incoming wave characteristics (Mallayachari and Sundar, 1995; Chiu et al., 2007; Yu et al., 2015) or of the deep-water wave characteristics (Gurhan and Unsalan, 2005). In this report, an other approach is followed. The wave characteristics directly at the wall (= local) are used. This is substantiated by the following two advantages:

- Avoids computation time of the reflection coefficient.
- Avoids inaccuracy in the calculation of the reflection coefficient.

The second argument is related to the observed numerical dissipation, as discussed in Appendix C. In addition, design formulae of Goda and Sainflou assume inherently 100% reflection. By rephrasing the formulae as functions of the local wave parameters, an equal comparison can be made with the local conditions.

The increase in mean water level is defined as the time averaged surface elevation $\overline{\eta}(x)$ over the x-axis. This local increase is compared to the still water level, which is defined to be equal to the space and time averaged water elevation $\overline{\eta(x,t)}$ [1]. The expected deviation in mean water level shows a sinus of which the maximum is located under the anti-nodes of the wave field and a minimum is found under the nodes. The increase in mean water $h_0$ is defined as the difference between $\overline{\eta}(0)$ and $\overline{\eta(x,t)}$. Figure 3.3 presents for both a regular and irregular wave field a sketch of the expected surface elevation and increase in mean water level.

[1] SWASH simulations showed small deviations between the zero water level $\overline{\eta(x,t)}$ and the original water $\eta(x,0)$. Therefore, SWL is defined as $\overline{\eta(x,t)}$. This agrees with the assumption that there is no loss of water volume in the model.

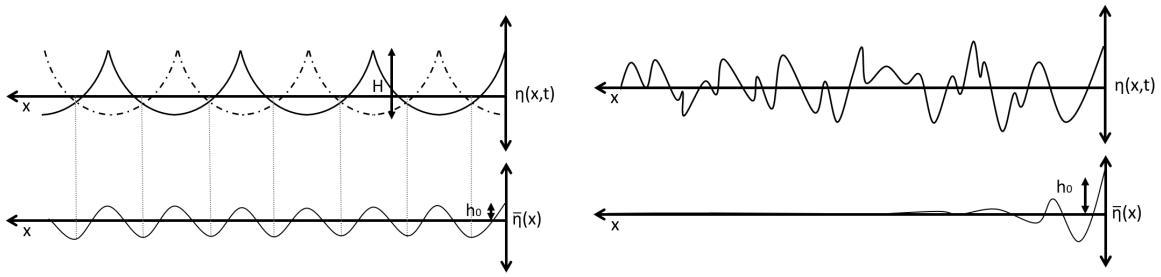


(a) Regular wave field

(b) Irregular wave field

Figure 3.3: Sketch of the increase in mean water level for an regular and irregular wave field. Top figures present the surface elevation over the x-axis. The solid line indicates the moment t = $t_1$, in which a wave crest is present at the wall. The dash-dot line (left) presents the moment t = $t_1$+ 1/2 T with a wave through at the wall. The bottom figures present the mean elevation of the water surface, averaged with respect to time. $h_0$ is defined as the increase in mean water level at the location of the anti-node at the wall. Relative increase in mean water level for an increasing wave steepness from the waves in an irregular wave field.

## 3.2. SWASH Model set-up

SWASH (acronym of Simulating WAves till SHore) is a recently developed numerical model at the TU Delft by The SWASH Team (2017) and based on the work of Stelling and Duinmeijer (2003), Stelling and Zijlema (2003), Zijlema and Stelling (2005), Zijlema and Stelling (2008) and Smit et al. (2013). The model is intended to be used for predicting transformation of surface waves and rapidly varied shallow water flows in coastal waters and is able to simulate in one, two or three dimensions (Zijlema et al., 2011). SWASH is a phase-resolved model and is able to present the vertical pressure distribution in the time domain. Because of this, SWASH can verify both the individual wave force (due to non-linear conditions) as well as wave heights and forces in the probability domain. The open source code of SWASH is available on http://swash.sourceforge.net. For this study, SWASH 4.01A is used.

**Model equations**

The governing equations in SWASH are the non-linear shallow water equations with the addition of a vertical momentum equation and non-hydrostatic pressure in the horizontal momentum equations. This non-hydrostatic pressure component is of importance since in the application of this study, the model is used for simulating short waves (Zijlema, 2015). The governing equations are the Navier-Stokes equations for the flow of an incompressible, inviscid fluid with a constant density and given by (Zijlema and Stelling, 2008):

$$\frac{\delta u}{\delta x} + \frac{\delta w}{\delta z} = 0 \tag{3.1}$$

$$\frac{\delta u}{\delta t} + \frac{\delta u^2}{\delta x} + \frac{\delta uw}{\delta z} + \frac{g}{\rho}\frac{\delta \zeta}{\delta x} + \frac{1}{\rho}\frac{\delta q}{\delta x} = 0 \tag{3.2}$$

$$\frac{\delta w}{\delta t} + \frac{\delta w^2}{\delta z} + \frac{\delta uw}{\delta x} + \frac{1}{\rho}\frac{\delta q}{\delta z} = 0 \tag{3.3}$$

$$\frac{\delta \zeta}{\delta t} + \frac{\delta Q}{\delta x} = 0, \qquad Q = \int_{-d}^{\zeta} u \mathrm{d}z \tag{3.4}$$

where:

| | | |
|---|---|---|
| $u$ | = Horizontal (particle) velocity | [m] |
| $q$ | = Non-hydrostatic pressure | [N/m$^2$] |
| $\zeta$ | = Surface elevation | [m] |
| $h$ | = Total water depth ( = $\zeta + d$ ) | [-] |
| $x$ | = Horizontal location | [m] |
| $z$ | = Vertical location | [m] |
| $c_f$ | = Chezy friction coefficient | [m$^{1/2}$/s] |
| $\tau_{xx}$ | = Horizontal turbulent stress | [N/m$^2$] |

**Boundary conditions and assumptions**
In the SWASH model several assumptions and boundary conditions are implemented, of which the following are the most relevant. At the free surface, pressure is zero and it is assumed that there is no wind interaction with the water. At the bottom, the assumption is made that the bottom friction is zero and the velocity perpendicular on the bottom is zero. The offshore boundary condition is defined with a deviating surface elevation $\zeta(t)$, resulting in an incoming (linear) wave or a system of linear waves (representing irregular waves). The shoreline boundary is modelled with a sponge layer, to absorb all incoming waves. To account for the reflective vertical wall, an additional modification is made to the grid cells as will be explained later.

Several approximations are made within the model. The advection approximation is strictly momentum conservative. Depth induced breaking is described by Smit et al. (2013). However, this does not cover wave breaking in infinite depths (white-capping). Baroclinic forcing is not present, which may be assumed to be right due to the small scale under consideration.

**Finite volume discretisation**
In SWASH, the geometry is schematised with a Cartesian coordinate system, using a one dimensional grid with a grid size $\Delta x$ of 0.25 m (see also Appendix C. The main section of the grid consists of wet points that represent the water basin. The vertical wall on the east boundary condition is modelled by wet grid points with small porosity. Riezebos (2014) describes the modelling of reflective structures by non-porous wet grid points. The value of reflection is maximum at a porosity of 0.1. The length of this porous layer is 10 m. East from this porous layer, a sponge layer is modelled to absorb the penetrated wave energy through the porous layer or undisturbed waves in case of simulating progressive waves. A schematization of the numerical grid and the location of the data output point is presented in Figure 3.4.

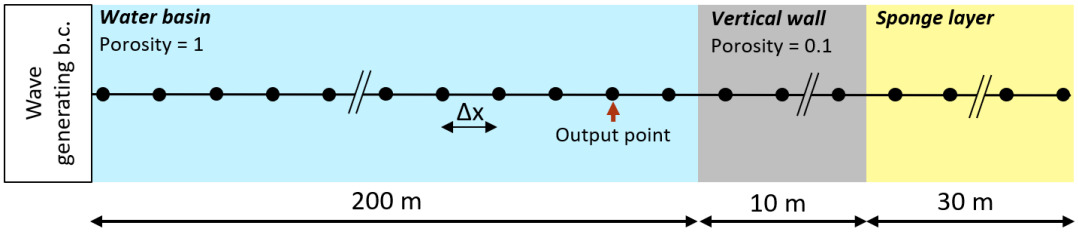


Figure 3.4: Schematization of the 1 dimensional SWASH grid. (Not on scale)

On the west boundary condition, a wave generating boundary condition is present. SWASH is applied with either the option of regular wave generation or manually generated wave spectra based on an input file. Reflected waves propagate back into the west boundary condition. This boundary condition is modelled as a weakly reflective and thereby avoiding (excessive) resonance in the system.

The discretized physical domain is elaborated in Zijlema and Stelling (2008) and summarized as follows. The horizontal plane is considered as a regular grid $\{x_{i+1/2} | x_{i+1/2} = i\Delta x, i = 0, .., I\}$ with $\Delta x$ the length of the cell and here chosen as 0.25 m. The cell centre is located at $x_i = (x_{i-1/2} + x_{i+1/2})/2$. The vertical domain is divided into $K = 6$ layers. The interface between the layers is defined as $z_{k+1/2}(x,t)$, with $k = 0, .., K$ and the layer thickness as $h_k = z_{k+1/2} - z_{k-1/2}$. The grid is boundary-fitted: at the water level $z_{K+1/2} = \zeta$ and at the bottom level $z_{1/2} = -d$ at $x = x_i$. Thereby, it makes the vertical layers equally distributed. The vertical spaces $h_k$ stay constant in the vertical dimension, but can fluctuate over the horizontal axis and over time. The (not equally distributed) vertical grid can be seen in Figure 3.5.

Time integration in SWASH is done with the midpoint rule and the space integration with the central differences scheme. This leads to the explicit leapfrog scheme with a second order time step for the advection terms, see Figure 3.6a. The viscosity term is integrated with a first order explicit time step and the non-hydrostatic part by a first order implicit time step.

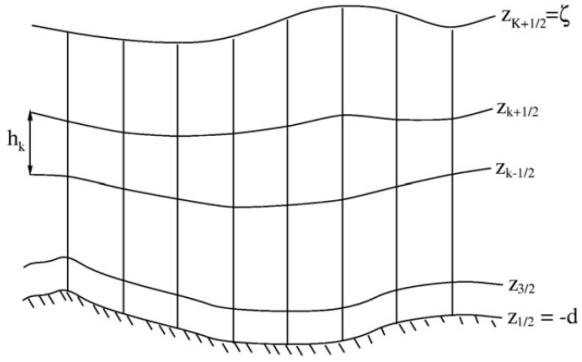


Figure 3.5: Schematization of the vertical layers in SWASH. Note that in this figure the vertical layers are not equidistant distributed. Based on: Zijlema and Stelling (2008)

Multiple schemes are available for the horizontal co-ordinates of the (for example) horizontal $u$-momentum. The default option is the second order BDF scheme. The pressure term in SWASH is separated in a hydrostatic and non-hydrostatic part. In calculating the non-hydrostatic pressure term, the Poisson equation is solved. Two linear solvers are incorporated in SWASH to solve this equation (Zijlema and Stelling, 2005). The vertical pressure gradient is solved with the central differencing layout, see Figure 3.6b. This is an important exception to the default option, needed for applications where vertical structures are important (The SWASH Team, 2017).

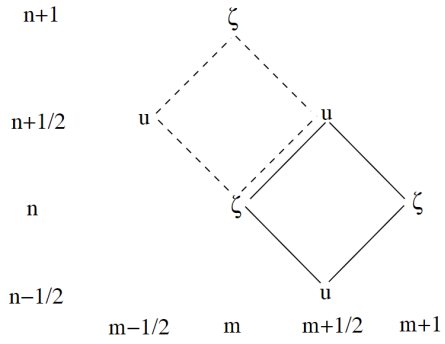


(a) Stencil of the leapfrog scheme. Based on: Zijlema (2015).

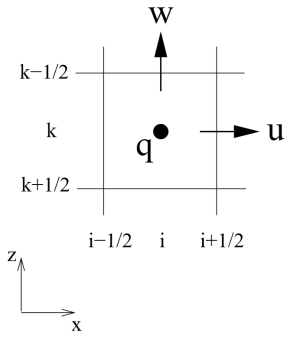


(b) A central differences integration scheme is used for the vertical pressure gradient. Based on: The SWASH Team (2017).

Figure 3.6: Numerical schemes of SWASH.

**Data output location**

SWASH is used with two different types of data output. One option is the BLOCK option, which gives the surface elevation over the complete spatial domain (x-axis) with a time interval of 0.2 s. The second option is the TABLE option, in which a specific location is chosen on which the surface elevation, depth, pressure on each layer and vertical position of each layer is obtained with a time interval of 0.1 s. The location is chosen 2 grid points before the wall is modelled, as indicated in Figure 3.4. The first point before the wall is disregarded since it showed to be subjective to local effects of the porous layer.

**Validation of SWASH**

Before the SWASH model is validated, an optimization of the grid size discretisation was performed. With the chosen grid size, an upper limit of the frequency range became visible. Numerical dissipation occurred for frequencies higher larger than 0.3 Hz. WIth the fixed water depth of 20 m, this also induced limitations to the relative depths simulated.

After this, SWASH results were compared with a physical experiment by Gurhan and Unsalan (2005). SWASH presented an accurate increase in wave pressure for increasing wave steepness. However, overall the SWASH

results were a percentage of about 15% lower than the experiment. This underestimation might be a consistency caused by an inaccurate reproduction of the experiment.

Further experiences in SWASH showed a correlation between the simulation of steep waves in irregular wave fields and. It could be that a SWASH runs fails in case the deep water breaking limit is reached (which is more likely to occur in irregular waves due the randomness). More information can be found in Appendix C.

From these observations it is concluded that SWASH is capable of simulating gentle waves. For the application where SWASH simulations are compared to each other, SWASH is assumed to give good results. For a representation of the realistic wave pressure, the SWASH model should be further validated.

## 3.3. SWASH Simulations

This section elaborates and argues the selection of simulations carried out in the SWASH model. The simulations are divided in four parts. The first three parts consider the different types of boundary conditions: regular waves, a uni-modal wave spectrum and a bimodal wave spectrum. In addition, simulations are carried out for the uni-modal and bimodal spectrum with the focus on the probability distribution of wave heights and force peaks.

For each part of the simulations the purpose is explained, follow by the choice on input parameters. Finally, an overview is given on the ranges of the local output parameters at the location of the wall, which will be the parameters for which the results are presented.

The ranges in which the incoming boundary conditions are taken are based on the IJmuiden case (see Figure 1.2). In this wave spectrum, the frequency range is approximately from 0.05 Hz up to 0.8 Hz. The maximum variance at the peak frequency is 1.25 $m^2$/Hz and the maximum variance at the smaller swell peak is 0.1 $m^2$/Hz. With the main objective of this research in mind, the ranges of the boundary conditions are partially adjusted with respect to the starting point, based on the following three assumptions:

- High frequency wave variance (> 0.3 Hz) is less of interest due the small contribution to the total horizontal induced wave force (according to the linear wave theory). In addition, due to the discretization high frequency waves are unable to simulate properly.
- More wave variance in the wave spectrum is of interest to investigate more severe wave conditions.
- A relatively large swell component is interesting for investigating the potential influence of the swell component on the total horizontal force.

### 3.3.1. Regular waves

Various wave theories such as the linear wave theory and Sainflou (1928) are based on regular waves. By simulating a regular wave field, these theories can accurately be compared with the SWASH model. For the formula of Sainflou this also comprises a verification of the expression of the increase in mean water level $h_0$. Besides these regular wave theories, the resulting horizontal wave force according to Goda can be examined for an individual wave. Therefore, the focus of the simulations of a regular wave field are:

- Analysis on the increase in mean water level
- Comparison of design guidelines for the horizontal wave force of regular waves (individual wave force)

**Input parameters**

For both of these aspects it is desirable to obtain results in a wide range of sea states. The rise in mean water level and the verification of the horizontal induced wave force are addressed for physical input parameters presented in Table 3.1.

Table 3.1: Range of input parameters for 36 simulations of a regular wave field. For a full overview of the input parameters for each simulation is referred to Appendix C.4

| Parameter | Range | Increment |
|---|---|---|
| $H_{inc}$ | 0.5 m - 3 m | 0.5 m |
| $f$ | 0.05 Hz - 0.25 Hz | 0.05 Hz |
| $T$ | 20 s - 3.33 s | *varies* |
| $L$ | 270 m - 17 m | *varies* |

### 3.3.2. Uni-modal wave spectrum

As explained in Section 3.1, also in an irregular wave field an increase in mean water level is expected. Furthermore, the horizontal wave force from the SWASH model can be compared with the design guidelines and spectral calculation. Unlike a regular wave field, wave heights, wave periods and force peaks obtained in the time domain are randomly distributed. Therefore, a comparison is carried out with the characteristic wave parameters. The two topics addressed for a uni-modal wave spectrum are:

- Analysis on the increase in mean water level
- Comparison of design guidelines for the characteristic horizontal wave force

**Description of the wave spectrum**

A common way to express an irregular wave field is by means of a wave spectrum. Amongst engineers, the most widely used method of directly modelling a wave spectrum $S_{var}(f)$ has its origin by JONSWAP (JOint North Sea WAve Project) (Hasselmann et al., 1973). The so called JONSWAP spectrum is based on the shape of the Pierson and Moskowitz spectrum (Pierson and Moskowitz, 1964), but enhanced with a peak enhancement factor $\gamma$. With this peak enhancement factor the spectrum can be assigned with a sharp peak, to account for a specific wave conditions such as a young sea state ($\gamma = 3.3$) or swell ($\gamma = 20$). The JONSWAP spectrum is often used for representing a developing sea state, which is often the case for storm conditions and is therefore well applicable to engineering purposes. The JONSWAP spectrum is given by:

$$S_{var}(f) = \alpha g^2 (2\pi)^{-4} f^{-5} \exp\left[-\frac{5}{4}\left(\frac{f}{f_p}\right)^{-4}\right] \gamma^{\exp\left[-\frac{1}{2}\left(\frac{(f/f_{peak})-1}{\sigma}\right)^2\right]} \tag{3.5}$$

Where:

| | | |
|---|---|---|
| $\alpha$ | = Energy scale parameter | [-] |
| $f$ | = Frequency | [Hz] |
| $f_p$ | = Peak frequency | [Hz] |
| $\gamma$ | = Peak enhancement factor (= 3.3) | [-] |
| $\sigma$ | = Shape parameter | [-] |
| $\sigma_a$ | = Shape parameter for $f \leq f_{peak}$ (= 0.7) | [-] |
| $\sigma_b$ | = Shape parameter for $f > f_{peak}$ (= 0.9) | [-] |

Where the values for $\gamma$, $\sigma_a$ and $\sigma_b$ are based on (Hasselmann et al., 1973, p. 37). The total variance of the spectrum is related to the significant wave height by:

$$H_{m_0} \approx 4\sqrt{\int_0^\infty S_{var}(f)\mathrm{d}f} \tag{3.6}$$

With this expression, a more evident way to express the wave variance density is obtained. In defining the range of input parameters, the energy scale parameter $\alpha$ is rewritten in such a way that it is depended on the input of a significant wave height $H_{m_0}$. With assumptions for the invariable parameters $\gamma$, $\sigma_a$ and $\sigma_b$ two input parameters remain: $H_{m_0,inc}$ and $f_p$.

**Input parameters**

The increase in mean water level and the characteristic horizontal wave force are considered for different wave fields. Table 3.2 presents the physical parameters that are used as input parameters for the simulations of these irregular wave fields. The peak enhancement factor is assigned with $\gamma = 3.3$. The simulated peak frequencies are less scattered over the frequency range compared to the simulations of regular waves, since the wave spectra comprise a frequency range inherent to the irregular wave field[2].

[2] From the 32 simulations, 29 simulations were performed successfully. Three runs with the highest expected steepness failed.

Table 3.2: Range of input parameters for 32 simulations of an irregular wave field. For a full overview of the input parameters for each simulation is referred to Appendix C.4

| Parameter | Range | Increment |
|---|---|---|
| $H_{m_0,inc}$ | 0.25 m - 3 m | *varies* |
| $f_p$ | 0.1 Hz - 0.25 Hz | 0.05 Hz |
| $T_p$ | 10 s - 4 s | *varies* |
| $L_p$ | 121 m - 17 m | *varies* |

### 3.3.3. Bimodal wave spectrum

Up to so far, "conventional" wave conditions were treated including regular waves and uni-modal wave spectra. Because the analysis of wave loads of bimodal spectra is an extension to this, the simulations are built up in steps. The following three topics are considered:

- First indication of the influence of swell
- Quantification of the influence of swell parameters
- Influence of swell in different sea states

**Description of the bimodal wave spectrum**

A bimodal wave spectrum can be created by adding two JONSWAP spectra with different parameters, resulting in:

$$\begin{aligned} S_{var}(f) =& \alpha_1 g^2 (2\pi)^{-4} f^{-5} \exp\Big[-\frac{5}{4}\Big(\frac{f}{f_{p1}}\Big)^{-4}\Big] \gamma_1^{\exp\left[-\frac{1}{2}\left(\frac{(f/f_{p1})-1}{\sigma}\right)^2\right]} \\ &+ \alpha_2 g^2 (2\pi)^{-4} f^{-5} \exp\Big[-\frac{5}{4}\Big(\frac{f}{f_{p2}}\Big)^{-4}\Big] \gamma_2^{\exp\left[-\frac{1}{2}\left(\frac{(f/f_{p2})-1}{\sigma}\right)^2\right]} \end{aligned} \tag{3.7}$$

where:

| | | |
|---|---|---|
| $\alpha_1$ | = Energy scale parameter of swell component | [-] |
| $\alpha_2$ | = Energy scale parameter of wind sea component | [-] |
| $f_{p1}$ | = Peak frequency of the swell component | [Hz] |
| $f_{p2}$ | = Peak frequency of the wind sea component | [Hz] |
| $\gamma_1$ | = Peak enhancement factor of swell component | [-] |
| $\gamma_2$ | = Peak enhancement factor of wind sea component | [-] |

In a same fashion as for the uni-modal wave spectrum, the $\alpha_1$ and $\alpha_2$ input parameters are exchanged for input parameters $H_{m_{01}}$ and $H_{m_{02}}$.

**Input parameters**

For each of the three topics under consideration, different input parameters are defined. The influence of swell on the characteristic wave force is assessed by decomposing a bimodal spectrum. This implies comparing the simulation of a bimodal spectrum with (the sum of) simulations of the swell component and wind sea component. Because of this decomposition, this example is referred to as "decomposition of the bimodal wave spectrum". An example is made with a steep wave field in relatively deep water (classification is mostly influenced by the wind sea component), because the difference between the peak frequencies and wave heights is the largest.

The influence of the swell characteristics is consequently addressed by taking the same wind sea component of the spectrum, and varying the peak frequency $f_{p1}$ and significant wave height $H_{m_{01},inc}$ of the swell component. This is referred to as "influence of swell parameters"[3].

Lastly, to investigate the influence of swell in a wider range of wave fields also the input parameters of the wind sea component are varied. To simulate wave spectra with increasing swell but constant wave characteristics, an intermediate step in the generation of wave spectra was implemented. This is explained in Appendix C.3.

[3]From the 31 simulations, 29 simulations were performed successfully. Two runs with the highest expected steepness failed.

In this way, the influence for a relative amount of swell can be determined. The range of input parameters for the three described topics are presented in Table 3.3.

Table 3.3: Range of input parameters for the simulations of irregular wave fields with a bimodal spectra. For a full overview of the input parameters for each simulation is referred to Appendix C.4

| Parameter | Decomposed spectrum | Swell paramters | Sea states |
|---|---|---|---|
| $H_{m_{01},inc}$ | 0.2 m | 0 - 0.75 m | 0 - 0.8 m |
| $H_{m_{02},inc}$ | 1.5 m | 1.5 m | 0.3 - 1.5 m |
| $f_{p1}$ | 0.075 Hz | 0.05 - 0.15 Hz | 0.05 - 0.09 Hz |
| $f_{p2}$ | 0.2 Hz | 0.2 Hz | 0.13 - 0.23 Hz |

### 3.3.4. Probability distribution

The probability distribution of wave heights and force peaks can be analysed by a long SWASH simulation where numerous values exceed the characteristic value. The observed distributions can consequently be compared with the theoretical Rayleigh distribution, for both uni-modal and bimodal wave spectra. The approach to compare this probability distribution with the Rayleigh distribution is divided into two steps:

- Comparison of the probability distribution of a uni-modal wave spectrum with bimodal spectrum to indicate potential deviations
- Quantification of deviations from the Rayleigh distribution for different wave conditions

**Input parameters**

For the first step two simulations with a simulation time of 10 hours are carried out. The input parameters for the uni-modal spectrum and bimodal spectrum are presented in Table 3.4. The input parameters are chosen in such a way that the observed wave steepness and relative depth at the wall are comparable. The observed wave spectra at the wall are indicated in Figure 3.7.

Table 3.4: Input parameters for the simulation of the uni-modal and bimodal spectrum for the comparison of the probability distribution.

| Parameter | Unimodal | Bimodal |
|---|---|---|
| $H_{m_{01},inc}$ | - | 0.5 m |
| $H_{m_{02},inc}$ | 1 m | 1 m |
| $f_{p1}$ | - | 0.05 Hz |
| $f_{p2}$ | 0.167 Hz | 0.2 Hz |

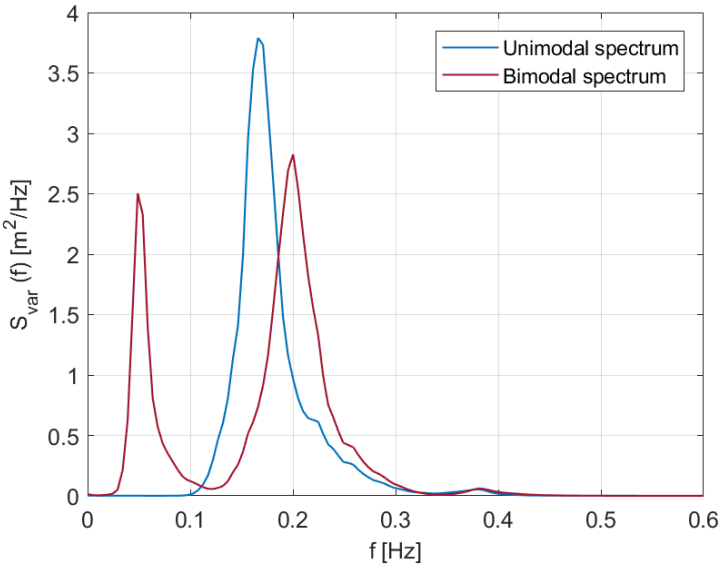


Figure 3.7: The observed wave spectra of the uni-modal and bimodal spectrum used for the comparison of the probability distribution.
$H_{1/3,loc}/L_{1/3} = 0.034$ , $d/L_{1/3} = 0.395$ (uni-modal)
$H_{1/3,loc}/L_{1/3} = 0.030$, $d/L_{1/3} = 0.363$ (bimodal)

In the second step, multiple simulation with a simulation time of 12 hours are carried out. The input parameters are in the same range as the values in the last column of Table 3.3. An complete overview of the input parameters of the simulations is presented in Appendix C.4.

### 3.3.5. Non-dimensional output parameters

After the spin-up time of the model, the model reaches a steady state solution. Depended on the amount of reflection, wave-wave interactions and numerical influences, the local wave parameters at the wall deviate from the input parameters. The wave period and wave length remain largely unaltered ($T_{loc} = T$ and $L_{loc} = L$). The wave height $H_{loc}$ shows mostly a magnification, as reflection is the most dominant effect.

The non-dimensional parameters on which is being hold on to are $d/L$ to present the relative depth and $H_{loc}/L$ to describe the wave steepness. In an irregular wave field these non-dimensional parameters are described by the characteristic values and become $d/L_{1/3}$ and $H_{1/3,loc}/L_{1/3}$ respectively.

**Introduction of swell parameters**

To make a distinction between the swell component and the wind sea component a boundary in the frequency domain is defined. This boundary is indicated by $f_{tr}$ and defined as the frequency located between $f_{p1}$ and $f_{p2}$ at which the wave variance is minimum. This divides the wave variance in the swell variance $m_{01}$ and the wind sea variance $m_{02}$.

To quantify the swell component in relation to the total spectrum, two new parameters are introduced. Most evident of influence is the wave variance underneath the swell peak with respect to the total wave variance. This will be defined as the *relative swell variance* and is given by:

$$M_{Sw} = \frac{m_{01}}{m_{01} + m_{02}} \tag{3.8}$$

From the theory of the response function, the presumption is that the lower the frequency of the swell peak, the more it contributes to the force. The influence of the frequency is defined as the *relative swell peak frequency*, which presents the distance between the peaks, over the peak frequency of the wind sea peak:

$$\Phi_{Sw} = \frac{f_{p2} - f_{p1}}{f_{p2}} \tag{3.9}$$

Both parameters are denoted in such a way that a larger value corresponds with a larger expected wave force. In Figure 3.8, a bimodal spectrum is showed with $H_{m_0 1} = 0.3$ m, $H_{m_0 2} = 1.3$ m, $f_{p1} = 0.05$ Hz and $f_{p2} = 0.18$ Hz.

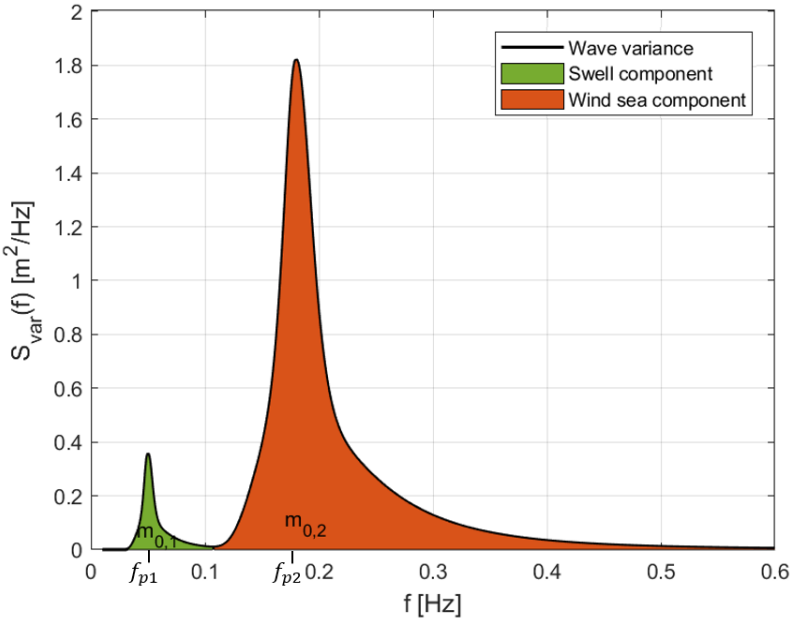


Figure 3.8: Example of a bimodal spectrum in which the swell and wind sea component are distinguished.

For this example, the relative swell parameters can be determined as follows:

$$M_{Sw} = \frac{m_{01}}{m_{01} + m_{02}} = \frac{0.0056}{0.0056 + 0.1058} = 0.05 \tag{3.10}$$

and

$$\Phi_{Sw} = \frac{f_{p2} - f_{p1}}{f_{p2}} = \frac{0.18 - 0.05}{0.18} = 0.72 \tag{3.11}$$

A wave spectrum with a value of $M_{Sw} = 0.05$ can be interpreted as a wave spectrum with 5% of swell.

**Overview**

For all the simulations carried out, including the simulations for the validation of SWASH, the range of non-dimensional parameters are presented in Table 3.5. This overview function also as a reference to the validity of the results and conclusions of this study.

Table 3.5: Ranges of relative depth, wave steepness and swell for which the simulations are carried out. *For regular waves, the statistical wave parameters $H_{1/3}$ and $L_{1/3}$ are equal to $H$ and $L$ respectively.

| Simulations | Relative depth $d/L_{1/3}$ [-] | Wave steepness $H_{1/3,loc}/L_{1/3}$ [-] | Relative swell variance $M_{Sw}$ [-] | Relative swell peak frequency $\Phi_{Sw}$ [-] |
|---|---|---|---|---|
| IJmuiden case | 0.64 | 0.057 | 0.02 | 0.62 |
| Validation SWASH | 0.123 | 0.036 - 0.092 | - | - |
| Regular waves* | 0.07 - 0.8 | 0 - 0.11 | - | - |
| Uni-modal spectrum | 0.18 - 0.77 | 0 - 0.06 | - | - |
| Bimodal spectrum | 0.26 - 0.48 | 0.017 - 0.045 | 0 - 0.25 | 0.4 - 0.75 |
| Probability distribution | 0.26 - 0.48 | 0.017 - 0.045 | 0 - 0.25 | 0.6 |

To obtain insight in the type of waves which are simulated, different wave theories that apply for progressive waves are indicated in Figure 3.9. The non-dimensional depth in terms of $d/(gT^2)$ is presented on the

horizontal axis. On the the vertical axis the wave steepness is indicated in terms of $H/(gT^2)$. Since in the simulations standing waves are generated, the non-dimensional wave characteristics do not directly apply to progressive waves. To still get a grip on the wave theories that apply to the simulated waves, the progressive wave characteristics are approximated.

By comparing the deep water breaking criterion of Miche (1944) and Danel (1952) it can be seen that the ratio of progressive waves with respect to standing waves is 0.142 : 0.218, which is approximately a factor 1.5. This factor could be used to divide the standing wave by to arrive at an indication of a progressive wave characteristics. An other theory, is that in case of 100% reflection, the standing wave is equal to half the incoming progressive wave.

To give the most rough indication of the wave characteristics observed in the simulations, the observed standing wave and second approximation of the wave characteristics are plotted:

- $H = H_{loc,1/3}$
- $H = 0.5\ H_{loc,1/3} \approx H_{inc,1/3}$ (assume 100% reflection)

These the wave characteristics are visualized in Figure 3.9 for the different simulations. The wide range in non-dimensional parameters show a dense distribution in the figure due to the logarithmic scale. It is observed that most simulations may theoretically not be described the linear wave theory. Furthermore, as the simulated wave conditions get more complex (from regular to uni-modal to bimodal), the range in which the simulations are carried out is smaller. Although the simulated waves are mainly classified as gentle waves, the waves do not fall in the region where they may be described by the linear wave theory.

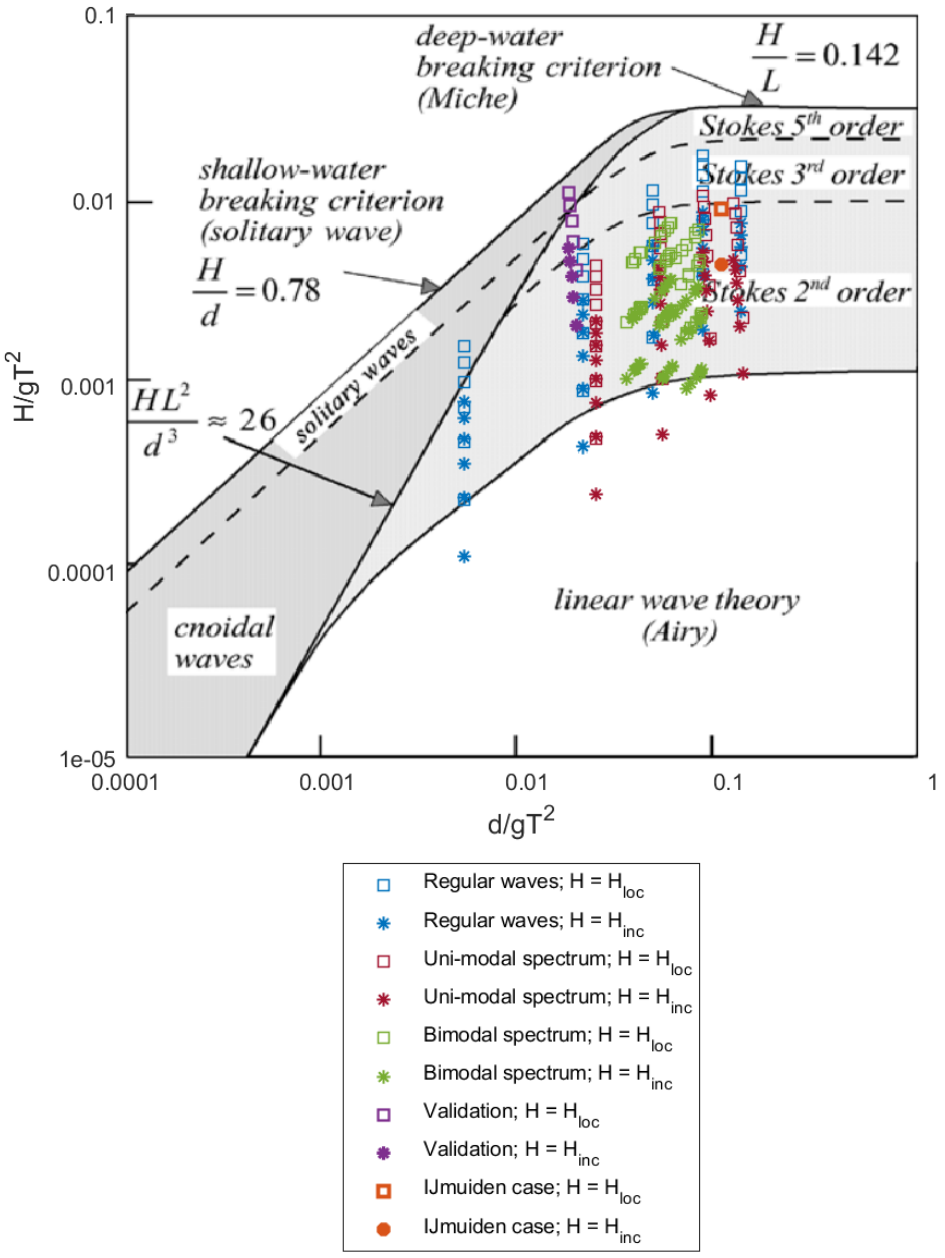


Figure 3.9: Non-dimensional plane of wave steepness $H/gT^2$ and relative depth $d/gT^2$ and accordingly the wave theories that describe progressive waves. The coloured markers indicate two possible options of where the obtained wave parameter of a standing wave would be indicated. Based on: Holthuijsen (2007)

## 3.4. Application of design methods

This section covers the application of the design methods to determine the horizontal wave force $F_h$. The following standard quantities are based on the SWASH model:

$$\rho_w = 1023 \text{ kg/m}^3 \tag{3.12}$$

$$g = 9.813 \text{ m/s}^2 \tag{3.13}$$

where $\rho_w$ is the density of water and will be denoted as $\rho$ throughout this report. These quantities are used in the other design methods as well.

### 3.4.1. SWASH

**Force calculation**

The output from the SWASH model necessary for the determination of the horizontal wave force consists of: the surface elevation, the water pressure at each vertical grid point, the vertical location of each vertical grid point. This data is obtained in front of the vertical wall (x = -0.25 m) with a time step of $\Delta t$ = 0.1 s. With a few steps the water pressure $p_{tot}$ is translated to a horizontal wave force $F_h$.

The vertical grid points extracted from the SWASH output range from the sea bottom up to the bottom of the top layer. Therefore, to get a complete discretization of the vertical grid, the first step is adding the zero pressure at the surface elevation. Subsequently, the pressure can be linear interpolated between the vertical grid points, resulting in $p_{tot}(z,t)$. The hydrostatic water pressure is given by:

$$p_{hydro}(z) = -\rho g z \tag{3.14}$$

and is subtracted from the total pressure between $z = -d$ and $z = 0$, resulting in $p_{wave}(z,t)$. With a standard Matlab operation, the wave pressure is integrated with linear interpolation from $z = -d$ to $z = \eta(t)$, to obtain the wave induced force $F_h(t)$.

**Probability distribution**

With the zero-down crossing method, both wave heights $\underline{H}$ and wave force peaks $\underline{F}$ can be identified. The wave heights are determined by max($\eta(t)$) - min($\eta(t)$), whereas the force peaks are determined by max($F(t)$), both within two successive zero-down crossings of respectively $\eta(t)$ and $F(t)$. After ordering the wave heights and force peaks on magnitude, the probability of each value is given by:

$$p(\underline{H}_i) = \frac{i}{N}, \qquad \text{where } i = 1,2,...N = \text{rank of wave, based on wave height} \tag{3.15}$$

$$p(\underline{F}_i) = \frac{i}{N}, \qquad \text{where } i = 1,2,...N = \text{rank of wave, based on force peak} \tag{3.16}$$

with $N$ the amount of wave heights and force peaks respectively in the time series.

The characteristic horizontal wave force is based on the average of the heighest 1/3$^{\text{rd}}$ of the force peaks $F_{1/3}$.

### 3.4.2. Design formulae

Here, the applications of the three design formulae (linear wave theory, Sainflou and Goda) are elaborated. The design formulae consists of three design steps (step 4, 5 and 2 from Figure 1.3). Design step 4, the simplification of the wave spectrum by wave characteristics, is indirectly addressed, by comparing results for differently shaped spectra.

As input parameters for the design guidelines, wave characteristics $H_{1/3}$ and $T_{1/3}$ are used. Thereby, the suggestions of the design guidelines are neglected. The significant wave parameters are chosen as it is argued that these characteristics give a direct (and most basic) representation of the wave field. Furthermore, for regular waves a spectral analysis results in inaccurate results. Design step 2 (the determination of the individual wave force) and design step 5 (the determination of the design characteristics) are presented here.

**Force calculation**
The design formulae are rewritten in a way they can be used with the local input parameters. The input parameters include the effect of reflection caused by the vertical wall. The outcome is the wave induced pressure accounting for the wave conditions (no additional safety).

Sainflou (based on the version in Leidraad Kunstwerken) simplifies to:

$$p_1 = \rho g(a_{loc} + h_0), \tag{3.17}$$

$$p_0 = \frac{\rho g a_{loc}}{\cosh(kd)}, \tag{3.18}$$

$$h_0 = \frac{1}{2} k a_{loc}^2 \coth(kd), \tag{3.19}$$

$$h_p = h_0 + a_{loc} \tag{3.20}$$

with $a_{loc} = 0.5 H_{loc}$.

Goda reduces considerably when adjusted for the geometry under consideration. This procedure is presented in Appendix B, and results in:

$$p_1 = \left(0.6 + \frac{1}{2}\left[\frac{2kd}{\sinh(2kd)}\right]^2 + \frac{4d}{H_{loc}}\right)\rho g \frac{1}{2} H_{loc}, \tag{3.21}$$

$$p_0 = \frac{p_1}{\cosh(kd)}, \tag{3.22}$$

$$h_p = 0.75 H_{loc} \tag{3.23}$$

Note: Instead of the unreflected $H_{inc}$ in the original Goda formula, here the local (reflected) $H_{loc}$ is implemented.

For the LWT, the pressure distribution below SWL is not linear distributed. Therefore, instead of the pressure at the bottom $p_0$, the pressure below SWL is described in the function of $p_{sub}(z)$:

$$p_1 = \rho g a_{loc}, \tag{3.24}$$

$$p_{sub}(z) = \rho g a_{loc} \frac{\cosh(k(d+z))}{\cosh(kd)}, \tag{3.25}$$

$$h_p = a_{loc} \tag{3.26}$$

For a linear distributed wave pressure (Goda and Sainflou), the horizontal force is derived by the expression:

$$F_h = \frac{1}{2} d(p_1 + p_0) + \frac{1}{2} h_p p_1 \tag{3.27}$$

In the linear wave theory, the force is found by the sum of the sector above and below the SWL, in which for the section below SWL integration of the pressure over depth is necessary:

$$F_h = F_{top} + F_{sub} \tag{3.28}$$

where

$$F_{top} = \frac{1}{2} h_p p_1 \tag{3.29}$$

and

$$F_{sub} = \rho g a_{loc} \int_{-d}^{0} \frac{\cosh(k(d+z))}{\cosh(kd)} \mathrm{d}z, \tag{3.30}$$

**Probability distribution**
In case of a regular wave field, the wave heights and wave periods of the wave field are constant in time

for a fixed location. The input variables of the design formulae at the wall become $H_{loc} = H_{1/3} = H$ and $T_{loc} = T_{1/3} = T$. Due to the stationary wave conditions, a probability distribution is not considered.

However, in the case of an irregular wave field, wave heights and wave periods vary in time at the location of measurement and a decision has to be made on the values of $H_{loc}$ and $T$ to insert in the formula. For comparing characteristic values, the significant wave height $H_{1/3}$ and wave period $T_{1/3}$ are chosen.
The design wave height is determined by the Rayleigh distribution, and given by:

$$H_d = \sqrt{-2m_0 \ln\left(1 - \Pr\{\underline{H} < H_d\}\right)} = \gamma_d H_{1/3} \tag{3.31}$$

The wave period is not related to a probability distribution. Predominantly, the significant wave period $T_{1/3}$ will be used for the application of the design formulae. In some cases, also $T_p$ and $T_{m-1,0}$ are used as design wave period.

### 3.4.3. Spectral calculation

The spectral calculation method is a method which applies the linear wave theory on the entire wave spectrum to end up with a force spectrum. This corresponds with design step 3 from Figure 1.3 and gives thereby and expression of the characteristic wave force. With the assumption that the force spectrum follows a Rayleigh distribution of force peaks, it can be used to a design force (design step 6 in Figure 1.3). Here, the derivation of the horizontal wave force from a wave spectrum is briefly presented. A complete elaboration on the spectral calculation method can be found in Appendix A.

**Force calculation**

The wave spectrum is obtained at the location of the interface between the wall and the water and includes the reflection from the wall. The measured wave variance is multiplied by the response function to obtain the force spectrum:

$$S_F(f) = \left(R_{sub}(f) + R_{top}\right)^2 S_{var}(f) \tag{3.32}$$

with

$$R_{sub}(f) = \rho\, g \int_{-d}^{0} \frac{\cosh(k(f)(d+z))}{\cosh(k(f)(-d))}\, \mathrm{d}z \tag{3.33}$$

$$R_{top} = \frac{1}{2}\, \rho\, g\, a_{ref} \tag{3.34}$$

The characteristic horizontal wave force is obtained by:

$$F_{m0} = 2\sqrt{\int_0^{\infty} S_F(f)\mathrm{d}f} \tag{3.35}$$

**Probability distribution**

With the assumption of Rayleigh distributed force peaks, for every probability of exceedance a design force can be determined.

$$F_d = \sqrt{-2m_{0,F}\, \ln\left(\Pr\{1 - \underline{F} < F_D\}\right)} = \gamma_d F_{m0} \tag{3.36}$$

### 3.4.4. Pressure distribution

In Figure 3.10, the pressure distribution over the vertical axis for the different design formulae is given. The pressure is made non-dimensional by dividing by ($\rho g h$) and the vertical axis is made non-dimensional (partial depth) by dividing by $d$. In this example, the different design methods are addressed for the significant load the simulation of the IJmuiden wave conditions. For design guidelines $H_{1/3}$ and $T_{1/3}$ are used as input paramters. The spectral calculation is applied for $F_{m0}$. For the SWASH, the pressure distribution that corresponds with $F_{1/3}$ is plotted.

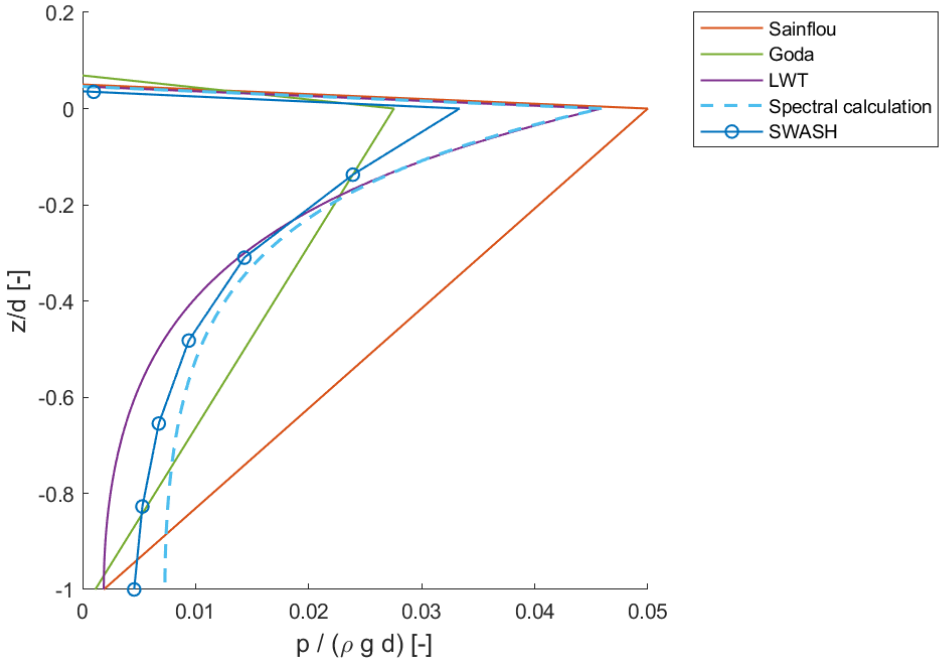


Figure 3.10: Application of the design methods on the distribution over the vertical axis.

In this example it can be observed how the pressure distributions differ between the design methods. The Sainflou and Goda give a simplified linear pressure distribution below SWL. The LWT gives a more accurate estimation of the pressure distribution of the SWASH simulation, but underestimates in greater partial depth. The spectral calculation method accounts for the swell component.

# 4

# Results

This chapter presents the results from the simulations in SWASH and calculations by the design guidelines and the spectral calculation method. The results are presented in the same order as the simulations from Section 3.3.

First, the results from regular wave fields are treated. This contains an analysis on the increase in mean water level and the horizontal wave force for an individual wave (regular wave) estimated by SWASH and the different design formulae. In the next section, irregular wave fields described with uni-modal spectra are addressed. Also here, first the increase in mean water level is analysed. Subsequently, the characteristic horizontal wave force according to the various design methods is compared. After that, the results for wave fields with a bimodal spectrum are presented. This includes three parts. First, the influence of swell on the characteristic wave force is examined by means of decomposing a bimodal spectrum. After that, the influence of the swell parameters $M_{Sw}$ and $\Phi_{Sw}$ are considered for the addition of swell components. Finally, the influence of swell in different sea states is presented. Ultimately, the distribution of the extreme values within storm conditions are considered. For long simulation lengths of irregular wave fields from uni-modal and bimodal spectra, the wave heights and force peaks are analysed.

## 4.1. Regular waves

### 4.1.1. Increase in mean water level

As discussed in Section 3.1, it is expected that a standing wave profile leads to an increase in mean water level. Figure 4.1 gives an example of a simulation in SWASH where the time averaged surface elevation is plotted over the basin length and compared with the expression $h_0$ according to Sainflou (see Equation 2.30). This expression indicates the increase in means water level at the wall. The location of the wall is at x = 0 m and the wave generating boundary condition at x = -200 m. As a reference, also the wave height $H$ is plotted, indicating the nodes and anti-nodes of the wave field.

From the figure it can be seen that an increase in mean water level is present at the anti-nodes and a decrease in mean water level is present at the nodes. Furthermore, it is visible that the expression by Sainflou is in this case overestimating the increase in mean water level at the wall.

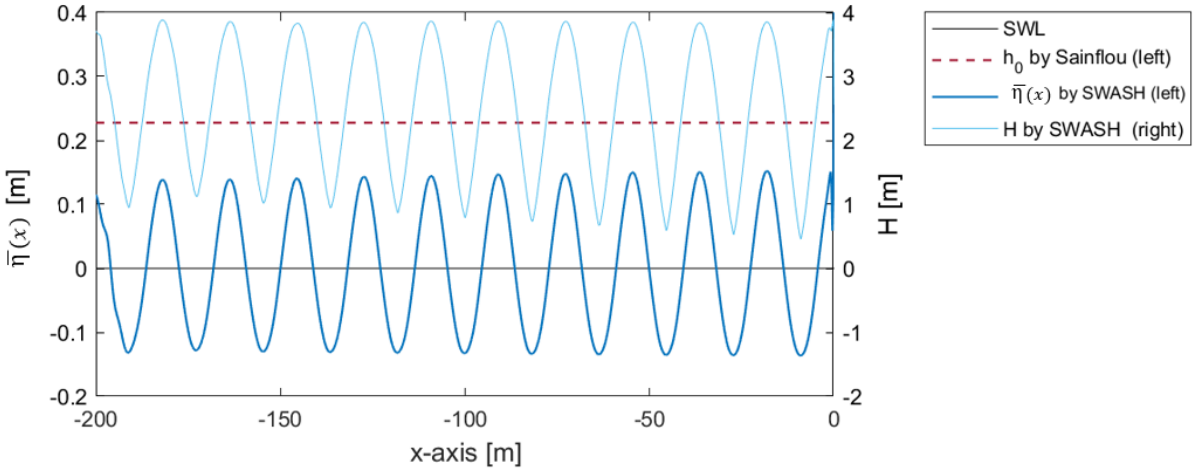


Figure 4.1: Example of the time averaged surface elevation and time wave height over the x-axis for a regular wave field with $H_{loc}/L = 0.1$ and $d/L = 0.51$

The increase in mean water level $h_0$ in front of the wall is divided by the local wave height, resulting in the expression $h_0/H_{loc}$. Results from the SWASH model are compared with the solution by Sainflou as presented in Leidraad Kunstwerken. Figure 4.2 plots the relative increase in mean water level for an increasing wave steepness $H_{loc}/L$, indicated on the x-axis. The SWASH results are indicated by dots and the analytical solutions by Sainflou is indicated by the solid lines. The different colours indicate the solutions for various relative depths.

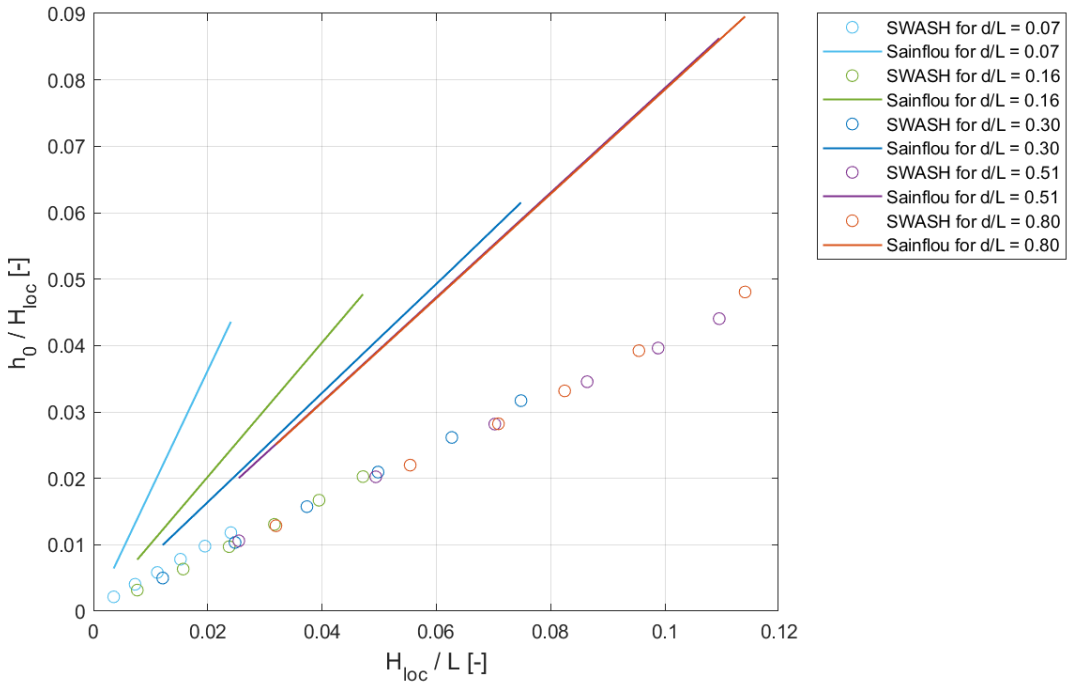


Figure 4.2: Relative increase in mean water level due to regular waves, plotted for an increasing wave steepness.

The Sainflou expression shows a linear increase for an increasing wave steepness. In very shallow waters ($d/L < 0.2$), $h_0/H_{loc}$ increases more than in deeper water. The SWASH simulations show clearly a linear relation to the wave steepness as well. However, the results by SWASH show a increase in mean water level of approximately a factor 2 smaller. Also the larger increase in mean water level for very shallow water is not present.

### 4.1.2. Horizontal wave force

Here, the horizontal wave force induced by the regular wave field is presented for a range of wave steepness and relative depth. The results of SWASH are compared with design guidelines. The horizontal wave force $F_h$ is made non-dimensional by dividing over the term ( $\rho g d^2$) and plotted on the vertical axis. The horizontal axis indicates the wave steepness. The various relative depths are indicated by colours. The computed results by SWASH are assigned with dots. In a similar range of $H_{loc}/L$ the analytical results of Sainflou, Goda and the LWT are plotted by de dashed-dot line, dashed line and solid line respectively.

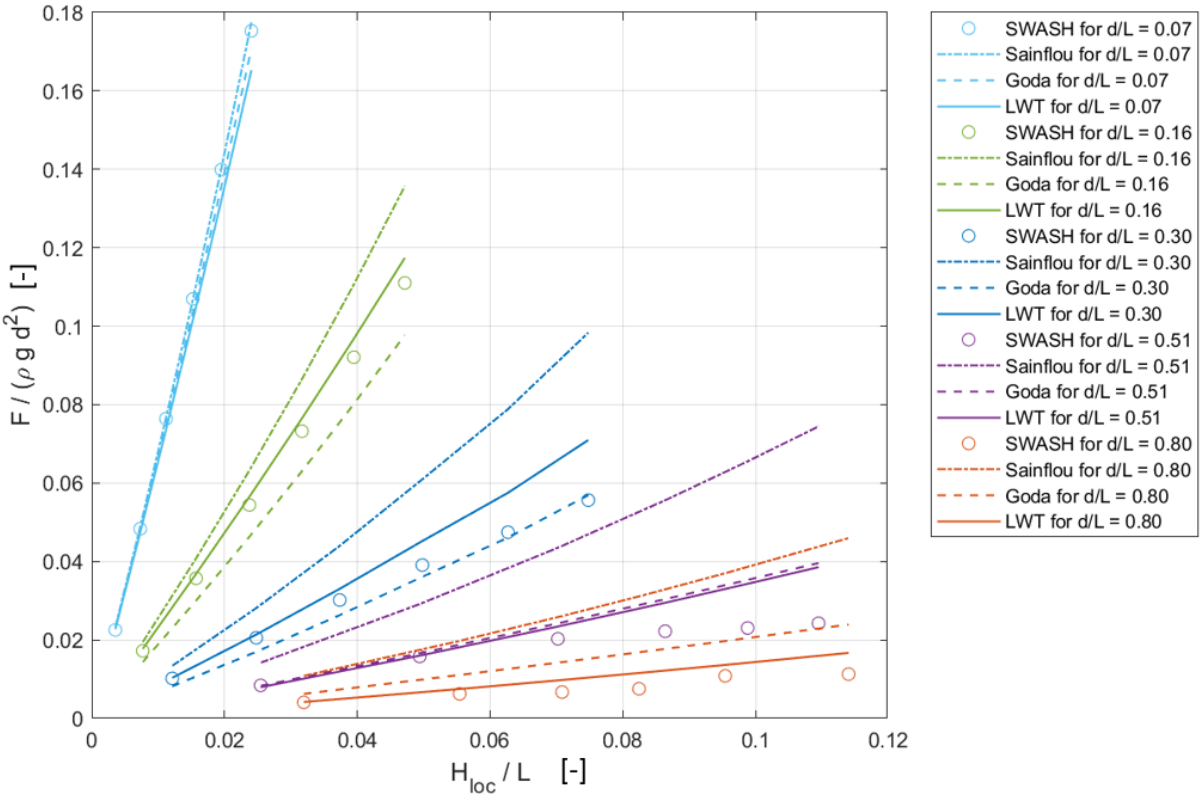


Figure 4.3: Non dimensional horizontal wave force in regular wave fields, plotted for an increasing wave steepness and for various relative depths. Numerical results are indicated by dots and the lines present the solutions by the design formulae.

From the figure, several observations are made:

- The SWASH simulations show a reasonable linear increase of the horizontal wave force for an increasing wave steepness. For very steep waves, the results show a small negative deflection of this linearity.
- In very shallow water, all the design methods give a good correspondence with the SWASH force. This can be explained by the similar shape of the vertical pressure distribution of all the models for long waves in shallow water.
- In relatively deeper water, Sainflou is overestimating the force compared to SWASH to a large amount. Reason for this is the second order pressure at still water level $p_1$ (high compared to Goda and LWT) and the linear distribution between $p_1$ and $p_0$, providing a conservative description of the wave pressure distribution.
- Goda presents an underestimation of the wave force in shallow water ($d/L = 0.16$), a good correspondence for $d/L = 0.3$, and an overestimation of the force in deeper water. The latter could be due to the linear approximation of the pressure distribution below SWL, which may cause a rough estimation for short waves in deep waters.
- The LWT provides for small wave steepness an accurate computation of the wave force. For steeper waves the LWT overestimates the wave force compared to the SWASH simulations.
- It is noticeable that solutions by Goda and the LWT present a different dependency on relative depth $d/L$. Where Goda provides a larger force for deep and shallow waters, the LWT is more conservative for

intermediate water depths. This can be explained by the linear pressure distribution of Goda compared to the LWT.

## 4.2. Uni-modal wave spectrum

### 4.2.1. Increase in mean water level

In an irregular wave field the features of the standing wave profile are only present locally at the wall, as explained in Section 3.1. A regular wave field showed an increase in mean water level under the anti-nodes and a decrease in mean water level under the nodes. For an irregular wave field, a similar deviation in mean water level is expected near the wall. Figure 4.4 gives an example of a simulation in SWASH where the time averaged surface elevation $h_0$ is plotted over the basin length. The formulae of Sainflou is applied with the average wave height. Since the increase in mean water level according to Sainflou is theoretically derived for regular waves, it is expected that the average value gives a better approximation of this derivative of the wave height than the significant value. In addition to the increase in mean water level, also the average wave height $H_{avg}$ is plotted, indicating the local nodes and anti-nodes.

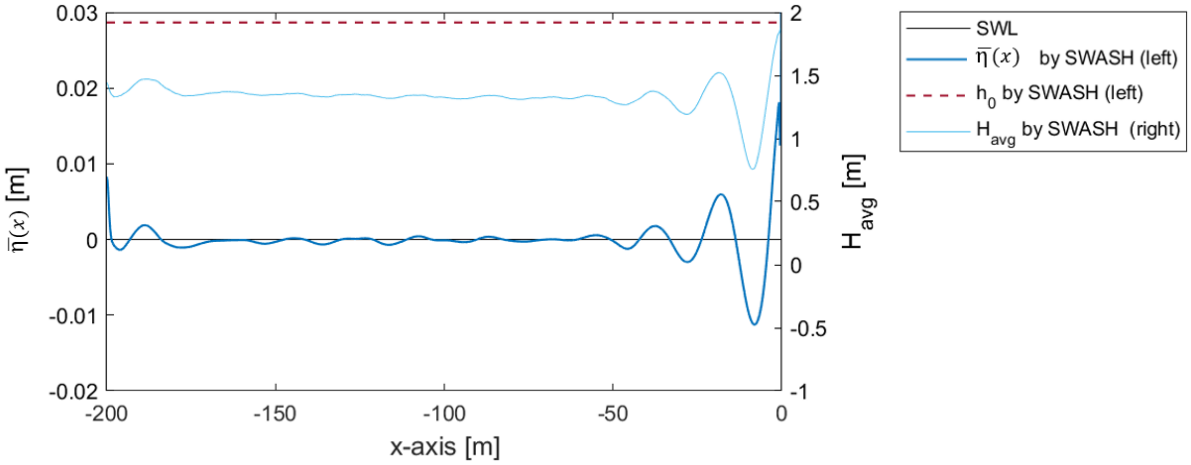


Figure 4.4: Example of the time averaged surface elevation and time averaged wave height over the x-axis for an irregular wave field with $H_{1/3,loc}/L_{1/3} = 0.05$ and $d/L_{1/3} = 0.54$

From the figure it can be seen that for approximately two wave lengths from the wall a standing wave profile is recognized. This profile is however reduced in the direction away from the wall. The Sainflou expression overestimates the increase in mean water level of SWASH. At the wave generating boundary condition also signs of standing wave profile are visible. This can be explained by the fact that the wave maker functions as an anti-node, which was also visible in the regular wave field.

In Figure 4.5, the normalized increase in mean water level $h_0/H_{avg,loc}$ is presented. The SWASH simulations are plotted by dots for various relative depths, indicated by colours. The analytical expression by Sainflou according Leidraad Kunstwerken is plotted with solid lines.

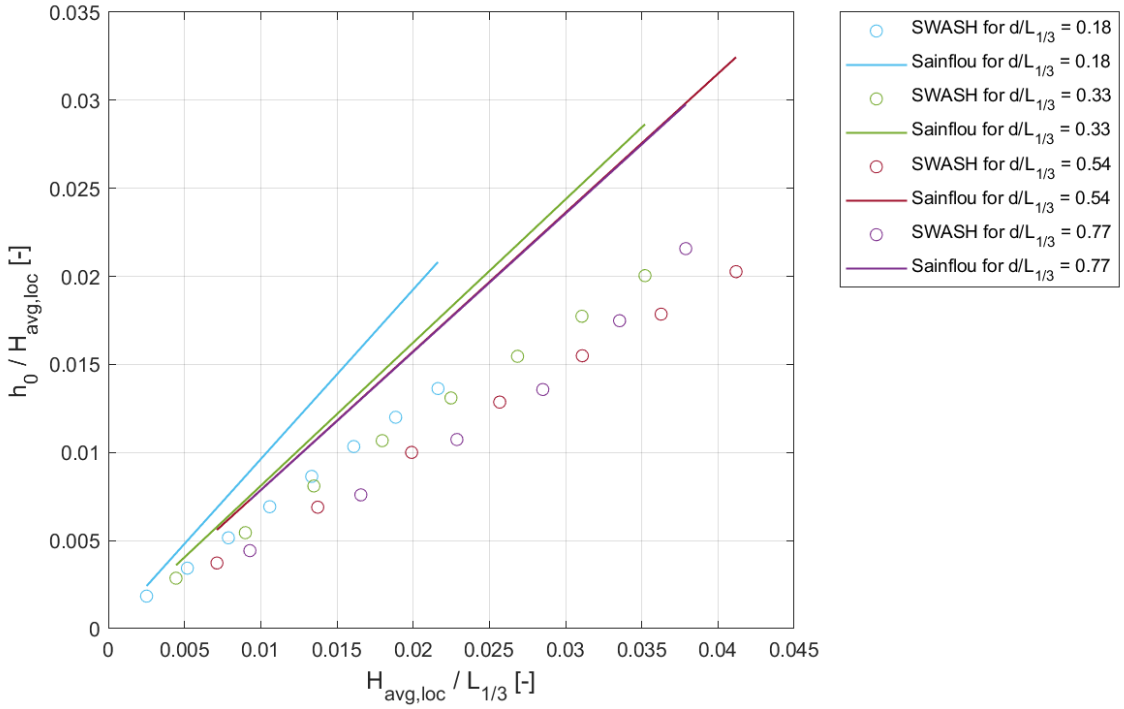


Figure 4.5: Relative increase in mean water level due to irregular waves, plotted for an increasing wave steepness. $h_0$ by Sainflou is estimated with $H_{avg}$

From the figure, it can be noticed that there is indeed an increase of mean water level for an increasing wave steepness $H_{avg,loc}/L_{1/3}$. The magnitude of this increase is smaller than the Sainflou expression. However, compared to a regular wave field, the solution by Sainflou based on the average wave height is closer to the SWASH expression. The same figure can also be made by replacing the average wave height with the significant wave height, see Appendix D. Here, the difference between the Sainflou expression and SWASH is larger.

### 4.2.2. Horizontal wave force

This paragraph compares the characteristic horizontal wave force in an irregular wave field from the various design methods. The characteristics value refers to the value with a probability of exceedance of 0.135 and corresponds with the significant wave height $H_{1/3}$ and significant wave force $F_{1/3}$ [1]. In Figure 4.6, the design guidelines and spectral calculation method are compared with the SWASH results for various uni-modal wave spectra with different wave steepness and relative depth. The design guidelines are applied with $H_{1/3}$ and $T_{1/3}$. On the vertical axis, the $F_{1/3}$ is made non-dimensional by dividing by $(\rho g d^2)$. The wave force is plotted for various relative depths $d/L_{1/3}$ (indicated by the different colours) over the wave steepness $H_{1/3,loc}/L_{1/3}$ on the x-axis. Compared to the results of regular waves, the range concerning wave steepness, based on the statistical values of $H_{1/3}$ and $L_{1/3}$, is smaller.

[1] For the spectral calculation method, $F_{1/3}$ is taken as $F_{m0}$.

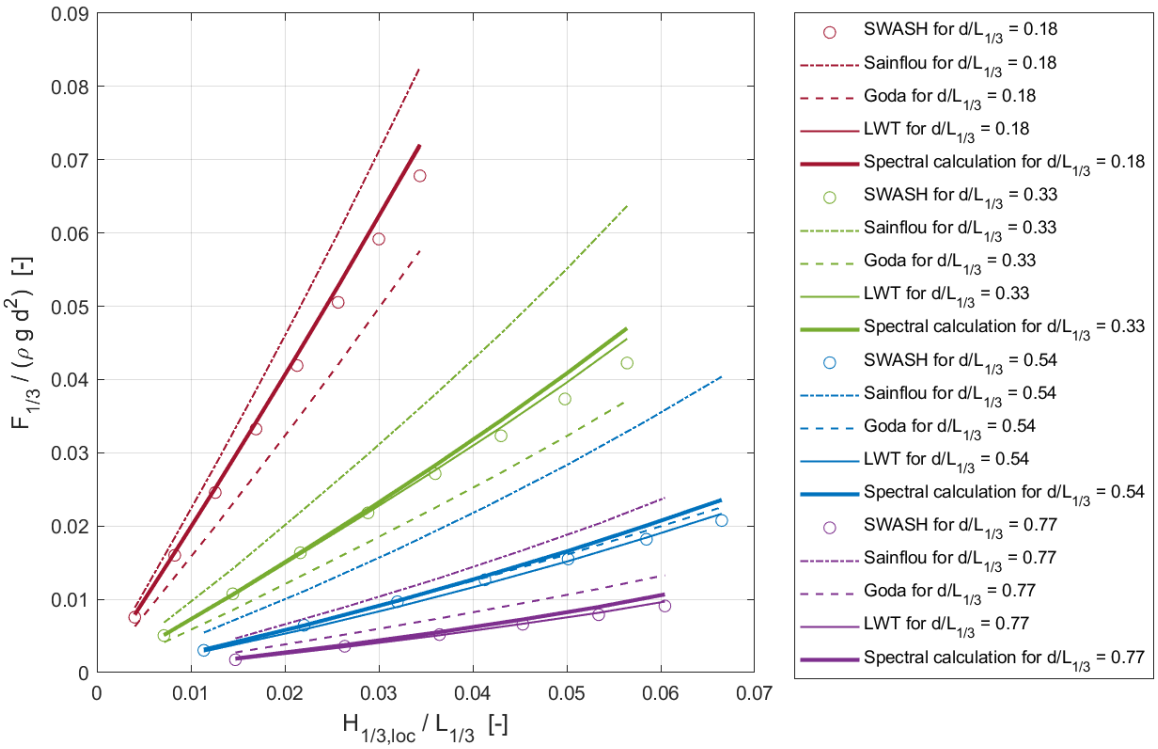


Figure 4.6: Non dimensional significant force $F_{1/3}$ for an increasing wave steepness, plotted for various relative depths. Numerical results are indicated by dots and the continuous lines presents the analytical solutions of design guidelines.

The following observations and accompanying explanations are made:

- The SWASH simulations presents a linear increase in wave force for an increase in wave steepness.
- Sainflou overestimates the force of the SWASH simulations for an increasing wave steepness and an increasing depth up to a value of more than 2. The increase due the wave steepness is explained by the incorporation of $h_0$, which accounts for second order components. The increase due the relative depth is explained by the linear pressure distribution which is a rough simplification of the actual pressure distribution, especially in greater depths.
- Goda underestimates the forces for shallow waters ($d/L_{1/3}$ is 0.18 and $d/L_{1/3}$ = 0.33) by approximately 15%. In deeper waters, Goda gives a overestimation of the force of 5 to 20%. The same observation was made for regular waves. The overestimation of the horizontal wave force in deeper waters is, similar as Sainflou, due to the linear pressure distribution which is a rough simplification for short waves in deep waters.
- The linear wave theory gives a good representation of the force simulated by SWASH, except for steep waves in intermediate water depth where it gives a small overestimation of about 10%.
- The spectral calculation gives similar results as the LWT. The increase in force for greater depths can be explained by the fact that there is more wave variance in the spectral domain located below the design wave frequency used in the LWT ( = $1/T_{1/3}$). This makes spectral method compared to the LWT more sensitive for low frequencies. In deeper waters, these low frequencies weigh relatively heavier than in shallow waters, making the spectral calculation positively biased (= conservative) for an increasing depth.

Where the SWASH results tend to deflect negatively for an increasing steepness compared to the LWT, it would be expected that the SWASH results show an exponentiation increase for wave steepness, since higher order pressure components add to the linear wave pressure. An explanation could be due the out of phase behaviour of the second order components of the wave pressure, as explained in section C.3.4.

## 4.3. Bimodal wave spectrum

This section presents the results for bimodal spectra in three steps. First, a decomposition of a bimodal spectrum is considered to indicate the influence of a swell component. After that, this swell component is varied in peak frequency and variance. The horizontal wave force is examined for different values of relative swell variance $M_{Sw}$ and relative peak frequency $\Phi_{Sw}$. Ultimately, the influence of swell on the characteristic wave force is indicated for a wide range of wave fields.

### 4.3.1. Decomposition of a bimodal wave spectrum

Three simulations in SWASH are carried out by simulating a swell component, a wind sea component and a bimodal spectrum as a sum of these two components. The obtained wave spectra at the wall for each of the simulations are plotted in Figure 4.7. It can be seen that sum of the wave variance of the decomposed parts (swell + wind sea) is approximately equal to the bimodal spectrum.

It stands out that an additional peak is present at 0.38 Hz. It is expected that this peak is created in the SWASH model, since the wave generating boundary condition in SWASH is based on a linear model. Steep waves (= non-linear) are imposed by the sum of a harmonic plus a bounded super-harmonic wave, comparable to the stokes formula in Equation 2.20. These bounded super-harmonic waves have a frequency of two times the size of harmonic wave. The reason why the peak is located at 0.38 Hz and not 0.4 Hz could be the numerical dissipation for high frequencies, see Appendix C.

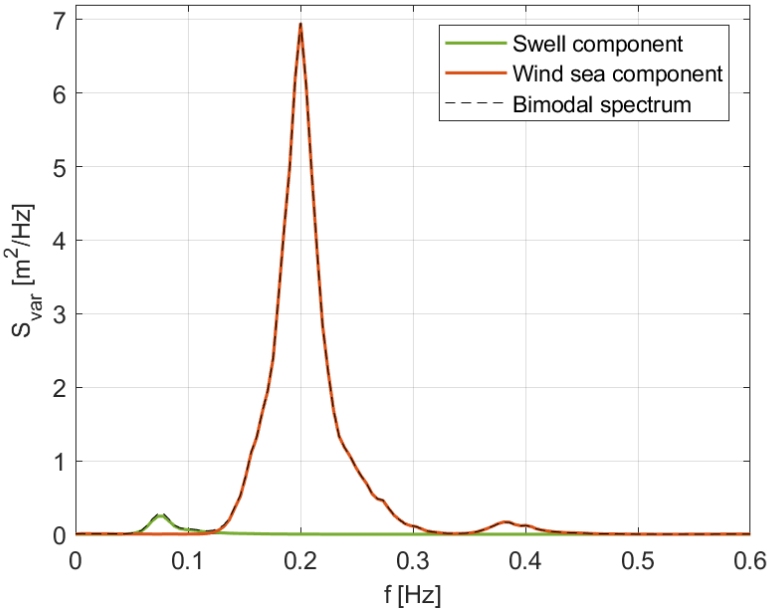


Figure 4.7: Local wave variance for the simulations of a swell component, wind sea component and bimodal spectrum.

It may look trivial that the horizontal wave force of a bimodal spectrum is equal to the sum of the horizontal wave force by the decomposed parts of the spectrum. Therefore, Table 4.1 presents an overview of the results of the three simulations. The first and second column show the characteristics of the quantity under consideration and the corresponding unit. The third and fourth column present the values for the simulated swell and wind component respectively. The column with the header "superposition" applies a linear superposition of the swell and wind sea components. For the spectral moment $m_0$, this implies the sum of the two components which is possible due to the conservation of energy (energy ≡ variance). Since the significant wave height $H_{m0}$ is related to the square root of the variance, superposition is carried out quadratically:

$$H_{m0,sum} = \sqrt{H^2_{m0,swell} + H^2_{m0,wind}} \tag{4.1}$$

With the assumption that the characteristic wave force present in the sea state is linear related to the energy in the wave field, linear superposition on the forces is applied. In the sixth column, the results from the

simulated bimodal spectrum are presented. The last column indicates the relative increase of the bimodal spectrum, with respect to the wind sea spectrum. Design formulae are calculated with $H_{1/3}$ and $T_{1/3}$.

Table 4.1: Characteristics of the wave field of the decomposed bimodal wave spectrum, compared with the values of superposition and the original bimodal spectrum.

| Symbol | Unit | Swell component | Wind sea component | Superposition | Bimodal spectrum | Increase due to swell [%] |
|---|---|---|---|---|---|---|
| $m_0$ | [m$^2$] | 0.008 | 0.334 | 0.342 | 0.343 | 2.1 |
| $m_{-1}$ | [s m$^2$] | 0.099 | 1.664 | - | 1.775 | 6.7 |
| $H_{m_0}$ | [m] | 0.36 | 2.31 | 2.34 | 2.34 | 1.3 |
| $T_p$ | [s] | 12.80 | 5.00 | - | 5.00 | 0 |
| $T_{1/3}$ | [s] | 12.44 | 4.90 | - | 4.94 | 0.8 |
| $T_{m-1,0}$ | [s] | 12.11 | 4.98 | - | 5.17 | 3.8 |
| $F_{1/3,Sainflou}$ | [kN/m] | 32.34 | 144.17 | 176.51 | 146.42 | 1.6 |
| $F_{1/3,Goda}$ | [kN/m] | 27.23 | 81.22 | 108.45 | 82.41 | 1.5 |
| $F_{1/3,LWT}$ | [kN/m] | 30.78 | 78.27 | 109.05 | 79.43 | 1.5 |
| $F_{m_0,Spectral}$ | [kN/m] | 29.31 | 80.97 | 110.28 | 87.15 | 7.8 |
| $F_{1/3,SWASH}$ | [kN/m] | 28.05 | 72.79 | 100.84 | 78.91 | 8.4 |

From the table, the following observations are made:

- Superposition of $H_{m_0}$ and $m_0$ results in the same values as observed in the bimodal spectrum. Hence, the bimodal spectrum gives a good representation of the sum of the swell and wind se component.
- For the simulating the swell component (relative shallow water), all design methods present quite accurate computations. In deeper water, the design methods present overstimations of approximately 10% (Goda, LWT, Spectral calculation) or 100% (Sainflou). These observations are similar to Figure 4.3.
- Superposition of the swell and wind sea component by all design methods results in an overestimation of the design force present in a bimodal wave spectrum. Goda, spectral calculation and SWASH overestimates the force compared to the force calculated for the bimodal spectrum.
- The LWT and Goda gives accurate estimation of the horizontal wave force induced by the bimodal spectrum. The spectral calculation method overestimates with approximately 10% and Sainflou with approximatley 100%.
- Due to swell, the significant horizontal wave force increase by 8.41% while the wave variance $m_0$, significant wave height $H_{m_0}$ and significant wave period $T_{1/3}$ only increase with 2.1%, 1.3% and 0.82% respectively. The spectral wave period increases with 6.7% under the influence of the swell component. This comes close to the increase in horizontal wave force by SWASH. $F_{1/3,Spectral}$ accounts for a similar increase as $F_{1/3,SWASH}$.

Based on these observations it can be concluded that the superposition of the SWASH calculated swell and wind force does not result in the wave force induced by a bimodal spectrum. Neither does this seem to work for the design guidelines, since a rough overestimation of the force is established. However, there is distinct increase due the swell component, as the increase in horizontal wave force is out of proportion with the increase in wave variance. The extend of this increase in force is not clearly indicated by the wave characteristics under consideration.

Goda and the LWT seems to give an accurate estimation of the wave force of the bimodal spectrum. However, it is argued that this is the result of the overestimation of the wind sea component and underestimation of the swell component. The spectral calculation provides a stable (over)estimation of the SWASH force.

### 4.3.2. Influence of swell parameters

Now the influence of a swell component is demonstrated, the influence on the horizontal wave force is quantified for different values of the swell component. Simulations are made with the same wind sea component from Figure 4.7. The swell component is simulated with different peak frequencies and different wave variance. In this way, different values of the relative swell variance $M_{Sw}$ and relative swell peak frequency $\Phi_{Sw}$ are obtained.

In Figure 4.8, the non-dimensional force by the different design methods is plotted over the relative swell variance on the x-axis. Different values for the realtive peak frequency are indicated by the different colors. Similar to the comparison of the horizontal wave force, the SWASH results are indicated by dots and the analytical solution by the solid and dashed lines.

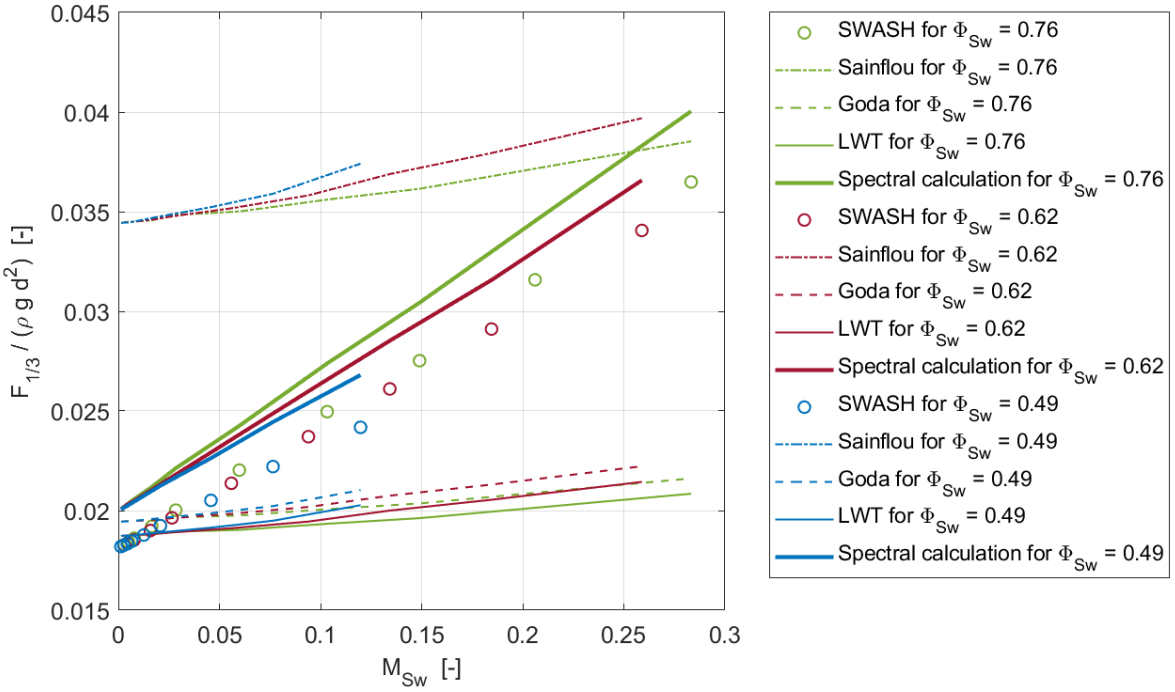


Figure 4.8: Increase in Relative characteristic force of spectral calculation method and Goda formula relative to the SWASH model for an increasing swell component. Goda is applied with with input parameters $H_{1/3}$ and $T_{m-1,0}$

The wind sea component (result for $M_{Sw} = 0$) is classified with a wave steepness $H_{1/3,loc}/L_{1/3}$ of 0.058 and a relative depth $d/L_{1/3}$ of 0.51. As the swell component increases, the values of $T_{1/3}$ and $H_{1/3}$ are increasing as well, leading to a decrease in wave steepness (increase in $L$ is dominant over increase in $H$) and a decrease in relative depth.For the simulation without swell ($M_{Sw} = 0$) the relation between the design methods can be recognized from Figure 4.6.

From the figure, the following observations are made:

- The horizontal wave force by SWASH increases considerably due to the swell component. With the addition of 15% swell, the force increases 50%. For 30% of swell, the horizontal wave force is expected to be doubled.
- The relative swell variance $M_{Sw}$ is for the ranges under consideration more influential than the different values of the relative swell peak frequency $\Phi_{Sw}$.
- The design formulae of Sainflou, Goda and the LWT show an increase of approximately 5% with the addition of 15% swell. This can be explained due to the small increase of the wave input characteristics $H_{1/3}$ and $T_{1/3}$.
- The spectral calculation gives for both the relative swell variance and the relative swell peak frequency an accurate increase in wave force.
- For this example, the LWT and Goda formula underestimate the SWASH force after about 2.5% of swell. The formula of Sainflou remains conservative but decreases significantly in the overestimation for large values of $M_{Sw}$.

The force estimation from the design methods presented in Figure 4.8 can be taken relative to the SWASH force. This is done the spectral calculation method and one of the design formulae (Goda). Figure 4.9 presents the relative force for different values of the relative swell parameters. From the figure is clearly visible that the

spectral calculation method gives a constant overestimation of the wave force, independent of the relative swell parameters. The formula of Goda shows an abrupt change from overestimation to underestimation under the influence of swell.

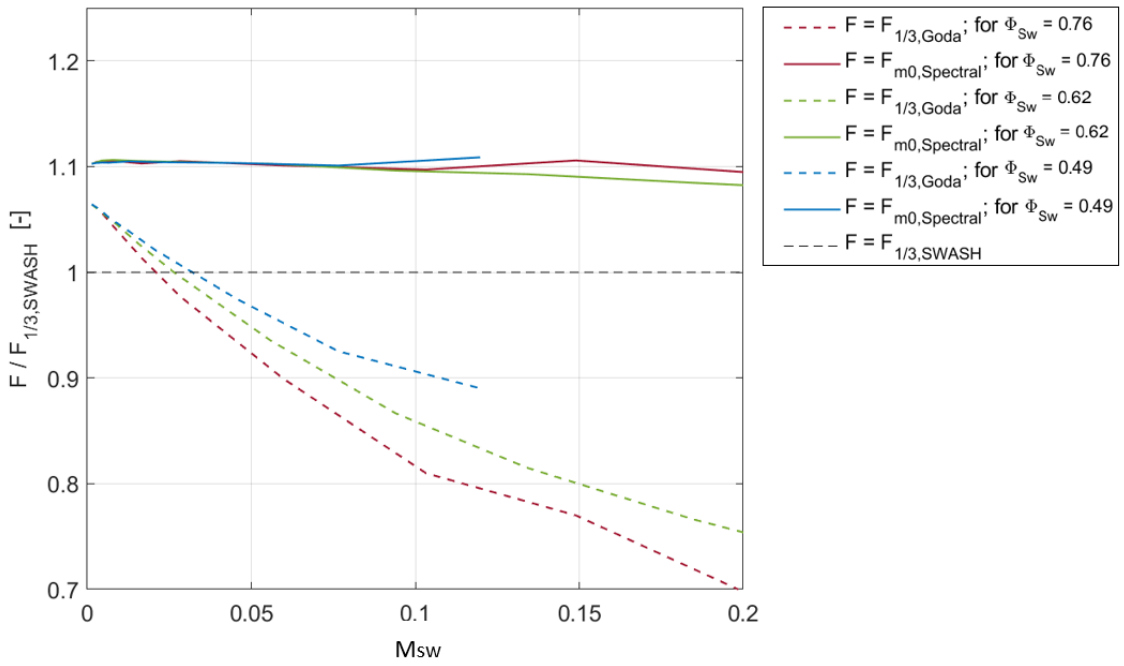


Figure 4.9: Relative force of the spectral calculation method and Goda for different bimodal wave spectra (linear interpolated). Goda is applied with $H_{1/3}$ and $T_{1/3}$

In Appendix D, additional plots are made where different design wave periods are used such as $T_p$ and $T_{m-1,0}$. From here, it can be seen that also for these input parameters the formula of Goda underestimates the influence of the swell.

### 4.3.3. Relative bimodal horizontal wave force

Up to now, the influence of a swell component is quantified for one sea state. This paragraph addresses the influence of the relative swell parameter $M_{Sw}$ for different sea states. Due to the small influence of the relative peak frequency $\Phi_{Sw}$, this parameter is kept constant ($\Phi_{Sw}$ = 0.6) throughout the following simulations.

This paragraph differs from previous paragraph that the bimodal wave spectra simulated are based on an inclusion of the swell component, rather than the addition of swell component. It was already observed that as the swell component increases, the values of $T_{1/3}$ and $H_{1/3}$ are increasing as well, leading to a decrease in wave steepness (increase in $L$ is dominant over increase in $H$) and a decrease in relative depth. Here, it is aimed that the inclusion of a swell component is not influencing the relative depth and wave steepness. Appendix C.3 elaborates on the method of simulating bimodal wave spectra for constant non-dimensional wave parameters.

Since it was already seen that the design formulae do not take account the swell component accurately, only the spectral calculation method is compared with the SWASH results. Furthermore, a new parameter is introduced to define the relative increase in force for a bimodal wave spectrum:

$$\Delta F_{bi,1/3} = \frac{F_{bi,1/3} - F_{uni,1/3}}{F_{uni,1/3}} \tag{4.2}$$

In Figure 4.10, $\Delta F_{bi,1/3}$ is plotted for an increasing relative swell variance $M_{Sw}$ for different sea states. The sea states of the simulations vary in wave steepness $H_{loc,1/3}/L_{1/3}$ indicated by the markers (dots, triangles, squares), and relative depth $d/L_{1/3}$ indicated by the type of colour. The force estimation by SWASH (markers) is compared with the force estimation by the spectral calculation method (lines).

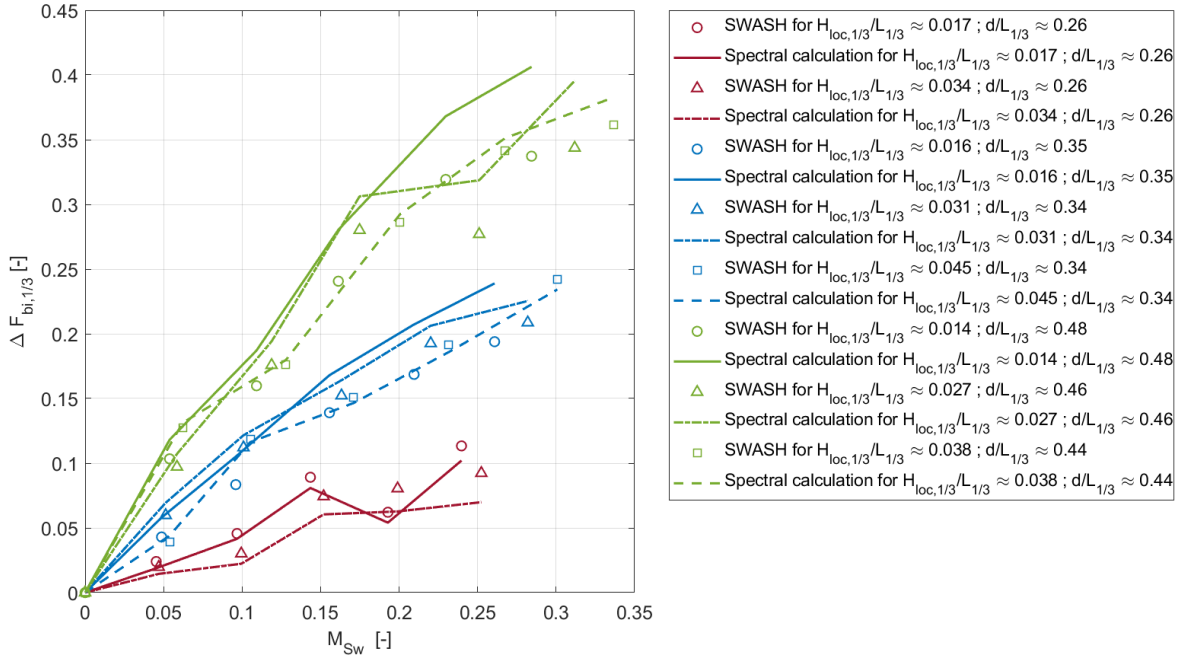


Figure 4.10: Relative increase in force for a bimodal spectra, indicated for different relative swell variance, wave steepness and relative depth.

From the figure the following observations are made:

- The SWASH results show an increase in $\Delta F_{bi,1/3}$, for an increasing $M_{Sw}$, as expected from the previous paragraph.
- $\Delta F_{bi,1/3}$ shows a strong correlation with relative depth $d/L_{1/3}$ and no clear correlation with wave steepness $H_{loc,1/3}/L_{1/3}$.
- The spectral calculation method gives roughly an accurate estimation for different values of relative depth and wave steepness. However, the spectral calculation method is presenting an overestimation of up to 15% in deeper water an underestimation of about 20% in shallow water.

## 4.4. Probability distribution

This section validates the probability distribution of the wave heights and force peaks in irregular wave fields. As explained in Section 3.3, first a comparison is made between a uni-modal and bimodal spectrum with a large swell component. From this example is derived what the potential influence of a swell component on the probability distribution is. After that, the deviation of the force peaks from the Rayleigh distribution is quantified for a broader range of wave fields for different amounts of swell.

### 4.4.1. Comparison between uni-modal and bimodal spectrum

The observed wave spectra for the uni-modal and bimodal spectrum under consideration are plotted in Figure 3.7. This figure represents the observed wave variance at the wall, for a 10 hour simulation time. Both simulations include similar parameters for the wave steepness and relative depth. With the simulation length of this time series a good judgement can be made up to a probability of exceedance of approximately 0.5%.

#### Uni-modal spectrum

For the uni-modal spectrum, > 6500 waves heights and > 6000 peaks force peaks were observed with a time domain analysis[2]. The wave steepness was $H_{1/3,loc}/L_{1/3}$ = 0.034 and relative depth $d/L_{1/3}$ = 0.395. Figure 4.11 plots the wave heights normalized by the significant wave height (= $H/H_{1/3}$) with blue dots and the force peaks normalized by the significant force peak (= $F/F_{1/3}$) with red crosses. The values of $H/H_{1/3}$ and $F/F_{1/3}$

[2]Not every wave height is related to a force peak.

are indicated on the x-axis. The corresponding probability of exceedance is located on the vertical axis. The theoretical Rayleigh distribution is plotted with a solid black line.

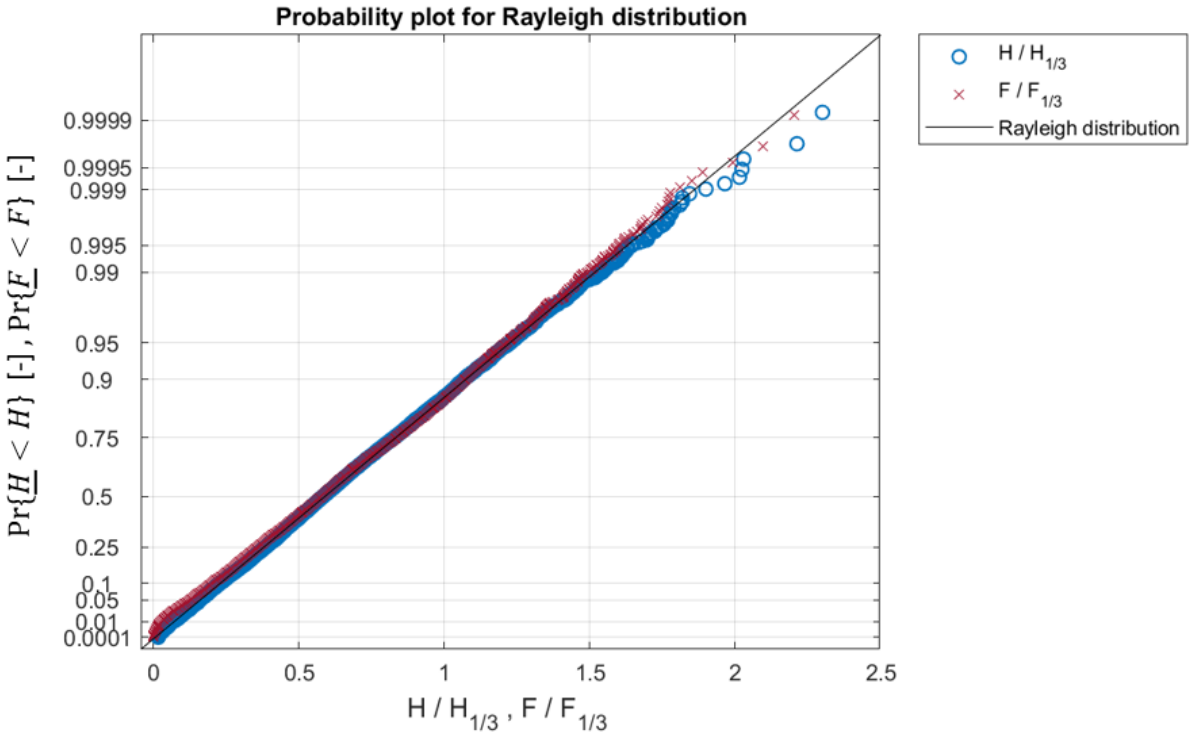


Figure 4.11: Probability plot (Rayleigh) of the normalized wave heights and normalized force peaks for a simulation in SWASH. $H_{1/3,loc}/L_{1/3} = 0.034$ , $d/L_{1/3} = 0.395$, $M_{Sw} = 0$, $\Phi_{Sw} = 0$.

It is observed that the normalized wave heights and normalized force peaks give both a good approximation of the theoretical Rayleigh distribution. Practically, this means that $H_d/H_{1/3} \approx F_d/F_{1/3}$. Hence, the ratio $F_d : H_d$ remains constant over the probability domain and the Rayleigh distribution is applicable for any design level.

**Bimodal spectrum**

The 10 hour simulation with the bimodal spectrum includes > 6500 waves and > 4000 force peaks. The sea state under consideration has a wave steepness of $H_{1/3,loc}/L_{1/3} = 0.03$ and a relative depth of $d/L_{1/3} = 0.363$. These parameters are comparable to the sea state of the previously discussed uni-modal spectrum. The relative swell parameters are $M_{Sw} = 0.27$ and $\Phi_{Sw} = 0.756$. Figure 4.12 plots the distribution of the normalized wave heights and the normalized force peaks. In addition, the Rayleigh distribution is indicated as a reference.

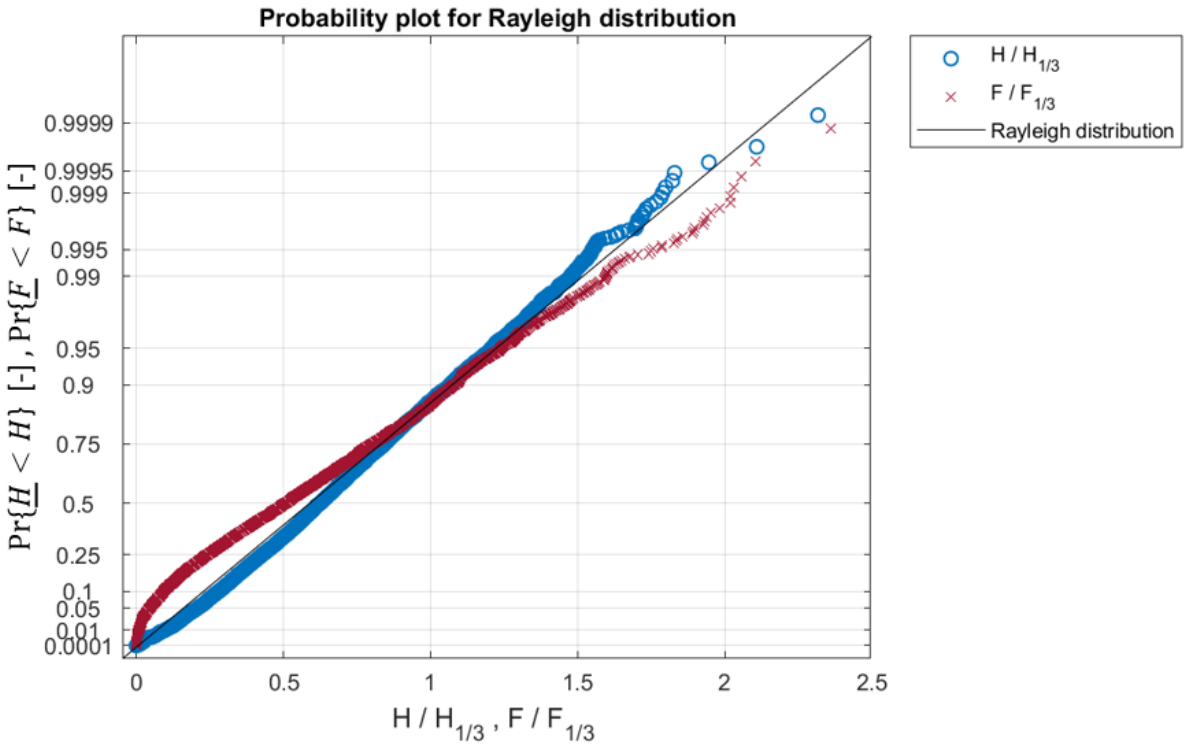


Figure 4.12: Probability plot (Rayleigh) of the normalized wave heights and normalized force peaks for a simulation in SWASH. $H_{1/3,loc}/L_{1/3} = 0.030$, $d/L_{1/3} = 0.36.$, $M_{Sw} = 0.27$, $\Phi_{Sw} = 0.76$.

Compared to the probability distribution that was observed for the simulation with a uni-modal spectrum, the bimodal spectrum shows less agreement with the Rayleigh distribution. The normalized wave heights present for higher safety levels (> 0.865) somewhat lower values compared to the Rayleigh distribution. On the other hand, the normalized force peaks show for higher safety levels (> 0.865) higher values compared to the Rayleigh distribution.

A physical explanation for the deviation of force peaks from the Rayleigh distribution could be as follows. Due to the larger range of wave variance in the frequency domain, the wave periods in the wave field are expected to be scattered more as well. Therefore, relative small wave periods in a uni-modal spectrum are smaller in a bimodal spectrum Similarly, the larger wave periods are a unimodal spectrum are even larger in a bimodal spectrum. From the wave theory it is known that larger wave periods contribute to a larger force on the wall. Consequently, for a bimodal spectrum small forces are smaller and large forces are larger compared to the force peaks in a uni-modal spectrum. This is what can be interpreted from the figure as well.

This deviation from the Rayleigh distribution has the following consequences to the design. When a design force is estimated on the Rayleigh distribution, for example $F_d = 1.5\ F_{1/3}$, it can be seen that the actual force that occurs in the wave field with this probability is $1.6\ F_{1/3}$. The other way around is the 1% probability of exceedance of the design force $F_d = 1.5\ F_{1/3}$ related to a lower probability of exceedcance in the SWASH model ($\approx 2\%$).

### 4.4.2. Deviation from the Rayleigh distribution

The previous paragraph showed an example of a bimodal spectrum which resulted in a wave field with force peaks that deviated from the Rayleigh distribution. This paragraph quantifies this deviation for different shapes of bimodal spectra and indicates the influence on the design factor $\gamma_d$. The design factor $\gamma_d$ was already obtained from Equation 2.27 for wave heights, but can also be derived for the force probability by:

$$\gamma_d = \frac{F_d}{F_{1/3}} = \sqrt{\frac{\ln(1 - \Pr\{\underline{F} < F\})}{-2}} \tag{4.3}$$

A similar expression of a design factor can be made for each observation of a force peak in SWASH, defined by:

$$\gamma_{SWASH} = \frac{F_{SWASH}}{F_{1/3}} \tag{4.4}$$

where $F_{SWASH}$ refers to the statistical values of the forces (e.g. $F_{5\%}$ or $F_{1\%}$). With these two design factors, the deviation from the Rayleigh distribution that is observed by SWASH can be quantified with the expression:

$$\Delta Ray = \frac{\gamma_{SWASH}}{\gamma_d} \tag{4.5}$$

Positive values of $\Delta Ray$ indicate that the Rayleigh distribution is underestimating the SWASH results. For the example of the bimodal spectrum from Figure 4.12, the deviation from the Rayleigh distribution $\Delta Ray$ is plotted in Figure D.4 for the upper part of the probability range. Because of the high variance for the extreme values, the data is smoothed to obtain a the trend of the deviation from the Rayleigh distribution [3].

Figure 4.13: Deviation from the Rayleigh distribution for a probability range between 0.9 and 1. In the probability range under consideration 407 force peaks are present.

From the figure, it can be seen that for values higher than 0.99, the simulated values start to show a larger scatter around the smoothed line. For the design level 1 % $\Delta Ray_{1\%} = 0.06$. For the design level of $\Delta Ray_{0.1\%} = 0.09$.

The same methodology is applied for a range of bimodal spectra with different wave steepness and relative depth, similar to the spectra presented in Section 4.3. Figure 4.14 presents the obtained values for $\Delta Ray_{0.1\%}$. for the different wave conditions (wave steepness and relative depth) with different values of relative swell variance.

[3] This MATLAB operation that applies smoothing of a dataset is described in Appendix C.6.

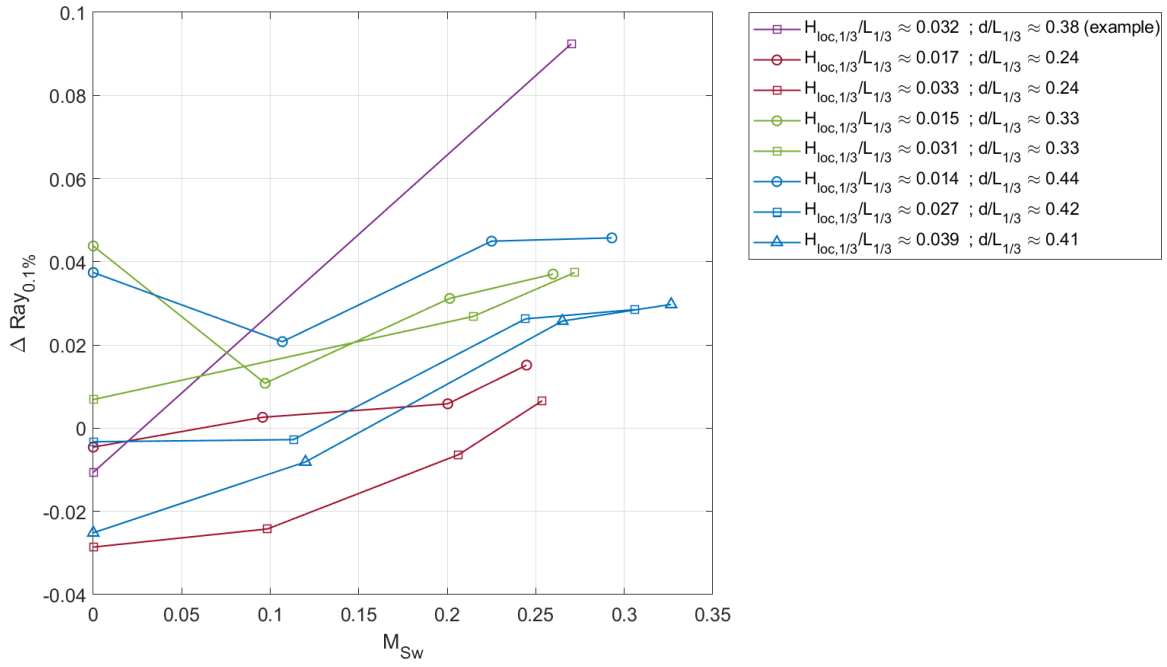


Figure 4.14: Relative deviation from the Rayleigh distribution for a probability of exceedance of 0.1%, determinied for various uni-modal and bimodal wave spectra.

The following observations are made:

- In the absence of swell ($M_{Sw} = 0$), the different wave fields are scatters over a deviation between -0.03 and 0.04.
- The two simulations introduced in the previous paragraph show a clear increase in $\Delta Ray_{0.1\%}$ of about 0.1.
- The influence of the wave steepness and relative depth on the deviation from the Rayleigh distribution is not present.
- A small influence of the relative swell variance on $\Delta Ray_{0.1\%}$ can be recognized between $M_{Sw} = 0.1$ and $M_{Sw} = 0.2$. Overall, the influence of the $M_{Sw}$ on $\Delta Ray_{0.1\%}$ is smaller than 0.05.
- In Appendix D, similar the results are plotted for $\Delta Ray_{5\%}$, $\Delta Ray_{2\%}$, $\Delta Ray_{1\%}$ and $\Delta Ray_{0.5\%}$. From here, similar observations are made.

# 5

# Discussion

This chapter presents a discussion in which is speculated about several topics of this study. Section 5.1 treats the limitations of the study concerning the applied approach, the scope and the used models. In the next section, Section 5.2, several new insights are discussed which were observed during this study.

## 5.1. Limitations of the study

First, considerations due to the applied approach are presented. Subsequently, several simplification of the scope are discussed. Lastly, some used models are addressed. For all topics, the relation to the interpretation of results is argued.

**Approach**

In the approach that is applied, the design methods are divided into design steps. Each design step is considered for various wave conditions. Therefore, the results present only the accuracy of a particular design step and not the accuracy of the complete design method. The advantage of this approach is that the accuracy of each design step is observed and that the origin of inaccuracy can be determined precisely. However, the total effect of the design guidelines is not verified for SWASH. For example, an overestimation of the individual wave force by Sainflou (design step 2) in combination with disregarding the swell component in a bimodal wave spectrum (design step 4) could in practice still lead to a safe design force with respect to SWASH. It can therefore not be concluded that the design guidelines are not safe. However, it is correct to conclude that the design process in such a case is inaccurate and may lead to underestimation.

**Occurrence of wave conditions**

The simulated wave spectra in this thesis are manually generated, based on the starting point of the IJmuiden case. After varying different aspects such as wave steepness, relative depth and relative swell parameters, the spectra were not validated with realistic scenarios. The small swell component from the IJmuiden case (1.5% swell) was intensified up to nearly 30% swell in the simulated spectra, covering a wide range of bimodal spectra. Apart from that, already interesting results were observed for swell contributions in the same order that was seen in the IJmuiden case. With the assumption that the boundary conditions of the IJmuiden case are not extremely rare, the relevance of the results is considerable.

**Impact on strength and stability**

Throughout this research, the only output analysed was the horizontal wave force $F_h$. The horizontal wave force is an important input parameter for the overall stability, such as sliding in case of quay walls (USACE, 2002). Reason for this particular output parameter was the large relation with an additional swell component. Other output parameters such as the moment around the bottom were not analysed (overturning failure mechanism). The point of exertion for swell waves is approximately in the middle of the vertical wall ($z = -\frac{1}{2}d$), where the shorter wind sea waves exert with a longer arm, viewed from the bottom. Therefore, the impact of swell waves on the overturning moment would be less big than the absolute force. After demonstrating the large influence of swell on the horizontal wave force $F_h$, the effect on the overturning moment might be worth investigating as well.

**Other geometries**
This thesis treats a rather general case of a perfectly flat bottom without the presence of rubble ballast or berm. In the consideration of coastal structures in practise, it is however very likely that the bottom is sloped from deep water offshore to shallow waters at the shoreline. For such geometries, wave shoaling may occur, which increases the wave steepness. This shoaling effect might apply earlier to the swell component (as large wave lengths "feel" the bottom earlier) than to the wind sea component. Therefore, the effect of incoming bimodal spectra over sloped foreshores might be interesting as well.

Besides a sloping bottom, coastal structures are often constructed on a rubble ballast or berm (see formulae by Goda). Reason for this could be to provide a robust foundation of the vertical structure on the seabed, a cost reduction of the vertical structure or to induce wave breaking and avoid the impact force on the particular structure Oumeraci et al. (1999). As soon as other type than non-breaking wave loads are present, the influence of a swell component might be less dominant than for strictly non-breaking waves.

**SWASH**
In the optimization of the grid discretization of SWASH, a limit was observed for simulating high frequency waves (> 0.3 Hz). Also, it was seen that super-harmonics occurred for steep waves, both in the surface elevation as the pressure distribution. The question rises if both of these super-harmonics are also subjected to the numerical dissipation of high frequency waves. If this would be the case, the representation of steep waves could be inaccurate.

An other limitation of the SWASH model is the disability of simulating white-capping[1]. It is unclear till what extend this type of breaking waves affects the load on the wall. A first train of though is that white-capping in a standing wave basin is not inducing excessive forces on the wall. This is because white-capping in a standing wave basin it is likely to be induced by both incoming and reflected waves, both waves propagating in opposite direction. Furthermore, the orbital motion of wave particles in a regular standing wave field in an antinode (where the waves are the most steep) is vertically directed. This might prevent waves from collapsing horizontally on the vertical wall.

**Rayleigh distribution**
The Rayleigh distribution is used for the extrapolation from a characteristic wave height to a design wave height within storm conditions. The assumption of Rayleigh distributed waves is however based on stationary storm conditions, deep water conditions and irregular waves from a narrow wave spectrum. Most of these assumptions were satisfied in the simulations carried out. In the scenario where the uni-modal spectrum was replaced by the excessive bimodal spectrum (not narrow), a small deviation from the Rayleigh distribution appeared.

Before concluding that the Rayleigh distribution is approached by wave heights and force peaks, it should be kept in mind that the conditions fell within the validity of the Rayleigh distribution: SWASH simulates in stationary conditions, the water depth was intermediate to deep and most spectra were narrow. A real sea storm is never stationary and in shallow water conditions the probability distribution may deviate (Battjes and Groenendijk, 2000).

**Vertical wall and quasi-static load**
The vertical wall is modelled in SWASH with a water point with a porosity of 0.1. Alternatives for the simulation of a reflective wall in SWASH are possible, however resulted rapidly in numerical instabilities. The porous layer shows visually a good approximation of a rigid wall, as a clear standing wave profile and less penetrating wave energy (in the form of wave variance) is visible. However, simulation of an impermeable wall by decreasing the porosity remains questionable.

The vertical wall is modelled as 100 % rigid on the horizontal axis, due the fixed location of the grid points on the x-axis. In practise however, a vertical structure will always show some response to the load. This could affect the actual load on the wall. In case of a movable structure such as a lock gate or movable storm surge barrier, this response may be more significant and cause dynamic responses. For that reason, it is important

[1] Not to be confused with depth induced wave breaking which is accounted for in SWASH (Smit et al., 2013).

to be aware that this study assumes a quasi-static load, which may not be the governing load.

## 5.2. New insights

This section discusses new insights that were obtained during the process of this study. First, it considers some key elements of the approach. After that, several interesting observations in the results are addressed in more detail. Ultimately, some comments are made on the practical implications of the results.

**Design formulae as function of local wave characteristics**
The design formulae are rewritten as a function of the local wave conditions. By doing this, inaccuracies in deriving the coefficient of reflection are bypassed. This is especially of interest, since design guidelines assume inherently 100% reflection. In case of partial reflection, the design guidelines do not overestimate the wave conditions. The reflection coefficient does not to be determined (saving computation time) and potential miscalculations are prevented.

**Probability distribution based on force peaks**
Leidraad Kunstwerken mentions that the application of a design factor can be based on the Rayleigh distribution, with the assumption that wave heights are Rayleigh distributed. However, instead of the probability of exceedance of a design wave height, more interest goes out to the probability of exceedance of a design wave force. Therefore, this study treats a few additional steps rather than simply analysing the distribution of wave heights.

For example, it was seen that the individual wave force increased proportionally with the wave steepness ($H \equiv F$). So if simply the design wave height may be determined with a design factor to come to a design force, it is inherently assumed that $H_d : H_{1/3} = F_d : F_{1/3}$. Thereby, indirectly also the distribution of force peaks is assumed. Therefore, more important than the distribution of wave heights is the distribution of force peaks.

**Superposition of horizontal wave force**
In the elaboration of the spectral calculation method, the wave variance $m_0$ was linearly transferred to the wave force variance $m_{0,F}$. This linear relation can be combined with the theory of quadratic superposition of wave heights. The hypothesis thereby becomes that the quadratic superposition of characteristic wave force is valid as well. A proof of the derivation and an example is given in Appendix E. This type of superposition is not applied in this study as one of the design methods.

If this approach gives accurate results, it could be a quick approach when the significant wave heights and peak periods of the swell and wind sea components are given. However, it should be noted that it is still a simplification of the spectral calculation method. If a complete wave spectrum is given, the determination of the significant wave height of the swell and wind sea do need spectral processing (the wave variance need to be cut in two parts and the wave heights must be estimated separately). In such a case it is questionable if the superpostition method is more efficient.

**Increase in mean water level**
Theories about the increase in mean water level for a standing wave profile were amongst others given by Sainflou (1928) and Miche (1953). These theories considered the local increase in mean sea level at the anti-node near the wall. In circulating design figures of the Sainflou formula, this increase is indicated as a constant value over the length of the basin. This might result in the interpretation of an increase in mean water level due to energy loss in the system, as it is known from coastal processes for sloped beaches (Bosboom and Stive, 2015). For example, (Vrijburcht, 2000, p. 11-32) mentions that the average level of the waves with respect to original average increases due the concentration of energy near the wall.

Penny and Price (1952) gave an expression of the deviation of mean water level over the horizontal axis. SWASH results confirmed such a deviation of mean water level over the x-axis: an increase in mean water level was present at the anti-nodes and a decrease at the location of nodes. The definition "deviation in mean water level" is therefore more appropriate than "increase in mean water level" . The magnitude of the local increase in mean water level appeared to be lower than the Sainflou expression of $h_0$. A good correlation with

the Sainflou expression is found when the local increase in mean water level would be defined as the difference between the mean water level at a node and anti-node.

This report extents the analysis on the increase in mean sea level from from regular waves to an irregular wave field. As described in Klopman and Van der Meer (1999) and visualized in Figure 3.2b, the irregular wave field can be seen as a sum of standing wave profiles of regular waves. This results in a locally standing wave field at the wall, but a grassy profile (not visible) of nodes and anti-nodes further from the wall. Based on this, it is expected that a deviation in mean water level is locally present in an irregular wave field. This hypothesis was confirmed by the SWASH model, since a clear deviation in mean water level was present, corresponding with the locations of the nodes and anti-nodes. The magnitude of the deviation in mean water level was depended on the statistical value of $H$ that was applied in the Sainflou formula. The input of $H_{1/3}$ and $H_{avg}$ did not result in the same results as was seen for regular waves.

**Double peaked pressure spectrum**
In the analysis of the individual wave force, several unexpected observations were made. Studies by Gurhan and Unsalan (2005) concluded an underestimation of the pressure at SWL by the linear wave theory for steep waves. However, the observed results for the total horizontal force $F_h$ do not correspond with this trend. Reason for this could be the overestimation of the individual wave force by the linear theory.

Nagai (1969), Fenton (1985) and Teo (2003) describe double peak phase behaviour in the pressure distribution for standing waves. Also a double peaked shape is visible in various plots of the wave force over a wave phase, such as Figure B.1a. Also in (Takahashi, 2002, p. 39) it was also seen that the offshore oriented pressure (in case of a wave trough at the wall) is larger than the structure oriented wave force. In Appendix C, an elaboration is made on the double peaked pressure spectrum in SWASH. The observations in SWASH support these descriptions from the literature. Thereby, it is also argued how these effects results in an overestimation of the LWT.

**Deviation from Rayleigh distribution**
The results of the analysis on an excessive bimodal spectrum showed a deviating distribution of force peaks, whereas wave heights were Rayleigh distributed. This gave the insight that even if wave heights in a wave field are Rayleigh distributed, force peaks might deviate from this. It is expected that the deviation might be even larger in case of deeper water and wave peaks that are more away from each other (larger $\Phi_{Sw}$).

**Practical implications**
One of the main observations in this study was the large influence of a small swell component on the horizontal wave force in deep water. The relative increase in force was plotted over the relative swell parameters. It should be noted that the quantification of the swell component by the relative swell parameters is a result of a spectral analysis. With the determination of wave characteristics based on a time domain analysis, a potential swell component stays completely unnoticed.

Proper understanding of the relation between the wave spectrum and the wave induced force is of great importance. Neglecting a nearly unnoticed swell component in a bimodal spectrum could lead to large underestimations of the wave force by the use of traditional formulae. In coastal areas that are vulnerable for larger relative swell components (still smaller compared to wind sea component), larger deviations between design guidelines and the SWASH model are expected. On the other hand, as soon as the swell component reaches an overruling amount of wave variance compared to the wind component, the design wave period $T_p$ adjust for this in the application of the design formula.

# 6

# Conclusions and recommendations

In this study, three types of design methods for non-breaking wave loads are compared. The design methods under consideration are the numerical model SWASH, a spectral calculation method and design formulae (Sainflou, Goda and the linear wave theory). Different type of wave conditions are simulated, such as regular waves, irregular waves from a uni-modal wave spectrum and irregular waves from a bimodal wave spectrum. Both the characteristic values as the design values are addressed. The application of design formulae and spectral method is decomposed into design steps and each step is verified by the SWASH model.

This chapter presents the conclusions and recommendations of this study. First, Section 6.1 presents a short summary of the results in relation to the design steps which were defined in the introduction. After that, the conclusions are formulated in Section 6.2 by answering the three main research questions of this study. Section 6.3 is subsequently providing an advise for the use of different design methods. This section fulfils the research objective by validating and improving the design guidelines of Leidraad Kunstwerken. Ultimately, Section 6.4 gives recommendations for further research.

## 6.1. Review on design steps

Based on the validation of the SWASH model and the observed results, the following comments can be made on the design steps (see also Figure 1.3):

1. **Validation of the SWASH model**
   Before the SWASH model was validated by measurement data, the grid discretisation was optimised. The vertical grid was discretised with 6 layers, and showed no effect of inaccuracies. The horizontal grid was defined with a grid step of 0.25 m. Thereby, the high frequency waves (> 0.3 Hz) showed numerical dissipation and limited the usable frequency range. With a fixed bottom of z = -20 m, this also induced limitations to the relative depth of the wave fields.

   The SWASH model was validated by the physical experiment from Gurhan and Unsalan (2005) and compared the SWL pressure at a relative depth of 0.12 for local wave steepness from 0.04 to 0.09. In this range, the SWASH model showed an underestimation of the experiment of about 15%. However, the increase in wave pressure due to the wave steepness was in correspondence with the experiment. It seemed that the reproduction of the experiment caused a consistent underestimation. From here it is concluded that the SWASH is useful for the relative force calculation between different sea states, but should be validated more accurately for a wider range of wave steepness and relative depth to verify the absolute values of the output.

2. **Estimation of the individual wave force (Design formulae)**
   By simulating regular waves, the individual wave force approximations of Sainflou, Goda and the LWT were validated. In very shallow water ($d/L < 0.1$), all design methods approached the SWASH results. For intermediate and deep waters Sainflou showed an overestimation up to a factor 2. Goda presented a small underestimation of approximately 10% for intermediate depth, but was accurate for deep water. The LWT showed to be accurate for all simulated regular wave fields.

In case of uni-modal wave spectra, the significant wave height and significant wave period were applied as input parameters for the design formulae. For the range of irregular wave fields that was overlapping with the range of regular waves, the results were in correspondence. From here, it is concluded that the significant wave force determined by design formulae is a representable estimation of the characteristic wave force present in a wave field described by uni-modal spectra.

In case of a bimodal spectrum, the characteristic wave force by SWASH was sensitive for the presence of swell, for constant wave characteristics. This caused in an underestimation of design formulae which is the result of the simplification of the wave spectrum by wave characteristics (described in design step 4).

3. **Determination of the force spectrum (Spectral calculation)**
   The force spectrum was validated by comparing the significant wave force $F_{m0}$ of the spectral calculation method with the characteristic wave height $F_{1/3}$ in SWASH. For uni-modal wave spectra the spectral calculation method gave accurate results for a wide range of wave steepness and relative depths. After the addition of a swell peak to the uni-modal spectrum, the spectral calculation method showed accurate results for different values of $M_{Sw}$ and $\Phi_{Sw}$. Also for a wider range of wave fields where a swell component was included, the spectral calculation followed the trend of the SWASH simulations. However, some underestimations of about 15% of the relative increase in force by the spectral calculation method were observed in shallow water and conservative results for deeper water.

4. **Simplification of the wave spectrum (Design formulae)**
   The consequences of the simplification of the wave spectrum by wave characteristics was assessed by comparing the results from bimodal spectra with a uni-modal spectrum. It was shown that by adding a swell component to a uni-modal spectrum, the wave characteristics increased to a lesser extent than the horizontal wave force. This resulted in deviations of the wave force calculation of design guidelines compared to the SWASH results.

   A trivial solution such as linear superposition of the wave force of the swell peak and wind sea peak resulted in an overestimation of the horizontal wave force. Also the use of the spectral wave period $T_{m-1,0}$ as the design wave period, which should account for low frequency variance, resulted in underestimations of the horizontal wave force.

5. **Extrapolation to design values (Design formulae)**
   Instead of only analysing the distribution of wave height, the probability distribution of the force peaks was considered for various wave fields. In an example with large relative swell parameters ($M_{Sw}$ = 0.27 and $\Phi_{Sw}$ = 0.76), a deviation from the Rayleigh distribution was observed of $\Delta Ray_{0.1\%}$ = 0.09. For the remainder bimodal spectra under consideration, the deviation from the Rayleigh distribution was limited to $\Delta Ray_{0.1\%} < 0.05$ and did not show a strong correlation with an increasing swell component. From this, it is concluded that the Rayleigh distribution can in most cases be used for the determination of a design value within storm conditions with a 5% accuracy.

6. **Extrapolation to design force (Spectral calculation)**
   Similar to the determination of the design wave height for the design formulae, is the determination of the design force by the spectral calculation based on the Rayleigh distribution. Similar conclusions can be drawn: the Rayleigh distribution can in most cases be used for the determination of a design value within storm conditions with a 5% accuracy.

## 6.2. Conclusions

The research questions of this study were if design guidelines are accurate for the calculation of wave conditions from uni-modal and bimodal wave spectra and if the spectral calculation method provides a good alternative.

For the simplified case of a vertical wall on a flat sea bed (no berm) the following conclusions are made for non-breaking wave loads. In the case wave conditions are described by a uni-modal wave spectrum, the Sainflou formula is too conservative. The formula of Goda is more accurate, but provides underestimations of about 10% in intermediate water depth. As an alternative, the linear wave theory is an accurate design method for gentle waves in a wide range of relative depths.

When wave conditions by a bimodal spectrum are considered, the influence of swell on the wave force can be considerable. Since wave characteristics ($H_{1/3}$ and $T_{1/3}$) do not distinguish a swell component, traditional design guidelines based on wave characteristics may underestimate the wave force. This underestimation is depended on the relative depth and the variance of the swell component.

A spectral calculation method in which the complete wave spectrum is translated to a force spectrum is an accurate design method for the estimation of non-breaking wave loads on vertical walls. The Rayleigh distribution can be used for the determination of a design force in a storm condition.

## 6.3. Remarks concerning design guidelines

This section is giving suggestions for additions to the design guidelines. Thereby, it connects the conclusions from this study to the research objective of this thesis. This section is written in such a way that it could be incorporated in Leidraad Kunstwerken Appendix B5. First, some remarks are made on the procurement of boundary conditions. After that, a discussion on the use of different design methods is provided. Finally, a basic description on the use of the spectral calculation method is given as an addition to currently used design methods.

**Boundary conditions**
In the procurement of the boundary conditions, usually wave characteristics such as $H_{m_0}$ and a $T_p$ are given. It should be realized that these physical values represent an irregular wave field. In practice it is found that for uni-modal shaped wave spectra, the characteristic wave force can be found by the application of wave characteristics in the appropriate design method. Subsequently, the Rayleigh distribution can be used for the extrapolation to a design value.

However, for other shapes of the wave spectrum, the wave characteristics may not give an accurate representation of the wave force. In this study it was seen that for similar wave characteristics, the wave force in a bimodal spectrum was considerably larger (30% larger if the spectrum included 20% swell) compared to a uni-modal spectrum. With a calculation method that takes into account the wave spectrum, the characteristic force represented by a bimodal spectrum can be determined accurately. Therefore, it is always recommended to be aware of the spectral shape that the wave characteristics are representing.

**Use of design methods**
Different design methods are available for the estimation of wave loads on vertical walls. A traditional but rather conservative design method is the formulae of Sainflou. Due to the large overestimations that are induced by the simplified pressure distribution, this formula is not advised to be used.

The formula of Goda is a design formula which appears often in design guidelines and literature. The formula is applicable to a wide range of geometrical parameters as well as both breaking and non-breaking wave loads. It should be realised that the validation of this formula was applied on many scenarios in which a vertical breakwater was present on berm. This study showed that in the scenario of a flat sea bed and no berm, the Goda formula underestimates the wave load in intermediate depth. Also, the wave induced breaking which this formula accounts for should not to be confused with white-capping. The use of the Goda formula is advised for the case when uni-modal wave conditions are assured and when the geometry is shaped with a sloping bottom or a vertical structure is located on a berm/rubble ballast.

For the simplistic case where the geometry of a vertical wall is present on a flat sea bed, the use of the linear wave theory is advised for wave loads by a uni-modal wave spectrum. This formula gives a realistic expression of the wave pressure distribution. For the case of steep waves (= non-linear) attention should be paid for underestimation of the linear wave theory, although these effects were not observed in this study.

If the wave spectrum is not described by a uni-modal spectrum, it is highly advised to carry out a spectral approach of the boundary conditions. With the current computation techniques such a spectral approach can be carried out without too much difficulties. For a vertical wall on a flat sea bed, this spectral calculation method provides an accurate computation of the wave force. If a more complex geometry is present, the use of linear theory which is implemented in the spectral calculation method, is not validated. Possibly,

the potential influence of the swell component could be addressed first by comparing the wave loads of a uni-modal spectrum and the considered spectrum for a simplified case to determine a factor $\gamma_{bi} = F_{bi}/F_{uni}$. Consequently, $\gamma_{bi}$ could be applied on the design force estimated by Goda.

According to Goda, the design wave height is denoted by $1.8H_{1/3}$. It is however recommended to discard this design factor and determine the design wave based on the Rayleigh distribution. The Goda formulae account inherently for a 100% reflection. The linear wave theory and spectral calculation give an expression of the force for the local conditions. Incoming wave conditions should therefore be multiplied with a factor 2 to account for full reflection.

$$H_d/H_{1/3} = \sqrt{\frac{\ln(-(\Pr\{\underline{H} < H_d\} - 1)}{-2}} \tag{6.1}$$

The term $\left(1 - \Pr\{\underline{H} < H_d\}\right)$ refers to the probability of exceedance of the wave height. For the 1% design load this term becomes: $\left(1 - \Pr\{\underline{H} < H_d\}\right)$ = 1 - 0.99 = 0.01.

**Spectral calculation method**
The spectral calculation method translates in a few steps the incoming wave spectrum to a force spectrum, based on the linear wave theory. From the force spectrum and the assumption of the Rayleigh distribution of force peaks, any statistical value for the design force can be estimated.

The first step is the formulation of the response function, which consists of a response function below SWL and a section above SWL:

$$R_{sub}(f) = \rho\, g \int_{-d}^{0} \frac{\cosh(k(f)(d+z))}{\cosh(k(f)(d))}\,\mathrm{d}z \tag{6.2}$$

$$R_{top} = \frac{1}{2}\,\rho\, g\, a_{ref} \tag{6.3}$$

with:

| | | |
|---|---|---|
| $\rho$ | = Density of water | [kg/m$^3$] |
| $g$ | = Gravitational acceleration | [m/s$^2$] |
| $d$ | = Water depth | [m] |
| $k(f)$ | = Wave number as a function of the frequency | [m$^{-1}$] |
| $z$ | = Vertical co-ordinate | [m] |
| $a_{ref}$ | = Reference amplitude (can be taken as 0.75 $H_{m_0}$) | [m] |

With the input of a wave variance spectrum $S_{var}(f)$, the force spectrum can be obtained:

$$S_F(f) = (R_{sub}(f) + R_{top})^2\, S_{var}(f) \tag{6.4}$$

Similar to the wave variance of a wave spectrum, the wave force spectrum has a wave force variance, which is a representation of the characteristic force presented in a sea state.

$$m_{0,F} = \int_0^\infty S_F(f)\mathrm{d}f \tag{6.5}$$

with this parameter, any statistical value for the design force can be determined, based on the Rayleigh distribution:

$$F_d = \sqrt{-2m_{0_F}\ln\left(1 - \Pr\{\underline{F} < F_d\}\right)} \tag{6.6}$$

The term $\left(1 - \Pr\{\underline{F} < F_d\}\right)$ refers to the probability of exceedance of the wave force. For the 1% design load this term becomes: $\left(1 - \Pr\{\underline{F} < F_d\}\right)$ = 1 - 0.99 = 0.01.

The significant wave force, exceeded by a probability of 13.5%, becomes:

$$F_{m_0} = \sqrt{-2m_{0_F}\ln\left(1 - 0.865\right)} = 2\sqrt{m_{0_F}} \tag{6.7}$$

## 6.4. Recommendations

This study was focussed on the comparison between different design methods for the calculation of the horizontal wave force in various sea states. As a consequence, the scope included several simplifications of the geometry and boundary conditions of which some are worth to investigate.

- It is recommended to extent this research by simulating waves in geometries with sloped sea beds and/or vertical structures on a berm. Also, the vertical structures in deeper water should be addressed, as it is expected that the influence of a swell component could be even larger.
- By extending the 2D simulation to a 3D simulation, several realistic effects could be included. These effects comprise for example oblique waves, short crested waves, and a boundary condition defined by a multi-directional wave spectrum.
- The boundary conditions addressed considered bimodal spectra defined by a dominant wind sea component and a small swell component. Scenarios with more than 2 peaks, wide wave spectra or differently shaped bimodal spectra (dominant swell component) could lead to other results. It is recommended to validate the design methods for these wave conditions.
- The wave steepness of the range of simulated bimodal spectra was limited to relative gentle waves. It is recommended to verify the design methods (in particular the LWT and spectral calculation method) for these non-linear wave conditions.
- To validate the relevance of this study, it is recommended to asses how realistic the occurrence of the bimodal spectra under consideration are.

The different design formulae and the spectral calculation method are validated by SWASH. Just like every model, SWASH has limitations. The effect of the most relevant limitations should be assessed in additional studies.

- SWASH is not able to model white-capping. It is interesting to investigate what the effect of this type of wave breaking on the wall is. Without doing this, the validity for steep wave conditions remains questionable. Since the simulated waves were also limited to gentle steepness, it is recommended to investigate the validity for steep non-breaking waves.
- A trade-off had to made between grid discretisation and computation time of SWASH. It was already shown that this led to numerical dissipation for high frequencies. Additional studies should look into the effects of numerical dissipation on the surface elevation and pressure distribution.
- The solid vertical wall was simulated by a nearly impermeable grid point. It is recommended to gain more understanding of the effect this simplification to be able to simulate a desired coefficient of reflection.

Besides the simplifications and limitations, several observations ask for further research. Here, some recommendations are listed that could be carried out as continuation on the observations in this study.

- A deviation in mean water level was compared with the expression by Sainflou. It should be (theoretically) assessed why the results for regular waves were a factor 2 smaller than the Sainflou expression. Subsequently, it can be investigated which statistical parameter of the wave height can be used for the determination of the increase in mean water level.
- It is recommended to validate more alternative design methods that could be applied on the bimodal spectra without applying a full spectral analysis. This could be done with a more representable wave period parameter $T_d$, an alternative method of superposition of forces (e.g. quadratic superposition of forces) of the swell and wind sea components or potentially with an analytical expression that includes the introduced relative swell parameters $M_{Sw}$ and $\Phi_{Sw}$.
- The observed double peaked wave pressure in the SWASH model should be compared with theoretical higher order derivations of the wave pressure. Accordingly, the effect of these non-linear effects should be related to the force estimations of the design methods.
- It is recommended to investigate the correlation of the deviation with the relative depth and spectral parameters such as $M_{Sw}$ and $\Phi_{Sw}$. Possibly a new probability distribution (e.g. Weibull) should be fitted to the observed distributions. It is also interesting to investigate the joint probability of wave heights and wave periods, as the forces in bimodal spectra seem to be not only depended on the design wave height.

Several of the most important recommendations can be verified by performing a physical experiment. This experiment should first of all verify the individual wave force for non breaking wave load on a vertical wall

on a flat sea bed. In addition, also the characteristic wave load must be verified for a range of uni-modal and bimodal spectra, preferably in line with the SWASH simulations carried out in this study. It is recommended to simulate steep waves as well, as the SWASH model was limited to gentle waves. Lastly, a possible deviation of force peaks from the Rayleigh distribution can be investigated for the physical experiment by running long simulations for severe cases of bimodal spectra.

Also it is recommended to carry out more numerical simulations to address simulations with bimodal spectra in different geometries, possibly in three dimensions.

# Bibliography


Airy, G. B.
1845. *Tides and waves*. London: Encyclopaedia Metropolitana.

Battjes, J. A. and H. W. Groenendijk
2000. Wave height distribution on shallow foreshores. *Coastal Engineering*, 40:161–182.

Bendat, J. S. and A. G. . Piersol
2010. *Random data: Analysis & measurement on procedures*, 4 edition. New Jersey: John Wiley & Sons.

Bosboom, J. and M. J. F. Stive
2015. *Coastal Dynamics 1: lecture notes CIE4305*. Delft: Delft University of Technology, Faculty of Civil Engineering and Geoscienses, Section of Hydraulic Engineering.

Chiu, Y.-f., J.-g. Lin, S.-c. Chang, Y.-j. Lin, and C.-h. Chen
2007. An experimental study of wave forces on vertical breakwater. *Journal of Marine Science and Application*, 15(3):158–170.

Danel, P.
1952. On the limiting clapotis, Gravity Waves. *National Bureau of Standards Circular*, 52:35–38.

Dingemans, M. W.
1997a. *Water wave propagation over uneven bottoms, Part 1 - Linear Wave Propagation*. Singapore: World Scientific.

Dingemans, M. W.
1997b. *Water wave propagation over Uneven Bottoms, Part 2 - Nonlinear Wave Propagation*. Singapore: World Scientific.

Fenton, J. D.
1985. Wave forces on vertical walls. *Journal of Waterway, Port, Coastal, and Ocean Engineering, ASCE*, 111:693–718.

Goda, Y.
1974. A new method of wave pressure calculation for the design of composite breakwaters. *Proceeding of 14th International Conference Coastal Engineering*, 14:1702–1720.

Goda, Y.
1988. Statistical variability of sea state parameters as a function of a wave spectrum. *Coastal Engineering in Japan*, 31(1):39–52.

Goda, Y.
2000. *Random seas and design of maritime structures*, 2nd edition. Singapore: World Scientific Publishing Co. Pte. Ltd.

Goda, Y. and T. Fukumori
1972. Laboratory investigation of wave pressures exerted upon vertial and composite walls. *Coastal Engineering in Japan*, 15:81–90.

Goda, Y. and S. Kakizai
1967. Study on finite amplitude standing waves and their pressures upon a vertical wall. *Coastal Engineering in Japan*, 10:1–11.

Guedes Soares, C.
1984. Representation of double-peaked sea wave spectra. *Ocean Engineering*, 11(2):185–207.

Gurhan, G. and D. Unsalan
2005. A comparative study of the first and second order theories and Goda's formula for wave-induced pressure on a vertical breakwater with irregular waves. *Ocean Engineering*, 32(17-18):2182–2194.

Hasselmann, K.
1974. On the spectral dissipation of ocean waves due to white capping. *Boundary-Layer Meteorology*, 6:107–127.

Hasselmann, K., T. P. Barnett, E. Bouws, H. Carlson, D. E. Cartwright, K. Enke, J. A. Ewing, H. Gienapp, D. E. Hasselmann, P. Kruseman, A. Meerburg, P. Muller, D. J. Olbers, K. Richter, W. Sell, and H. Walden
1973. Measurements of Wind-Wave Growth and Swell Decay during the Joint North Sea Wave Project (JONSWAP). *Ergnzungsheft zur Deutschen Hydrographischen Zeitschrift Reihe*, A(8)(8 0):p.95.

Hofland, B., X. Chen, C. Altomare, and P. Oosterlo
2017. Prediction formula for the spectral wave period Tm-1,0 on mildly sloping shallow foreshores. *Coastal Engineering*, 123(September 2016):21–28.

Holthuijsen, L. H.
2007. *Waves in oceanic and coastal waters*. New York: Cambridge University Press.

International Navigation Association
2003. PIANC: Breakwaters with Vertical and Inclined Concrete Walls. Technical report, PIANC, Brussels.

ISO 21650
2007. International standard: actions from waves and currents on coastal structure.

Ito, Y., M. Fujishima, and T. Kitatani
1966. On the stability of breakwaters. *Coastal Engineering in Japan*, 14:53–61.

Juhl, J. and J. W. Van der Meer
1992. Quasi-static wave forces on vertical structures, re-analysis of data at Danish Hydraulic Institute and Delft Hydraulics Report. Technical report, Prepared for MAST G6-S Coastal Structures.

Klopman, G. and J. W. Van der Meer
1999. Random wave measurements in front of a reflective structure. *Journal of waterway, port, coastal, and ocean engineering*, 125(6):322–330.

Korteweg, D. and G. De Vries
1895. On the change of form of long waves advancing in a rectangular canal, and a new type of long stationary waves. *Philosophical Magazine, Series 5*, 39:422–443.

Longuet-Higgins, M. S.
1975. On the joint distribution of the periods and amplitudes of sea waves. *Journal of Geophysical Research*, 80(June):2688–2694.

Lucas, C. and C. Guedes Soares
2015. On the modelling of swell spectra. *Ocean Engineering*, 108:749–759.

Mallayachari, V. and V. Sundar
1995. Standing wave pressures due to regular and random waves on a vertical wall. *Ocean Engineering*, 22(8):859–879.

Miche, R.
1944. Mouvements ondulatoires des mers en profundeur constante on décroisante. *Annales des Ponts et Chaussées*, 114:369–406.

Miche, R.
1953. The reflecting power of maritime works exposed to action of the waves. *Bulletin of the Beach Erosion Board*, 7(April):1–7.

Ministerie van Verkeer en Waterstaat
2001. *Hydraulische Randvoorwaarden*. https://www.helpdeskwater.nl/: [publisher unknown].

Molenaar, W. and M. Voorendt
2017. *Manual Hydraulic Structures February 2017*, number 2. Delft: Delft University of Technology, Faculty of Civil Engineering and Geoscienses, Section of Hydraulic Engineering.

Nagai, S.
1969. Pressures of standing waves on vertical wall. *Journal of the Waterways and Harbors Division, ASCE*, 95:53–76.

Novak, P., A. I. B. Moffat, C. Nalluri, and R. Narayanan
2007. *Hydraulic structures*, 4th edition. Abingdon: Taylor & Francis Group.

Ochi, M. K.
1998. *Ocean waves, The stochastic approach.* New York: Cambridge University Press.

Ochi, M. K. . and E. N. Hubble
1976. On six-parameter wave spectra. *Proceedings of the 15th International Conference on Coastal Engineering*, 1:301–328.

Oumeraci, H., N. W. H. Allsop, M. B. de Groot, R. S. Crouch, and J. K. Vrijling
1999. Proverbs: Probabilistic Design Tools for Vertical Breakwaters.

Penny, W. G. and A. T. Price
1952. Finite periodic stationary gravity waves in a perfect liquid, Part II: "Some gravity wave problems in the motion of perfect liquids". *Philosophical Transactions of the Royal Society*, 244:254–84.

Pierson, W. J. and L. Moskowitz
1964. A proposed spectral form for fully developed wind seas based on the similarity theory of S. A. Kitaigorodskii. *Journal of Geophysical Research1*, 69(December):5181–5190.

Rayleigh, Lord
1880. XII. On the resultant of a large number of vibrations of the same pitch and of arbitrary phase. *Philosophical Magazine Series 5*, 10(60):73–78.

Rice, S. O.
1944. Mathematical analysis of random noise. *Bell System Technical Journal*, 23:282–332.

Riezebos, H. J.
2014. *Validation of SWASH for wave-channel interactions.* Additional thesis, Delft University of Technology.

Rundgren, L.
1958. *Water Wave Forces; Bulletin No. 54.* Stockhom: Royal Institute of Technology, Division of Hydraulics.

Sainflou, M.
1928. Essai sur les diques maritimes verticales. Technical report, Paris.

Smit, P. B., M. Zijlema, and G. S. Stelling
2013. Depth-induced wave breaking in a non-hydrostatic, near-shore wave model. *Coastal Engineering*, 76:1–16.

Stelling, G. S. and S. P. A. Duinmeijer
2003. A staggered conservativve scheme for every Froude number in rapidly varied shallow water flows. *International Journal for Numerical Methods in Fluids*, 43:1329–1354.

Stelling, G. S. and M. Zijlema
2003. An accurate and efficient finite-difference algorithm for non-hydrostatic free-surface flow with application to wave propagation. *International Journal for Numerical Methods in Fluids*, 43:1–23.

Stokes, G. G.
1847. On the theory of oscillatory waves. *Transactions of the Cambridge Philosophyical Society*, 8:441–455.

Strekalov, S. and S. Massel
1971. On the spectral Analysis of Wind Waves. Technical report, Gdansk, Poland.

Sverdrup, H. V. and W. H. Munk
1946. Empirical and theoretical relations between wind, sea and swell. *Transactions American Geophysical Union*, 27:823–827.

Tadjbaksh, I. and J. B. Kelle
1960. Standing surface waves of finite amplitude. *Journal of Fluid Mechanics*, 8:442–451.

Takahashi, S.
2002. Design of vertical breakwaters. *Port and airport research institute - Japan*, 1996(34):126.

Takahashi, S. and S. Hosoyamada
1994. Hydrodynamic characteristics of sloping top caissons. In *Proc. Int. Conf. on Hydro-Technical Eng. for Port and Harbour Construction.*, Pp. 733–746, Yokosuka, Japan. Port and Harbour Research Institute.

Takahashi, S., K. Tanimoto, and K. Shimosako
1993. Experimental study of impulsive pressures on composite breakwaters - Foundamental feature of impulsive pressure coefficient. *Rept of Port and Harbour Research Institute*, 31(5):33–72.

Tanimoto, K., K. Moto, S. Isizuka, and Y. Goda
1976. An investigation on design wave force formulae of composite-type breakwaters. *Proceedings of 23rd Japaneese Conference Coastal Engineering*, Pp. 11–16.

TAW
2003. Leidraad kunstwerken. Technical report, Delft.

Teo, H. T.
2003. Wave pressures on a vertical wall due to short-crested waves: Fifth-order approximation. *Ocean Engineering*, 30(16):2157–2166.

The SWASH Team
2017. *SWASH User manual.* Delft: TU Delft, Faculty of Civil Engineering and Geosciences.

Torsethaugen, K. and S. Haver
2004. Simplified double peak spectral model for ocean waves. *Proceedings of 14th international offshore and polar engineering conference. ISOPE*, 3:76–84.

Tuin, H. G., H. Voortman, T. Wijdense, W. Van der Stelt, D. Van Goolen, P. Van Lierop, and L. Lous
2018. Design of roller gates of the lock of Amsterdam using a transformation of the wave spectrum in a frictional force spectrum. *unpublished.*

USACE
1984. *Shore Protection Manual*, volume 2, 4th edition. Washington, DC: US Government Printing Office.

USACE
2002. *Coastal Engineering Manual*, volume 6/6. Washington, DC: U.S. Army Corps of Engineers.

Van der Meer, J. W., K. D'Angremond, and J. Juhl
1994. Probabilistic calculations of wave forces on vertical structures. *Proceeding of 23th International Conference on Coastal Engineering*, Pp. 1754–1768.

Van der Meer, J. W., J. Juhl, and G. Van Driel
1992. Probabilistic calculations of wave forces on vertical structures. *Proc. Final MAST G6-S Coastal Structures Workshop, Madrid.*

van Gent, M. R. A.
1999. Physical model investigations on coastal structures with shallow foreshores; 2D-model tests on the Petten Sea-defence. Technical report, Delft Hydraulics, Delft.

van Gent, M. R. A.
2001. Wave Runup on Dikes with Shallow Foreshores. *Journal of Waterway, Port, Coastal, and Ocean Engineering*, 127(March):254–262.

Van Vledder, G. P. and F. Enet
2014. Detaillering golfrandvoorwaarden Nieuwe Zeesluis IJmuiden. Rapport A13120R6, 28 nov. 2014. Technical report, BMT ARGOSS.

Verhagen, H. J. and J. Van den Bos
2017. *Breakwater design: Lecture notes CIE5308*, number Draft. Delft: Delft University of Technology, Faculty of Civil Engineering and Geoscienses, Section of Hydraulic Engineering.

Vrijburcht, A.
2000. *Ontwerp van schutsluizen*, deel 2 edition. Utrecht: Rijskwaterstaat Bouwdienst.

Wiegel, R. L.
1964. *Oceanographical Engineering*. Berkeley, California: Pentice-Hall International.

Yu, D., P. Tang, and Q. Song
2015. Feasibility study on common methods for wave force estimation of deep water combined breakwaters. *Journal of Ocean University of China*, 14(4):629–635.

Zijlema, M.
2015. *Computational Modelling of Flow and Transport*, number January. Delft: Delft University of Technology, Faculty of Civil Engineering and Geoscienses, Section of Hydraulic Engineering.

Zijlema, M. and G. S. Stelling
2005. Further experiences with computing non-hydrostatic free-surface flows involving water waves. *International Journal for Numerical Methods in Fluids*, 48:169–197.

Zijlema, M. and G. S. Stelling
2008. Efficient computation of surf zone waves using the nonlinear shallow water equations with non-hydrostatic pressure. *Coastal Engineering*, 55(10):780–790.

Zijlema, M., G. S. Stelling, and P. B. Smit
2011. SWASH: An operational public domain code for simulating wave fields and rapidly varied flows in coastal waters. *Coastal Engineering*, 58(10):992–1012.

ZUS
2016. ZUS ontwerpt grootste zeesluis ter wereld, Zones Urbaines Sensibles https://architectenweb.nl/.

# A

# Spectral calculation method

This section elaborates the spectral calculation method, which is an analytical design method that employs the entire wave spectrum to calculate the horizontal wave induced force on the wall. This is performed by means of a response function, which is elaborated in Section A.1. Subsequently, the horizontal wave force can be determined for any arbitrary probability of exceedance, based on the Rayleigh distribution. This is explained in Section A.2. After that, an expression for the vertical pressure distribution is given in Section A.3. Finally, Section A.4 presents an example of the application of the spectral calculation method on a bimodal wave spectrum.

## A.1. Response function

The concept of the response function is based on the theory that it is possible to transform the spectrum of a variable (excitation) to the spectrum of an other variable (response), as long as the two variables can be treated as a linear system (Holthuijsen, 2007). The example for that linear system that is used here is the relationship between the surface elevation as excitation, and the wave induced pressure below the water surface as a response:

$$\text{Excitation:} \qquad \eta(t,f) = \underbrace{(1+\chi)\,a(f)}_{\text{amplitude}} \underbrace{\sin(2\pi f t + \alpha(f))}_{\text{wave harmonic}} \tag{A.1}$$

$$\text{Response:} \qquad p_{sub}(t,f,z) = \underbrace{(1+\chi)\rho g a(f) \frac{\cosh(k(f)(d+z))}{\cosh(k(f)d)}}_{\text{amplitude}} \underbrace{\sin(2\pi f t + \alpha(f))}_{\text{wave harmonic}} \tag{A.2}$$

It can be seen that the two formulae contain the same wave harmonic. The amplitude part of the two equations contain both a linear relation to the amplitude $a(f)$ of the surface elevation. By dividing the amplitude of the response $p_{sub}$ by the amplitude of the water level elevation $\eta$, a response function is obtained.

However, in calculating the total horizontal wave force on the wall two more steps are performed before defining the response function. First, the wave induced pressure above SWL is taken into account:

$$p_{top}(t,f,z) = \underbrace{(a(f)(1+\chi) - z)\rho g}_{\text{amplitude}} \underbrace{\sin(2\pi f t + \alpha(f))}_{\text{wave harmonic}} \tag{A.3}$$

Likewise Equation A.1 and A.2, this equation contains the wave harmonic part and the amplitude part. Based on the linear relation between the amplitude of $p_{top}$ and $\eta$, the pressure above SWL could be implemented in a response function as well.

The second step before the response function is determined, is the integration of the pressure distribution over the vertical. By doing this, a function for the horizontal wave induced force is obtained. The wave

harmonic within the pressure equations are disregarded, since in the following interest goes out to the amplitudes of the function. The equations for the horizontal wave force become:

$$F_{sub}(f) = (1+\chi)\,\rho\,g\,a(f)\int_{-d}^{0}\frac{\cosh(k(f)(d+z))}{\cosh(k(f)(d))}\,\mathrm{d}z \tag{A.4}$$

for the force below SWL, and for the force above SWL:

$$F_{top}(f) = (1+\chi)^2\,\frac{1}{2}\,\rho\,g\;a^2(f) \tag{A.5}$$

By doing this, a new complication occurs for the force above SWL. Equation A.5 contains the term $a^2(f)$, which is not a linear term. This non-linear term can be deleted by linearising $F_{top}(f)$. Here, this is done by replacing one amplitude function $(a(f)(1+\chi))$ with a constant reference amplitude $a_{ref}$. For a first estimate this can be taken as a reasonable conservative value, for example $0.75H_{m_0}$. Later, the value of $a_{ref}$ can be determined with more precision, in a way it agrees with the probability of the calculated force. The linearised force formula becomes:

$$F_{top}(f) = (1+\chi)\,\frac{1}{2}\,\rho\,g\;a(f)\,a_{ref} \tag{A.6}$$

The definition of the response function is as follows:

$$R(f) = \frac{\text{amplitude of response}}{\text{amplitude of excitation}} = \frac{F(f)}{(1+\chi)a(f)} \tag{A.7}$$

One response function is determined for the top section and one for the sub section. For both response functions, the amplitude function of the surface elevation is deleted out of the response function since it is present in both the numerator and denominator of the response functions. The response functions are:

$$R_{sub}(f) = \rho\,g\int_{-d}^{0}\frac{\cosh(k(f)(d+z))}{\cosh(k(f)(d))}\,\mathrm{d}z \tag{A.8}$$

$$R_{top} = \frac{1}{2}\,\rho\,g\,a_{ref} \tag{A.9}$$

Where:

| | | |
|---|---|---|
| $R_{top}$ | = Response function for section above SWL | [N/m$^2$] |
| $R_{sub}(f)$ | = Response function for section below SWL | [N/m$^2$] |

The total response function is derived by combining the response functions of the force distribution above and below SWL. This is done taking the sum of the two response functions first, because the both responses are a function of the same excitation. After this, the response is squared. This is done, because the response functions were determined for the excitation function of the amplitude $a(f)$ and the variance spectrum is a function of the amplitude squared. The wave force spectrum is finally obtained by the multiplication of the total response function by the variance spectrum.

$$S_F(f) = (R_{sub}(f) + R_{top})^2\,S_{var}(f) \tag{A.10}$$

where $S_{var}(f)$ is the incoming wave spectrum and $S_F(f)$ is the incoming wave force spectrum. To obtain the local wave force spectrum, the local wave spectrum $S_{var,loc}(f)$ should be used.

## A.2. Probability distribution

With a force spectrum, no values of a characteristic force is obtained yet. However, together with the assumption of the Rayleigh distribution of the forces, force characteristics can be determined in the same way as wave characteristics from a wave variance spectrum. Ultimately, it leads to a distribution of the horizontal induced force in the probability domain. The handling of the wave force spectrum is analogous to the use of the wave spectrum. First, the wave force variance is determined by:

$$m_{0,F} = \int_0^\infty S_F(f)\mathrm{d}f \tag{A.11}$$

Now, also an expression of the significant wave force can be determined. However, first the difference in the relation between $m_{0,F}$ and $F_{m,0}$ is compared to the relation between $m_0$ and $H_{m0}$. The wave variance spectrum is a function of $\frac{1}{2}a^2 = \frac{1}{2}(\frac{1}{2}H)^2 = \frac{1}{8}H^2$. The wave force spectrum a function of the force peaks, which are the equal to solely the wave force amplitude: $\frac{1}{2}F_p^2$. Therefore, $m_0 \equiv 4m_{0,F}$. This lead to the following significant wave force:

$$F_{m0} = 2\sqrt{m_{0,F}} \tag{A.12}$$

The wave force variance can also be used in the probability density function of a single force peak:

$$p_{\underline{F}}(F) = \frac{F}{m_{0,F}}\exp\left(-\frac{F^2}{2m_{0,F}}\right) \tag{A.13}$$

or the cumulative distribution:

$$\Pr\{\underline{F} < F\} = 1 - \exp\left(-\frac{F^2}{2m_{0,F}}\right) \tag{A.14}$$

Since Equation 2.25 has a scale parameter which is completely independent of the wave variance, the wave height can be replaced by force peak and becomes:

$$\Pr\{\underline{F} < F\} = 1 - \exp\left[-2\left(F/F_{1/3}\right)^2\right] \tag{A.15}$$

where $F_{1/3}$ is the significant force peak, equal to the average of the highest $1/3^{\text{rd}}$ of the force peaks. By rewriting the cumulative distribution as a function of the probability of exceedance, a function is obtained to determine a design wave $F_d$ for a given force spectrum variance $m_{0_F}$. This function looks as follows:

$$F_d = \sqrt{-2m_{0_F}\ln\left(1 - \Pr\{\underline{F} < F_D\}\right)} \tag{A.16}$$

## A.3. Vertical pressure distribution

In the first part of this section the response function is determined for the horizontal wave force on the wall. By doing this, information about the pressure distribution over the vertical axis is left out. To analyse the pressure distribution of the spectral method over the vertical axis, an additional step before integrating the pressure is implemented.

First, the distinction between the sub section and the top section needs to be considered again. In integrating the pressure over the vertical for the section below SWL, the range of 0 to $d$ is split up in ranges of $\Delta d$, where $\Delta d << d$. For each $\Delta d$ a response function is determined. By taking the square of the response function and multiplying by the wave variance spectrum, a force spectrum for that particular location on the vertical axis is determined. Together with an assumption for the probability of exceedance, a value for the force can be assigned. The pressure on the location is obviously the force divided by $\Delta d$. This is done for the entire subsection and a vertical pressure distribution for the subsection is obtained. For the section below SWL the pressure becomes:

$$p_{sub}(z) = \lim_{\Delta d\to 0} \frac{R_{sub}(f)^2\, S_{var}(f)}{\Delta d}$$

$$= \lim_{\Delta d\to 0} \frac{\left(\rho\, g \int_{z-\frac{1}{2}\Delta d}^{z+\frac{1}{2}\Delta d} \frac{\cosh(k(f)[d+z])}{\cosh(k(f)(d)}\,\mathrm{d}z\right)^2 \quad S_{var}(f)}{\Delta d}, \qquad \text{for} \qquad -\frac{1}{2}\Delta d \geq z \geq -d + \frac{1}{2}\Delta d \tag{A.17}$$

For the section above SWL, the solution is more convenient. Since the response function above SWL is not a function of the frequency, but only of the $a_{ref}$, it is not need for the response function to be divided in vertical

layers. The pressure is linear distributed over the the section between z = 0 and z = $a_{ref}$. The pressure at z = $a_{ref}$ is 0 and the pressure at z = 0 is $a_{ref}\rho g$ .

$$p_{top}(z) = (a_{ref} - z)\rho g \tag{A.18}$$

## A.4. Example

A bimodal wave spectrum is generated with the input parameters: $H_{m_{01}}$ = 0.2 m, $f_{p1}$ = 0.08 Hz, $H_{m_{02}}$ = 1 m, $f_{p2}$ = 0.23 Hz. Figure A.1 plots the wave variance over the frequency domain. For this example, the assumption that this spectrum is measured at the interface between water and a vertical wall.

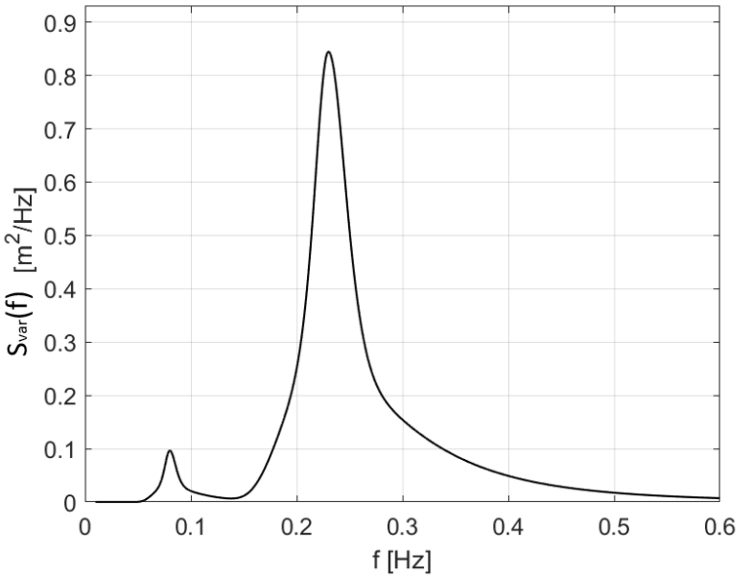


Figure A.1: Example of a bimodal wave spectrum.

To create the response functions, an assumption for an $a_{ref}$ is required. Here, a first value of 1.5 ($\frac{1}{2}H_{m_0}$) is taken. Later, based on the assumed probability, a safety factor is determined, on which the $a_{ref}$ can be adjusted. The response functions in the frequency domain are plotted in Figure A.2.

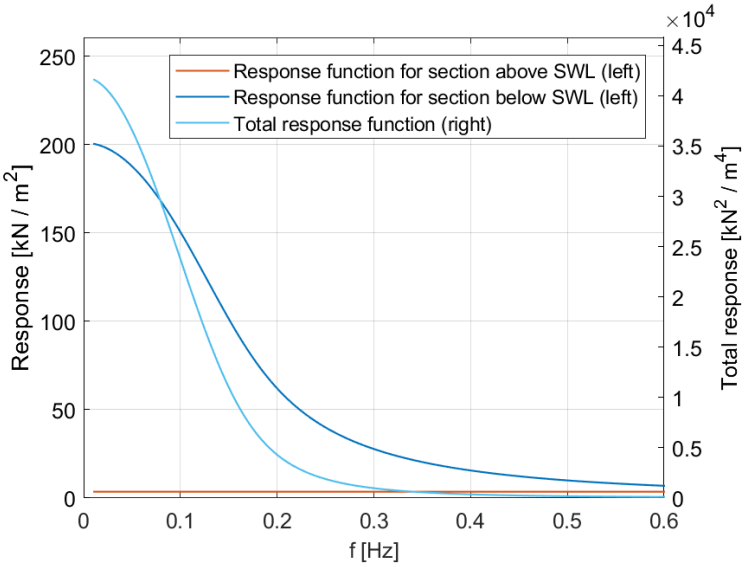


Figure A.2: Response function (top, sub, total) for an example case.

It can be noticed that the response for section above SWL remains constant in the frequency domain. This can be recognized in the equation as well, since it is not a function of the frequency $f$. The response for the section below SWL becomes high for lower frequencies. This is explained by the fact that low frequency waves have a long wave length and wave pressure persists in greater depth, see Figure A.3. Hence, the response function is sensitive for wave variance in the lower frequency range, especially in deep water. The total response function is the square of the sum of the top and sub response function. After multiplying the wave variance spectrum with the response function, the wave force spectrum is obtained.

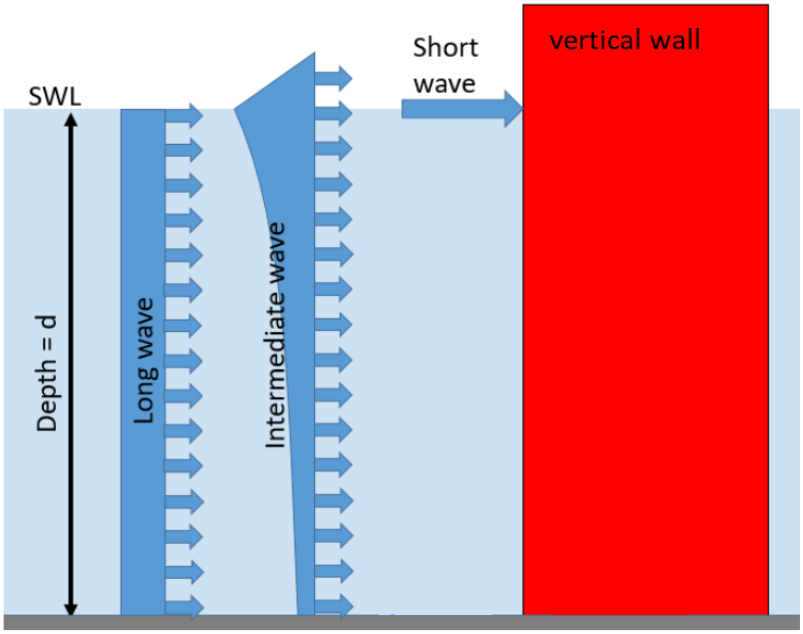


Figure A.3: Visualisation of the influence of the wave length on the penetration depth of the wave pressure. Based on: Tuin et al. (2018)

Figure A.4 plots both the variance spectrum and the wave force spectrum. It is noticable that the small peak at a low frequency in the variance spectrum causes a big peak in the wave force spectrum.

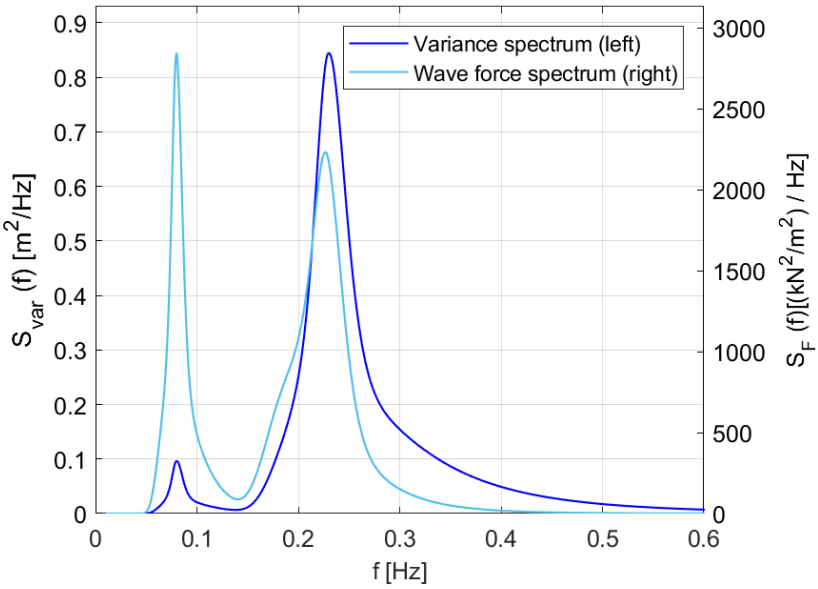


Figure A.4: Wave spectrum and wave force spectrum for an example case

The next step is to translate the wave force spectrum to the probability domain. This is done by measuring the force variance (zero'th moment of the wave force spectrum) and use it for the scale parameter in the Rayleigh distribution. It is important to note that an assumption is made on the validity of the Rayleigh distribution.

$$m_{0,F} = \int_0^\infty S_F(f)\mathrm{d}f = 202.5\,\mathrm{kN}^2/\mathrm{m}^2 \tag{A.19}$$

The significant wave force becomes:

$$F_{m0} = 2\sqrt{m_{0,F}} = 28.5\,\mathrm{kN\ /\ m} \tag{A.20}$$

From here, any probability of exceedance and corresponding wave force can be regarded. In this example, a probability of a wave exeedance of 0.02 is taken. This probability is inserted in the following formula:

$$F_d = \sqrt{-2m_{0,F}\,\ln\left(1-\Pr\{\underline{F} < F_D\}\right)} = \sqrt{-2m_{0,F}\ln\left(1-0.98\right)} = 39.9\,\mathrm{kN} \tag{A.21}$$

Now the design force is determined, a design factor can be found by the simple relationship:

$$\gamma_d = \frac{F_d}{F_{m0}} = 1.4 \tag{A.22}$$

This is slightly lower than the assumed safety factor of 1.5 before. With the new design factor the previous steps are repeated, but now with an accurate estimation of $a_{ref}$. Just one iteration is done, since the difference between old an new safety factor is low, and the influence of the response function above SWL is minor. The new design force becomes 39.8 kN.

The non-dimensional pressure distribution for the 2% design force is plotted over the partial depth in Figure A.5. In this example $\Delta d$ = d/100 = 0.2 m. For each vertical layer a local response function is made and multiplied by the wave variance to get to a local force spectrum. With the probability earlier discussed of 0.02, the design force for each vertical layer is calculated. By deviding this force over the height of the vertical layer $\Delta d$ , the local pressure is determined.

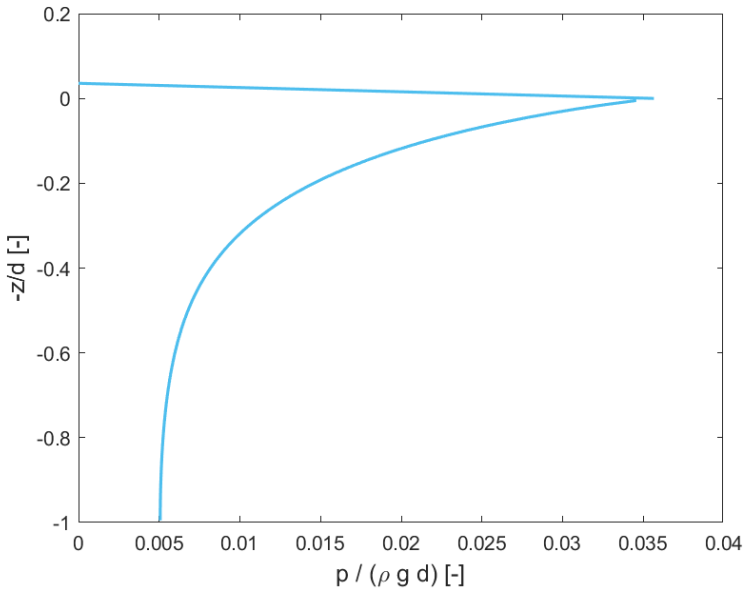


Figure A.5: Vertical pressure distribution of spectral calculation for the 2% design wave force $F_{2\%}$ for the example case.

# B

# Design guidelines

## B.1. Types of waves

According to the USACE (1984) and Ministerie van Verkeer en Waterstaat (2001) wave loads can roughly be divided in three types:

1. *Non-breaking waves*
   In this scenario a standing wave may occur. With complete reflectance and a non frictional wall, the wave amplitude will increase with a factor 2.
2. *(Slightly) breaking waves*
   Breaking waves can cause a huge force on the structure. This force is however limited to a very short time period in the order of 0.1 seconds. The load is therefore often classified as an impact.
3. *Broken waves*
   This type describes the case where already broken waves impact the structure and is characterised by a big amount of turbulence at the water surface.

Oumeraci et al. (1999) makes an additional distinction in breaking waves between slightly breaking waves and impact loads. Figure B.1 shows the plot of the force over the time for four different types of wave impact. According to Oumeraci et al. (1999), broken wave impact and slightly breaking wave impact doesn't occur for vertical breakwaters without a berm. Breaking waves may exert much greater forces due to dynamic effects of turbulent water and entrapped air pockets. In areas of protected regions, regions with a limited fetch and when the depth of the structure is greater than about 1.5 times the wave height non-breaking waves may occur (USACE, 1984). Non-breaking waves exert a load with a duration in the order of seconds and in most cases they do not cause any dynamic effects (Verhagen and Van den Bos, 2017). Therefore, non-breaking waves can be seen as a quasi static load.

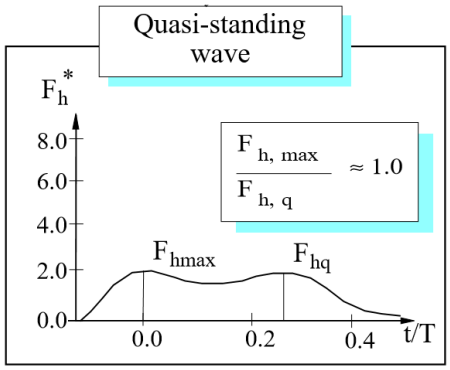


(a) Non-breaking wave load or quasi-standing wave load

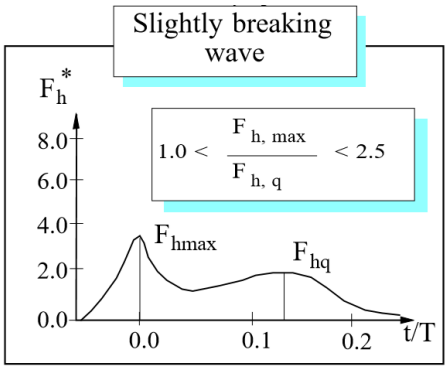


(b) Slightly breaking wave load

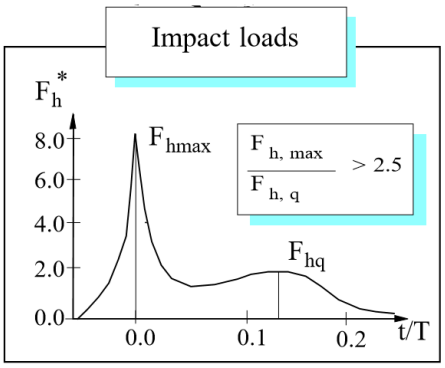


(c) Breaking wave load

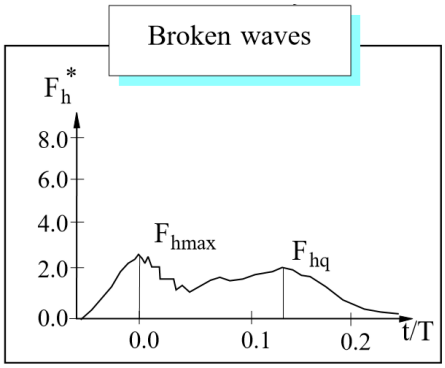


(d) Broken wave load

Figure B.1: Various types of wave load. Based on: Oumeraci et al. (1999)

## B.2. Failure mechanisms

Most literature about failure mechanisms for coastal structures with a vertical wall refer to caisson structures. In discussing the design and performance of coastal structures International Navigation Association (2003) defines failure as follows: "*Damage that results in performance and functionality of the structure below the minimum anticipated by design*". A distinction can be made between overall instability and local instability. The overall stability failure modes are: shoreward sliding, seaward sliding, slip failure in subsoil and settlement, slip failures in rubble foundations and subsoil, overturning around heel. Local instabilities are: Hydraulic instability of rubble foundation, seabed scour in front of structure, damage of structural elements(USACE, 2002; International Navigation Association, 2003). For overturning, shoreward sliding and breakage and damage of structural elements the maximum wave load will be an important parameter, see also Figure B.2.

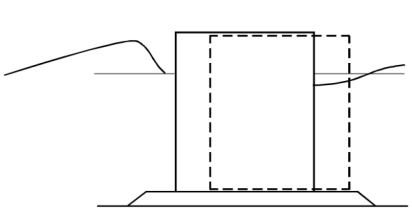

(a) Sliding

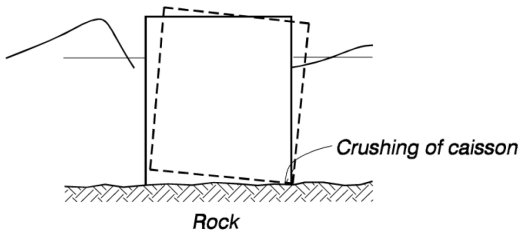


(b) Overturning

Figure B.2: Considered failure mechanisms, based on USACE (2002)

# B.3. Design formulae

## B.3.1. Sainflou

As described in Section 1.1, different versions of the Sainflou formula appear throughout the literature. The original Sainflou formula is originated from 1928. In Section 2.4, an other version of Sainflou is elaborated: the version that appears in Leidraad Kunstwerken and in Molenaar and Voorendt (2017).

A third version of the Sainflou formula appears in the Coastal Engineering Manual USACE (2002) and Verhagen and Van den Bos (2017). The formula is a close resemblance of the original formula. There is a difference in the definition for $p_1$. An other difference is that there is no distinction made between depths $d$ and $d'$; there is a flat sea bed in front of the structure. The pressure distribution between the points remains linear and the definition of $h_0$ stays identical.

A fourth version is found in the Shore Protection Manual USACE (1984). It states that the original form of the formula (version 3) gives good results for long waves with low steepness. However, Rundgren found in 1958 experimental data that showed that Sainflou method overestimates the wave force for steep waves. Rundgren adjusted the Sainflou formula based on a modified high order wave theory of Miche (1944). Which is the same as the second version above, but than a reflection coefficient implemented. Sainflou Miche/Rundgren is being used in the Shore protection manual (USACE, 1984) and works by means of design curves. In this formula, also a reflection coefficient $\chi$ is introduced, which should be taken to be 0.9 or 1. In USACE (2002), the successor of USACE (1984), the design curves are disappeared from the manual.

Table B.1 presents an comparison between the orinal Sainflou formula and the occurance of Sainflou in Leidraad Kunstwerken and the Coastal Engineering Manual [1].

Table B.1: Overview of different versions of the Sainflou formula.

| Symbol | Sainflou (1928) | Leidraad Kustwerken (2003) | CEM (2002) |
|---|---|---|---|
| $h_0$ | $kH_{inc}^2 \coth(\frac{1}{2}kd)$ | $\frac{1}{2}kH_{inc}^2 \coth(kd)$ | $\frac{1}{2}kH_{inc}^2 \coth(kd)$ |
| $h_p$ | $h_0 + 2H_{inc}$ | $h_0 + H_{inc}$ | $h_0 + 2H_{inc}$ |
| $p_0$ | $\rho g \frac{2H_{local}}{\cosh(\frac{1}{2}kd)}$ | $\rho g \frac{H_{inc}}{coshkd}$ | $\rho g \frac{2H_{inc}}{coshkd}$ |
| $p_1$ | $(p_0 + \rho g d)\frac{h_0+2H_{inc}}{d+h_0+2H_{inc}}$ | $\rho g(h_0 + H_{inc})$ | $(p_0 + \rho g d)\frac{h_0+2H_{inc}}{d+h_0+2H_{inc}}$ |

## B.3.2. Miche

Wiegel (1964) presents the second-order theory by Miche (1944) as the best description for pressure of a standing wave against a vertical wall. Miche describes the standing wave in finite depth to the second order for zero mass transport. At the bottom, the pressure is the same as Sainflou. The expression below sea level deviates from the Sainflou expression. For engineering purposes however, it states that it is adequate to use a linear pressure distribution taken as zero at the maximum/minimum surface elevation. With this assumption the pressure distribution becomes equal to Sainflou.

Miche also presents a $h_0$ value as an increase in the average waterlevel at an antinode as:

$$h_0 = \frac{\pi H^2}{4L}\left(1 + \frac{3}{4\sinh^2(2\pi d/L)} - \frac{1}{4\cosh^2(2\pi d\ L)}\right)\coth\frac{2\pi d}{L} \tag{B.1}$$

or can be simplified (to Sainflou), where $H$ is given as the wave height of the standing wave ($2\ H_{inc}$):

$$h_0 = \frac{\pi H^2}{4L}\coth\frac{2\pi d}{L} \tag{B.2}$$

[1] The symbol $h$ from the original Sainflou (1928) paper is interpreted as incoming wave height. Due to the French language use in the paper, this assumption remains uncertain.

### B.3.3. Goda

The presented formula of Goda in section 2.4.2 can be simplified with the assumptions for the geometry:

- $\beta = 0$ (no wave inclination)
- $\lambda_1 = \lambda_2 = \lambda_3 = 0$ (vertical wall, no curved or oblique elements.)
- $p_4 = p_2 = 0$ (infinite height of vertical wall, no wave overtopping)
- $\alpha_4 = 0$ (no wave overtopping)
- $h_w - h_c = h_s = d = h' = h$ (no rubble balast on which coastal structure is founded, also no vertical slope of bottom)
- $\eta^* < h_c$
- $h_b = d'$ (depth 5 wave lengths in front of structure)
- $p_u$ is left outsite of the scope.
- Compared to the original equation, $p_3$ is defined as $p_0$

This leads to the simplified Goda formula:

$$\eta^* = 1.5 H_d, \tag{B.3}$$

$$p_1 = (\alpha_1 + \alpha_2)\, \rho g H_d, \tag{B.4}$$

$$p_3 = \alpha_3 p_1, \tag{B.5}$$

with:

$$\alpha_1 = 0.6 + \frac{1}{2}\left[\frac{4\pi h / L_d}{\sinh(4\pi h / L_d)}\right]^2, \tag{B.6}$$

$$\alpha_2 = \frac{2d}{H_d}, \tag{B.7}$$

$$\alpha_3 = \frac{1}{\cosh(2\pi h / L_d)}, \tag{B.8}$$

A 100% reflection coefficient is assumed for Goda. The input parameter used is the unreflected wave height. To make the formula applicable for the reflected (local) wave height, the input parameter is halved ($H_d = 0.5$ $H$, assuming 100% reflectivity). After denoting $2\pi / L = k$, $h = d$ and $p_3 = p_0$ and rewriting the set of equations, the simplified Goda formula is given by:

$$h_p = 0.75 H, \tag{B.9}$$

$$p_1 = \left(0.6 + \frac{1}{2}\left[\frac{2kd}{\sinh(2kd)}\right]^2 + \frac{4d}{H_{loc}}\right)\rho g \frac{1}{2} H_{loc}, \tag{B.10}$$

$$p_0 = \frac{p_1}{\cosh(kd)}, \tag{B.11}$$

**Probability**

The design wave used in Goda is 1.8 $H_s$. Thereby, Goda states that the it accounts for the $H_{1/250}$ of a single wave (assuming a Rayleigh distribution). The reliablitiy of Goda's formulae is extensively re-analysed by Van der Meer et al. (1992). This is done by eleven cases of wave forces and moments on vertical structures from Juhl and Van der Meer (1992) and is summarized in Van der Meer et al. (1994). This concluded into a overestimation of $F_{Goda}$ with respect to $F_{0.4\%}$. From here it was deduced that Goda gives a good prediction for storms of 2000 to 3000 waves (So, you can increase $N$ from originally 250 waves to 2500 waves approximately). The physical modal test are given in USACE (2002).

## B.4. Design manuals

This section presents the most relevant design guidelines that can be found in literature. For Dutch standards, construction works must comply with the NEN standards. However, hydraulic loading is rather specific and not described in detail by the NEN. Leidraad kunstwerken is the dominant guideline for designing hydraulic structures (TAW, 2003). Additionally to the Dutch guidelines, there is a construction manual for locks in the Netherlands called Ontwerp van Schutsluizen by Vrijburcht (2000).

Internationally, the Coastal Engineering Manual by USACE (2002) is widely used. Also its predecessor, the Shore Protection Manual USACE (1984) is still often referred to. In the field of wave loads on vertical walls significant differences are found between these two manuals. In port development, the PIANC is a prominent organisation that presents the guidelines in various reports (International Navigation Association, 2003). Often is referred to the USACE (2002), but for a complete overview it is presented as well. The same accounts for ISO 21650 (2007).

### B.4.1. Leidraad kunstwerken (2003)

As the starting point for the calculations, Leidraad Kunstwerken is employed, as it is the most relevant (Dutch standard) and it gives a relatively comprehensive use of both the Sainflou and Goda formula.

Since the Eurocode doesn't specify guidelines with respect to hydraulic structures very extensively, TAW (2003) published national guidelines called Leidraad Kunstwerken that covers this aspect more in depth. Leidraad Kunstwerken is giving recommendations in the design and maintenance of all water retaining structures, in such a way that the different functions and values are optimized. The focus in this is on the retaining function. Leidraad kunstwerken describes how the wave loads in a probabilistic approach need to be applied.

The design wave height is chosen in such a way that the probability of exceedance of this value during a storm peak is 10%. The length of a storm duration is not presented, however, a storm duration $D$ is 6 hours is presented in an example for the calculation of wave overtopping. With the assumption of the Rayleigh distribution and a given average wave period, the storm duration can be determined, see section **??** For average Dutch conditions, a Rayleigh-distribution of the wave heights can be assumed and a safe value for the design wave height is chosen:

$$H_d = 2,2H_s \qquad \text{for} \qquad H_d \leq D_{0,5L} \tag{B.12}$$

Where $H_d$ is the design height of the incoming wave just in front of the construction and $D_{0,5L}$ is the water depth on a distance L/2 for the construction. After this, the design wave is multiplied by a factor of (1 + $\chi$), where $\chi$ is the reflection coefficient. This coefficient is for a vertical wall between 0.7 and 0.9. But to be conservative a value of 1 can be taken. The wave length and wave number are determined by the linear wave theory. Leidraad Kunstwerken addresses both the Sainflou and the Goda formula. Choice on the formula is as follows. For non-breaking waves, the method of Sainflou is often used. The formula is slightly conservative. For breaking waves or almost breaking waves, it is better to use Goda.

### B.4.2. Coastal Engineering Manual (2002)

The design manual of the US Army Corps of Engineers is more or less covering all design aspects of coastal engineering structures, including hydraulic load and morphology. This manual is the successor of the Shore Protection Manual from 1984 (USACE, 1984). The CEM presents both the Sainflou formula and the Goda formula.

#### Sainflou

For Sainflou, CEM gives recommendations for input variables. In case of irregular waves, H should be taken as a characteristic wave height. In Japan the $H_{1/3}$ is used. In other countries $H_{1/10}$ is used. $L$ is the local wave length.

In contrast to the version of Sainflou in Leidraad Kunstwerken, CEM presents a second version. This version also appears in (Verhagen and Van den Bos, 2017) and is given by:

$$p_1 = (p_0 + \rho g d)\frac{H + h_0}{d + H_d + h_0} \tag{B.13}$$

$$p_0 = \frac{\rho g H}{\cosh(kd)} \tag{B.14}$$

$$h_0 = \frac{1}{2} k H_i^2 \coth(kd) \tag{B.15}$$

A difference is that there is no distinction made between $d$ and $d'$. The is also a difference in the definition of $p_1$. The pressure distribution between the points remains linear. Also $h_0$ stays the same.

### B.4.3. Shore Protection Manual (1984)

The Shore Protection Manual (1984) is the predecessor of the CEM (2002) and describes the Sainflou method in more detail for non-breaking wave force. It states the original Sainflou (1928) and the addition of the higher order theory of Miche (1944). This is modified by Rundgren (1958) to reduce the overestimation for steep waves. Also the reflection coefficient can be chosen as either 1.0 or 0.9. The result is presented in design curves. Attention has to be paid to the figures representing the pressure distribution in SPM (1984), since they are not correctly showing the pressure distribution. The incoming wave height is not determined.

The original form of the formula gives good results for long waves with low steepness USACE (1984). However, Rundgren found in 1958 experimental data that showed that Sainflou method overestimates the wave force for steep waves. Rundgren adjusted the Sainflou formula based on a modified high order wave theory of Miche (1944). Sainflou Miche/Rundgren is being used in the Shore protection manual (USACE, 1984) and works by means of design curves. In this formula, also a reflection coefficient $\chi$ is introduced, which should be taken between 0.9 and 1. The single pressure formula given in USACE (1984) is the following:

$$p_0 = \left(\frac{1+\chi}{2}\right) \frac{\rho g H}{\cosh(2\pi d/L)} \tag{B.16}$$

It is stated that the pressure increases linearly from zero at the free water surface to $p_0$ + hydrostatic pressure. This gives:

$$p_1 = \frac{p_0 + \rho g d}{d + h_0 + H(\frac{1+\chi}{2})} (h_0 + H(\frac{1+\chi}{2})) = (p_0 + \rho g d) \frac{h_0 + H(\frac{1+\chi}{2}))}{d + h_0 + H(\frac{1+\chi}{2})} \tag{B.17}$$

Which is the same as the second version above, but with the implementation of a reflection coefficient.

The value of $h_0$ is not to be determined from a formula, but is obtained from the Miche Rundgren design curves. In total, there are six figures given. Three figures for a reflection coefficient of 1.0 and three for a reflection coefficient of 0.9. Here we consider only the curves with a reflection coefficient of 1.0. Figure B.3 and B.4 present data to obtain $h_0$ / $H$ and $F$ / $\rho g d^2$ respectively. Input for the curve is the wave steepness as a function of the wave height and wave period, on the x-axis. Subsequently the relative wave depth as a function of the wave height and depth can be found. This combination leads to the output value on the y-axis.

### B.4.4. Ontwerp van Schutsluizen (2000)

In contrast to the previous presented design guidelines, Vrijburcht (2000) presents the linear wave theory as method to estimate the wave forces for a standing wave on a vertical wall. However, just like the Sainflou model Vrijburcht also mentions an increase in the average water level. This can be calculated by means of design curves and are depended on the wave steepness and relative wave height. In addition, Vrijburcht (2000) also mentions that Goda is a widely used model that can be used as well.

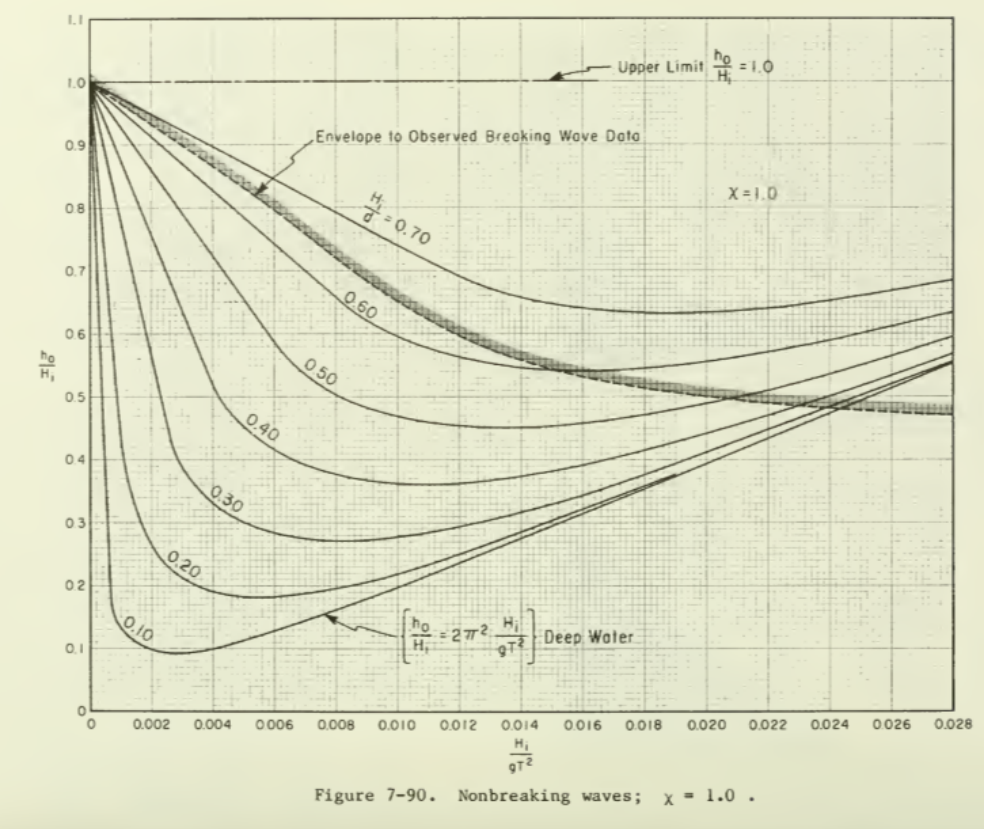


Figure B.3: Design curve of Miche/Rundgren for the normalised water level increase, based on USACE (1984)

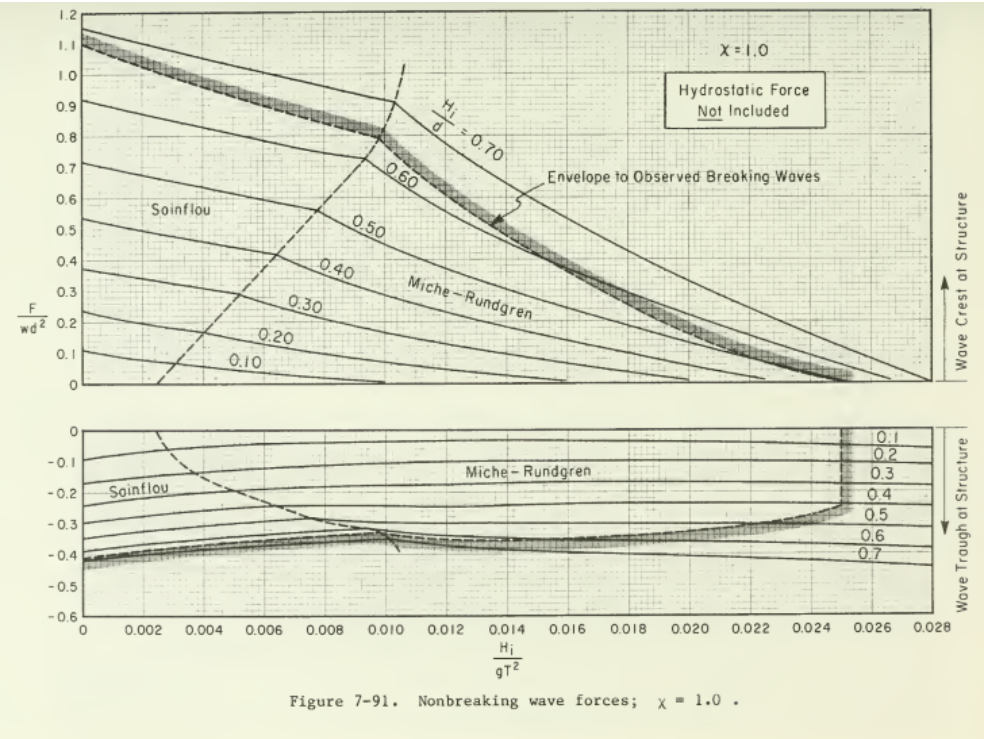


Figure B.4: Design curve of Miche/Rundgren for the normalised force, based on USACE (1984)

# C

# SWASH

This appendix elaborates on the use of SWASH for the study of simulating wave loads on vertical walls. In the first section, Section C.1, the model setup is explained. Section C.2 treats the validation of the SWASH model by comparing the results of SWASH with the results from a physical experiment by Gurhan and Unsalan (2005). In Section C.3, various subjects in the context of swash are given. These include experiences, generation of bimodal spectra and observed super-harmonics. Finally, Section C.4 presents an overview of the input parameters used.

## C.1. Model set up

SWASH works with an input file where all the necessary input parameters for a simulation are defined. These input parameters comprise start up commands, the model description, output commands and lock-up commands (The SWASH Team, 2017). The most relevant part for defining a specific geometry and the boundary conditions is the model description. The model description consists of the following elements: Computational grid, input grid and data, initial and boundary conditions, physics, numerics. The most important input parameter and considerations are discussed here.

**Time step**
SWASH uses a time integration of the explicit type. Therefore, a time step that is too big could lead to numerical instability solution. The computational time step is initially set on 0.0001 second. As will be discussed later, the time step is automatically adjusted by SWASH to satisfy the specified criteria of the CFL condition. Inserting a too big or too small time step is therefore not leading to computation errors.

**Computation time**
The computation time is depended on various factors. First of all, the observations in all scenarios should be based on stationary conditions. Due to the initial condition (surface elevation is zero) and the imposed boundary condition, the model will need time to reach a stationary condition. This is defined as the spin-up time of the system. For an incoming regular wave this time could theoretically be derived by assuming that it is the time it takes for a wave to travel to the wall and back to the open boundary again. In an irregular wave field it would be the time it takes for the highest frequency (slowest) wave to travel to the wall and back to the open boundary. The SWASH manual recommends to take approximately 10 to 15 % of the computation time.

In practice, it is most safe to also visually analyse the surface elevation in the time domain. For regular waves stationarity can be observed by identifying the time when the wave heights over time do not fluctuate any more. In an irregular wave field it is harder to observe this moment. Therefore, for irregular waves 5 minutes of start-up time is taken. In long simulations, this becomes less than the SWASH manual recommendation, however it does meet the condition that the slowest wave has travelled out of the system.

A second requirement for the computation time becomes of importance when addressing the statistical parameters of the wave parameters. Note: this is only applicable for irregular waves. In this research, two levels of probability levels will be treated. Initially, conclusions will be made based on the significant wave height,

which corresponds with a probability of exceedance of 0.135. Therefore, a "standard computation time" is taken to get reliable results to say something about the significant wave height. In this case, many waves should be in the range with the top 13.5%, so an amount of 100 waves are chosen. For irregular waves, the frequency range for these simulations is between 0.1 Hz to 0.3 Hz. The longest peak wave period is accordingly 10 s and so is the average wave height approximately. Based on this wave length, the computation time can be defined by multiplying the amount of total waves with the average wave period.
The second level of probability is looking into a wave height that could be seen as a design wave. This is here defined as the 1% exceedance percentage. To reduce the computation time, a value of 60 waves that exceed this value is assumed to be sufficient. The computations for the verification of the higher level of probability are excecuted with an average wave period of about 7 seconds.

Table C.1 presents an overview of the different computation times for irregular waves. Note that this is a starting point for the computations. For various computations exception may be made (e.g. when the average wave period is a lot shorter). The computation times are excluding the start up time.

Table C.1: Overview of the computation based on the determination of statistical values of the wave parameters.

| Type of wave | Percentage of exceedance | $N_{waves}$ | $T_{avg}$ | Computation time |
|---|---|---|---|---|
| $H_s$ | 13.5 % | 100 / 0.135 = 740 | 10 s | ≈2 hours |
| $H_{1\%}$ | 1 % | 60 / 0.01 = 6000 | 7 s | ≈ 12 hours |

**Length basin**
A length of 200 m is chosen for the water basin. Requirements for the length of a basin are that the wave conditions posed on the boundary condition can adjust to the spatial domain in which they are propagating. This is verified by applying an anlysis on the wave characteristics on the x-axis. It was observed that after approximately 30 m from the west boundary condition, the wave variance showed a constant value.

**Initial conditions**
Both the surface elevation and velocity components are initially zero.

**CFL condition and Courant number**
The CLF condition for 1D problems is given by:

$$\mathrm{CR} = \frac{\Delta t\left(\sqrt{gd} + |u|\right)}{\Delta x} \leq 1 \tag{C.1}$$

The CFL condition must be met to obtain numerical stability. In SWASH it is possible to dynamically adjust the time step $\Delta t$ if the Courant number is outside a range implemented by the user. The time step is either halved or doubled if it is respectively too big or too small. In this case, the minimum Courant number is given as 0.1 and the maximum Courant number is 0.5.

**Horizontal grid size**
The SWASH manual states the spatial resolution is important for possible energy loss in the system. It suggest a wave grid of at least 50 grid cells per wave length for low waves and 100 grid cells for high waves. The wave length can be found if the peak frequency is know. In a depth of 20 m and with a maximum peak frequency of 0.25 Hz[1], the wave length is 25 m. This would mean that a grid size of approximately 0.25 m is necessary.

$$\Delta x = \frac{L_{min}}{100} = \frac{25\mathrm{m}}{100} = 0.25\mathrm{m} \tag{C.2}$$

[1] Actually, also 0.3 Hz is simulated. However, these simulations were only carried out for the regular waves and indicate the upper limit of the frequency range of interest

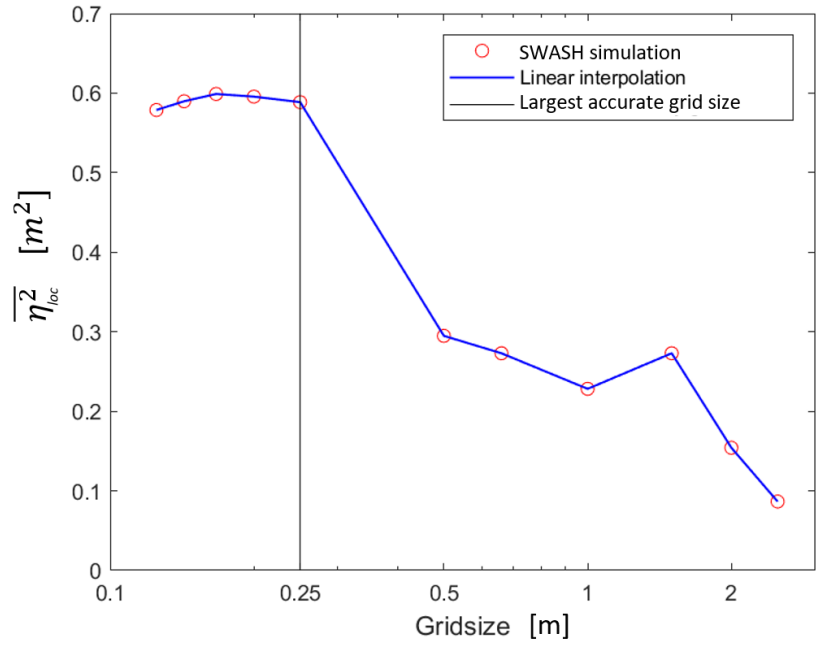


Figure C.1: Optimization of the horizontal grid size.
SWASH simulations are carried out with regular wave with $H_{inc}$ = 1, $T$ = 4 s. Wave variance is obtained at the wall.

**Vertical layers**

The number of vertical layers need to be optimized to get a proper pressure distribution over the vertical axis. However, more vertical layers is at the expense of a longer computation time. Figure C.2 shows an optimization of the vertical layers by regarding the wave variance obtained at the wall for an increasing amount of vertical layers. This is done for regular waves with different wave frequencies. It is observed that for long waves the amount of vertical layers is of minor influence. It is seen that especially waves with a frequency of 0.25 Hz are under influence of the number of vertical layers. For high frequencies, the measured variance remains relatively constant for more than 6 vertical layers.

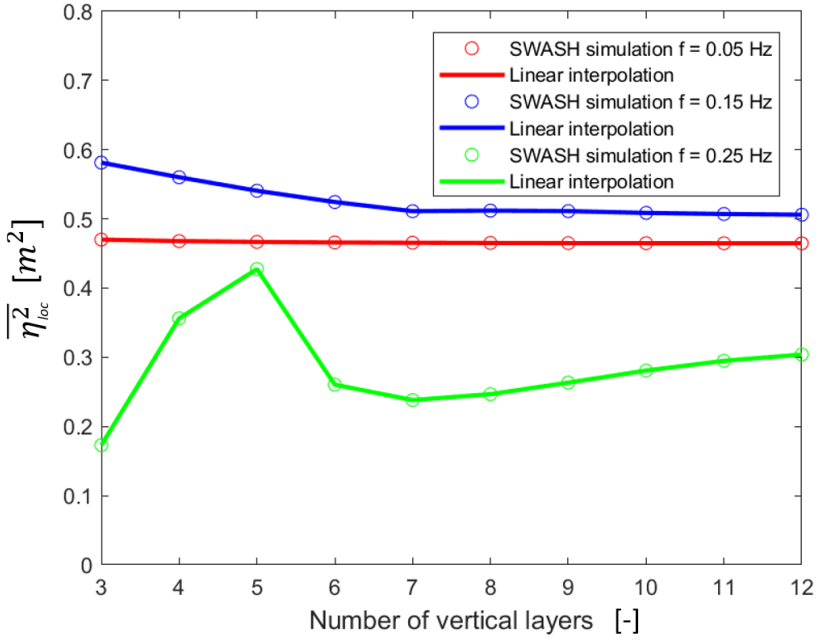


Figure C.2: Variance measured at the wall in a regular wave field with different frequencies, covering the frequency range of interest.
SWASH is simulated for various vertical layers. Depth = 20 m and wave heigth is 1 m.

**Location of measurement**
The location of measurement is chosen on two grid points before vertical wall is modelled. In an analysis on the wave characteristics over the horizontal axis, it turned out that the first grid point of the wall reached excessive values of surface elevation (and accordingly wave height and variance). This is explained by the numerical scheme, were some implicit discretizations are implemented. This causes that the first porous grid point of the vertical wall influences numerically the last wet grid point. The second-last grid point showed wave characteristics in line with the expectations from the rest of the wave field. Therefore, this measurement point was chosen.

**Breaking waves**
SWASH includes the option to correct for breaking waves due to depth induced wave breaking. For many coastal processes this is of valuable use. However, in this study no sloped bottom or berm is present, making depth-induced breaking impossible. Physically, waves could still break in such a scenario due the steepness of waves. This process is called white-capping. Since SWASH does not account for this feature, the option in SWASH to account for wave breaking may be set off.

## C.2. Validation of the model

In the model set up it appeared that SWASH results are sensitive for settings of the input files such as the discretization of the horizontal and vertical grid. Several optimizations were carried out to decide upon accurate discretization. However, a comparison with reality was not included op to now. By comparing the results from SWASH simulations with data from physical measurements, it can be concluded whether SWASH gives realistic values for the wave induced pressure. The assumption is made that these physical measurements approach reality. By comparing the results of experimental data in terms of non-dimensional parameters, they are scalable to the 1:1 scale in which the SWASH model is applied.

For the comparison, data from the journal paper *A comparative study of the first and second order theories and Goda's formula for wave-induced pressure on a vertical breakwater with irregular waves.* by Gurhan and Unsalan (2005) is used. This paper presents experimental results for irregular waves. Statistical values of the wave heights are determined by a zero up-crossing, and the corresponding wave pressure intensity statistics have been evaluated. This is done for the values $H_{avg}$, $H_{1/3}$, $H_{1/10}$ and $H_{max}$ and corresponding maximum pressure of a wave at SWL ($p_1$) that is found at the vertical wall.

The experiments were carried out for a vertical caisson type breakwater at the facilities of the Turkish Ministry of Transportation, State Ports and Airports Administration's Hydrodynamics Laboratory, Ankara. The wave flume has a length of 40 m, width of 0.6 m and a depth of 1.2 m. The water depth was 0.29 m in front of the caisson and was constant over the width of the flume. The model scale was 1/40. The flume bed had a slope of 1:40. Figure C.3 presents a schematic view of the experimental set-up.

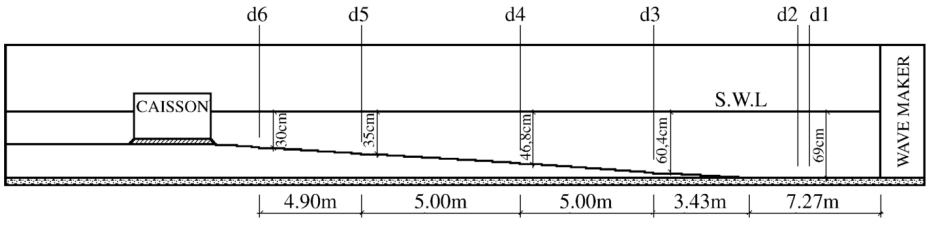


Figure C.3: Schematic diagram of wave flume and experimental set-up, by Gurhan and Unsalan (2005)

By multiplying the geometry of the experimental set up with the scale factor, the geometry in SWASH is obtained and can be seen in Figure C.4. The sloped bottom is modelled with an impermeable layer.

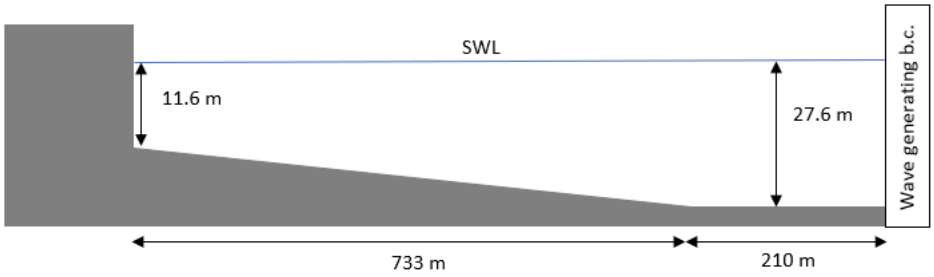


Figure C.4: SWASH replication of the wave flume and experimental set-up of Gurhan and Unsalan (2005)

In the experiment, the wave generating boundary condition simulated irregular waves described by the Bretschneider-Mitsuyasu spectrum, given by:

$$S(f) = 0.205 H_{1/3}^2 T_{1/3}^{-} 4 f^{-5} \exp(-0.75(T_{1/3} f)^{-4}) \tag{C.3}$$

Figure C.5 shows a comparison between the Bretschneider-Mitsuyasu spectrum as modified by Goda (1988) and the JONSWAP spectrum with $\gamma = 1$. It is observed that the spectral width of the two spectra is comparable. Deviations in the peak period or total wave variance between the spectra are not directly related to errors in the solution. Results of the wave induced pressure will be plotted as a function of the observed wave characteristics in the flume and not the generated wave characteristics.

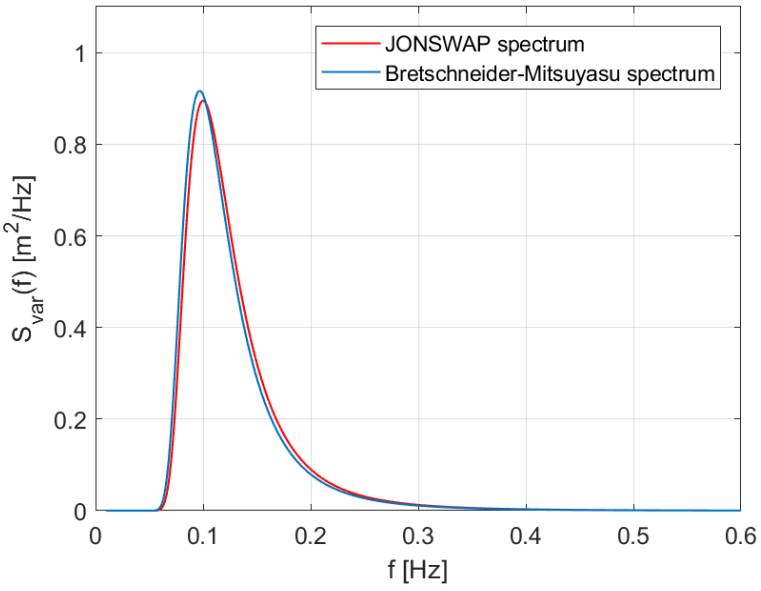


Figure C.5: Comparison between the Bretschneider-Mitsuyasu spectrum and JONSWAP spectrum with $\gamma = 1$. Input parameters in this example for JONSWAP spectrum are $H_{m_0}$ = 1 m , $T_p$ = 10 s and for the Bretschneider-Mitsuyasu spectrum $H_{1/3} = H_{m_0}$ / 1.05 = 0.95 m, $T_{1/3} = T_p$ / 1.1 = 9.09 s.

The wave pressure was measured by pressure transducers on the vertical front of the wall. The sample frequency amounted 12.5 Hz and each experiment included over 650 random waves. The wave steepness is based on deep water conditions $H_{1/3,0}/L_{1/3,0}$. Wave periods simulated amounted T = 1.26 s, T = 1.68 s and T = 2.02 s. Since the latter two wave periods lead to a relative depth which is outside the range of interest (too shallow water), only the simulations with the first wave period are considered. With the depth of measurement known (35 cm), the wave length can be found with the dispersion equation. The SWASH simulation aims on generating waves of a wave length which is 40 times bigger than the experiment. Table C.2 presents an overview of the parameters of the experiment and the simulation by SWASH.

Table C.2: Overview of depth and wave parameters before and after scaling from the experiment to the SWASH simulation. A scaling factor of 40 is used.

| Gurhan and Unsalan (2005) | SWASH |
|---|---|
| $d_0$ = 0.69 m | $d_0$ = 27.6 m |
| $d_{loc}$ = 0.29 m | $d_{loc}$ = 11.6 m |
| $T_{1/3,0}$ = 1.26 s | $T_{1/3,0}$ = 7.91 - 8.3 s |
| $L_{1/3,0}$ = 2.36 m | $L_{1/3,0}$ = 85.89 - 89.29 m |
| $d_0/L_{1/3,0}$ = 0.29 | $d_0/L_{1/3,0}$ = 0.321 - 0.309 |
| $d_{loc}/L_{1/3,0}$ = 0.123 | $d_{loc}/L_{1/3,0}$ = 0.135 - 0.130 |

Results are plotted as the relative wave pressure $p_1/(\rho g d)$ versus the deep water wave steepness $H_{1/3,0}/L_{1/3,0}$. Table C.3 gives the overview of the data from the SWASH experiment. The last column also presents the local wave steepness, as a reference for the simulations carried out in the main part of the report. Figure C.6 compared the results of the experiment (black) and the result of the SWASH simulation (red).

Table C.3: Output of the SWASH model.

| $H_{1/3,0}/L_{1/3,0}$ [-] | $p_{1,mean}/(\rho g d)$ [-] | $p_{1,1/3}/(\rho g d)$ [-] | $p_{1,1/10}/(\rho g d)$ [-] | $p_{1,max}/(\rho g d)$ [-] | $H_{1/3,loc}/L_{1/3,loc}$ [-] |
|---|---|---|---|---|---|
| 0.023 | 0.072 | 0.117 | 0.160 | 0.214 | 0.036 |
| 0.033 | 0.104 | 0.167 | 0.224 | 0.284 | 0.052 |
| 0.043 | 0.133 | 0.212 | 0.328 | 0.342 | 0.067 |
| 0.052 | 0.161 | 0.251 | 0.321 | 0.449 | 0.082 |
| 0.060 | 0.187 | 0.288 | 0.372 | 0.641 | 0.097 |

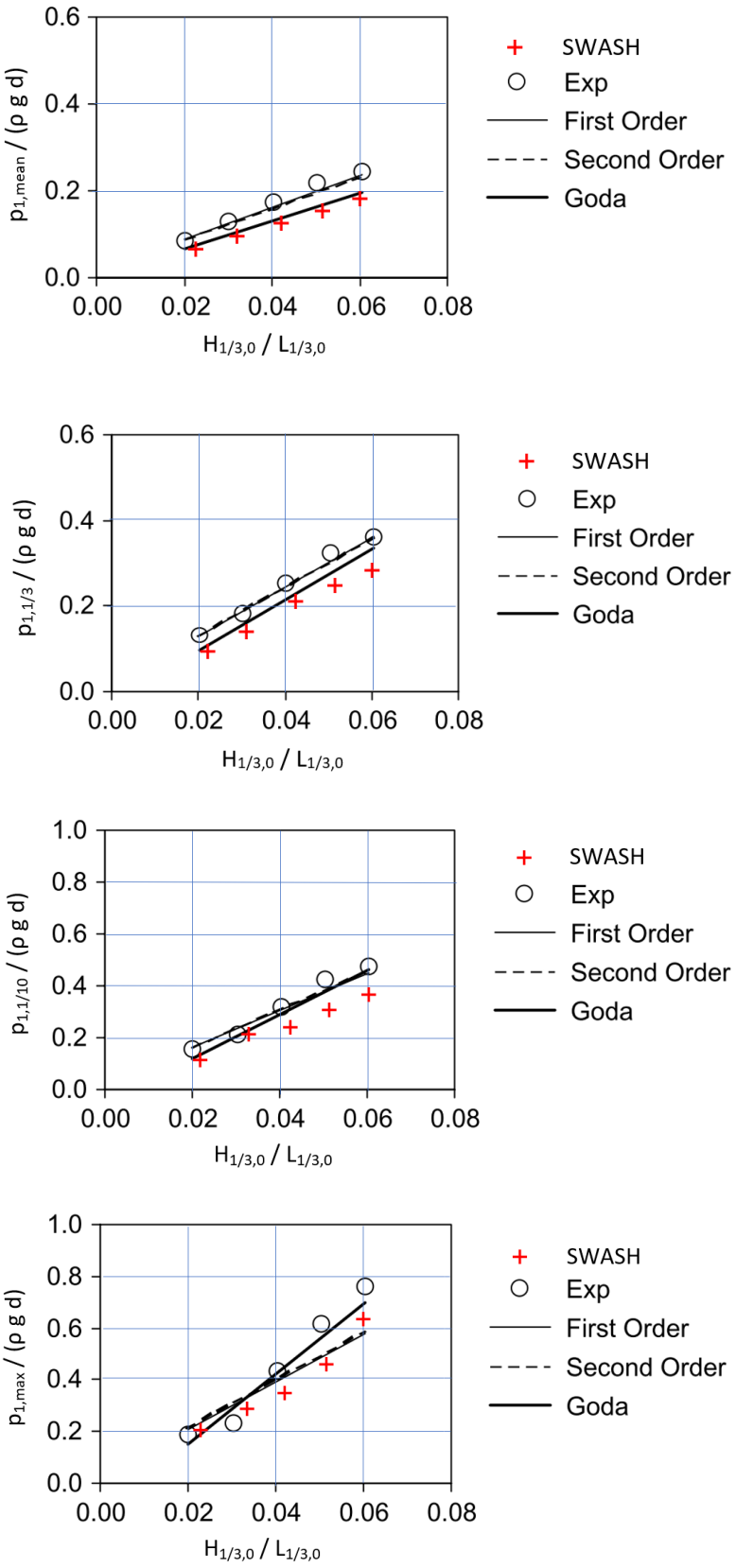


Figure C.6: Results for $d_0/L_{1/3,0}$ = 0.29 (Experiment), $d_0/L_{1/3,0}$ = 0.321 - 0.309 (SWASH). $N_{waves} > 1050$

**Conclusions**
By comparing the SWASH results with the experimental data, it is observed that the SWASH simulations underestimate the experiments for all values. The increase in wave pressure due to an increasing wave steepness is proportional to the experiment. However, over all it seems that the wave pressure by the experiment gives higher values than the SWASH model. The main hypothesis for this underestimation is that the SWASH model simulated waves in relatively deeper waters compared to the experiment. With the wave steepness being constant, waves in deeper water induce a greater horizontal force.

Based on this validation it is concluded that SWASH is an appropiate tool for simulating the wave pressure, as long as it is used for the relative comparison between wave fields. It should also be noted that the verification is limited to only one relative depth and only considers the wave pressure at SWL and not the total induced wave pressure. Therefore, it is recommended to compare the SWASH model with more experimental data.

## C.3. Experiences in SWASH

### C.3.1. Computation of bimodal spectra

In simulating bimodal wave spectra with a different amount of swell for different sea states, an extension in the determination of input parameters has been implemented. Reason for this is that by increasing the swell component in addition to the wind sea component, the total wave variance $m_0$ as well as the significant wave period $T_{1/3}$ increases. This has consequences to the sea state: the wave heights and the significant wave length increases. This causes that the wave steepness $H_{1/3,loc}/L_{1/3}$ and relative depth $d/L_{1/3}$ (which are aimed to keep constant) decrease ($H$ increased less than $L$). In this way, it would not be able to compare the wave force between the different sea states for varying swell but constant wave conditions.

This problem was solved by adding an intermediate step in the generation of the wave spectra. First, initial conditions for $T_{p2}$ and fixed values for $H_{m0}/L$ determined and initial wave spectra are computed. From these spectra, analytical time series are generated, resulting in the wave parameters $T_{1/3}$, $H_{1/3}$ and $L_{1/3}$ . For a uni-modal spectrum, the relation can be determined between $T_p$ and $T_{1/3}$ and assigned with a factor $Q_{uni}$. For bimodal spectra, this relation can be determined as well (= $Q_{bi}$) and be compared with the uni-modal spectrum. It will turn out that the value of $T_{1/3}$ and $Q_{bi}$ are higher, since a swell component was included. Since it is aimed to obtain a same $T_{1/3}$ for bimodal spectra, the new $T_{p1}$ and $T_{p2}$ in the generation of the bimodal spectra are decreased by a factor ($Q_{uni} - Q_{bi}$).

With the dispersion formula and fixed relation of $\Phi_{Sw}$, $H/L$, $M_{Sw}$, all input parameters could be determined. Since this is a very rough way of adapting the input parameters, still some fluctuation occurred in establishing constant local wave conditions. However, for swell conditions up to about 10%, almost constant conditions were achieved. Between 10 and 30%, small deviations occurred.

### C.3.2. Numerical dissipation

The vertical grid was discretised with 6 layers, and showed no effect of inaccuracies. The horizontal grid was defined with a grid step of 0.25 m. Thereby, the high frequency waves (> 0.3 Hz) showed numerical dissipation and limited the usable frequency range. With a fixed bottom of z = -20 m, this also induced limitations to the relative depth of the wave fields.

### C.3.3. Steep waves

In the simulations of irregular wave field, it was noticed that some swash runs leaded to errors. These failed swash runs were often related to the highest expected wave steepness. Possibly, waves occurred in the model that exceeded the (infinite depth) wave breaking limit. Since in longer simulations leaded to a larger scatter in wave heights, the simulated wave steepness was predominantly limited to gentle waves.

### C.3.4. Standing wave pressure profile

In figure C.7 an example is given of the surface elevation and wave force over time for a standing wave profile measured in the anti-node near the vertical wall. The wave characteristics of the wave field are a wave height of 1.9 m and a wave period 5 s.

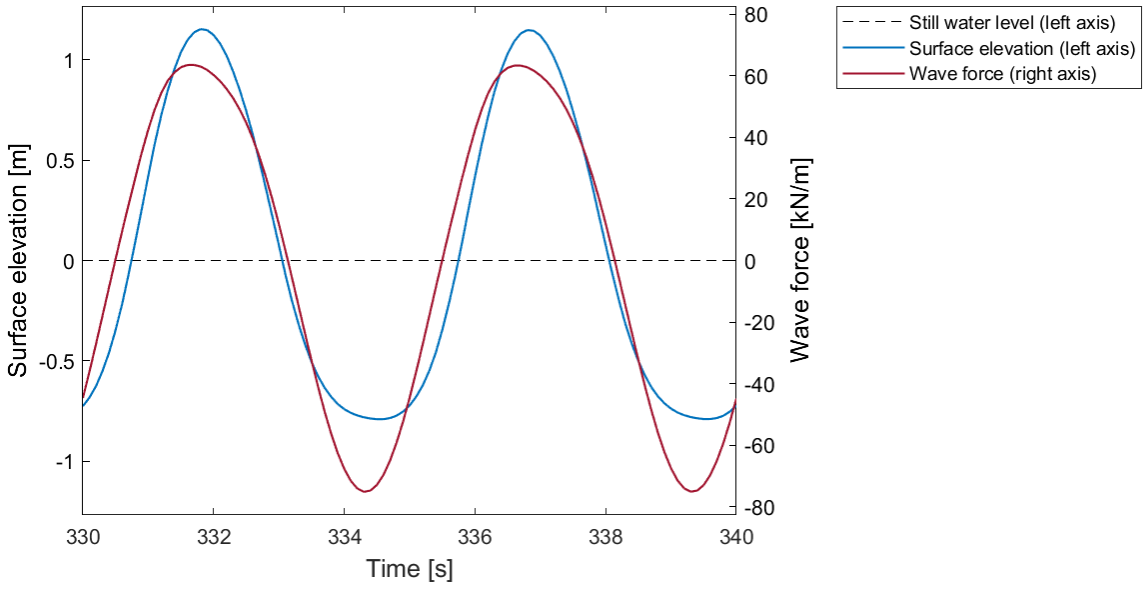


Figure C.7: Example of a time series of the surface elevation and wave induced horizontal force for a standing wave with $H/L = 0.05$ and $d/L = 0.514$, measured at the anti-node near the vertical wall.

It can be noticed that the surface elevation shows a positively peaked profile: the wave crests are relatively steep and the wave troughs are relatively shallow. The surface elevation is symmetric in the vertical axis and not symmetric in the horizontal axis. The wave force demonstrates a negatively peaked profile: the wave force troughs are sharper than the wave force crests. Furthermore the wave force looks weakly negatively skewed as well as weakly out of phase with the surface elevation. The wave force increases fast until it reaches a maximum, just before the surface elevation reaches the maximum. Similarly it decrease to a minimum which is reached a fraction before the surface elevation reaches a minimum.

More insight in the wave dynamics is obtained by comparing the vertical pressure distribution of a standing wave with a progressive wave in time. Figure C.8 plots for both a standing wave and a progressive wave the vertical pressure distribution on various moments in a wave phase. In both wave fields a wave height of 1.9 m and a wave period of 5 s is present. The complete wave phase is defined from the minimum surface elevation (t = 0 s) until the successive minimum surface elevation (t = 5 s). This is different than the traditional zero-down crossing, in order to make a good analysis on the complete increase and decrease in wave pressure. Snapshots are taken from t = 0.5 s until t = 4 s with an interval of 0.5 s. On the vertical axis, the partial depth is plotted. The wave induced pressure is made non-dimensional by taking a relative value with respect to the maximum hydrostatic pressure $\rho g d$ present at the bottom and plotted on the horizontal axis. Negative values of the wave pressure are due a total horizontal pressure that is smaller than the hydrostatic pressure.

At t = 0.5 s, the relative wave pressure for both waves is increasing to a positive value. From t = 0.5 s until t = 1.5 s, it can be seen that the standing wave increases faster in wave pressure than the progressive wave. A maximum value for the pressure at SWL for the standing wave is reached at t = 2 s. However, the pressure in greater depths already decreased in value with respect to the pressure at t = 1.5 s. The progressive wave reaches a maximum pressure both at SWL and in greater depths at t = 2.5 s. From this moment on, both standing wave and progressive wave decrease in a similar pace to a minimum value.

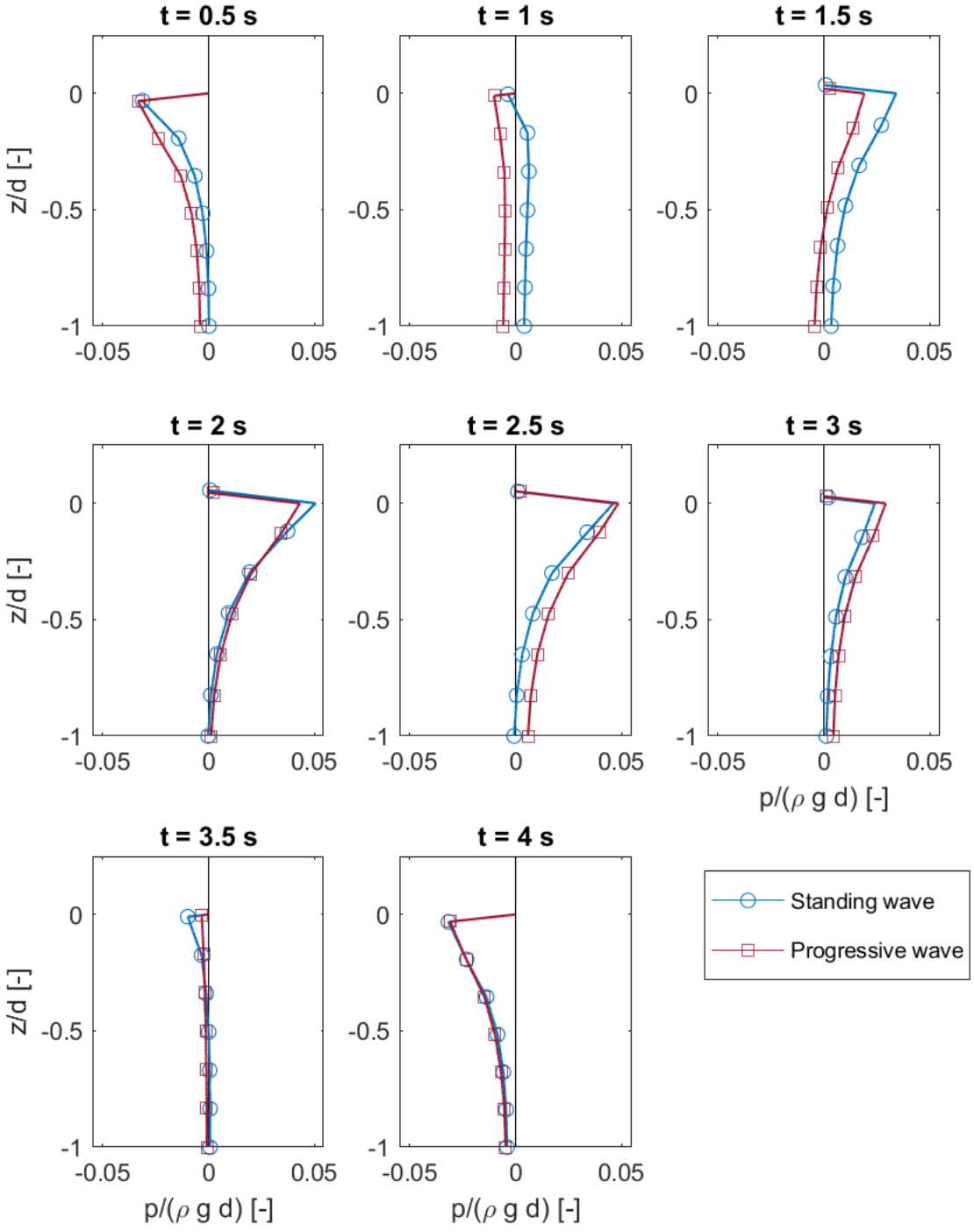


Figure C.8: Vertical pressure distribution for various moments in a wave period. The markers represent the computed values by SWASH and the solid line is a linear interpolation. The standing wave is indicated in blue and the progressive wave in red. In both wave fields the wave characteristics measured at the wall are approximately $H = 1.9$ m and $T = 5$ s.

The wave induced force of the standing wave is compared with the progressive wave in table C.4. Where the wave period and wave height are nearly similar, the maximum wave force in a wave phase is deviating more than 25%. From the visual analysis of the vertical pressure distribution in time, this is explained as a consequence of the unequal build up of maximum pressure over the vertical axis in a standing wave compared to the progressive wave.

Based on the measured wave characteristics at the wall the linear wave theory gives a wave force of 63.4 kN/m. This underestimation of the progressive wave can be explained due the wave steepness of the simulation. For the standing wave force however, the LWT is close to the value of the wave induced force by the standing wave.

Table C.4: Wave characteristics and wave force for a progressive wave and a standing wave.

| Type of wave | Wave period | Wave height | H/L | d/L | Wave force |
|---|---|---|---|---|---|
| Standing wave | 5 s | 1.93 m | 0.050 | 0.514 | 63.7 kN/m |
| Progressive wave | 5 s | 1.98 m | 0.051 | 0.514 | 81.9 kN/m |

**Phase difference**
In an analysis on the wave induced pressure on different depths it was noticed that in greater depths, the pressure showed a different pressure phase than at the SWL. The pressure $p$ can be plotted for various depths in the frequency domain, which is done in figure C.9. On the horizontal axis the relative wave frequency $f/f_p$ is plotted and on the vertical axis the relative pressure variance is plotted $dfS_{pr}(f)/m_{0,pr}$.

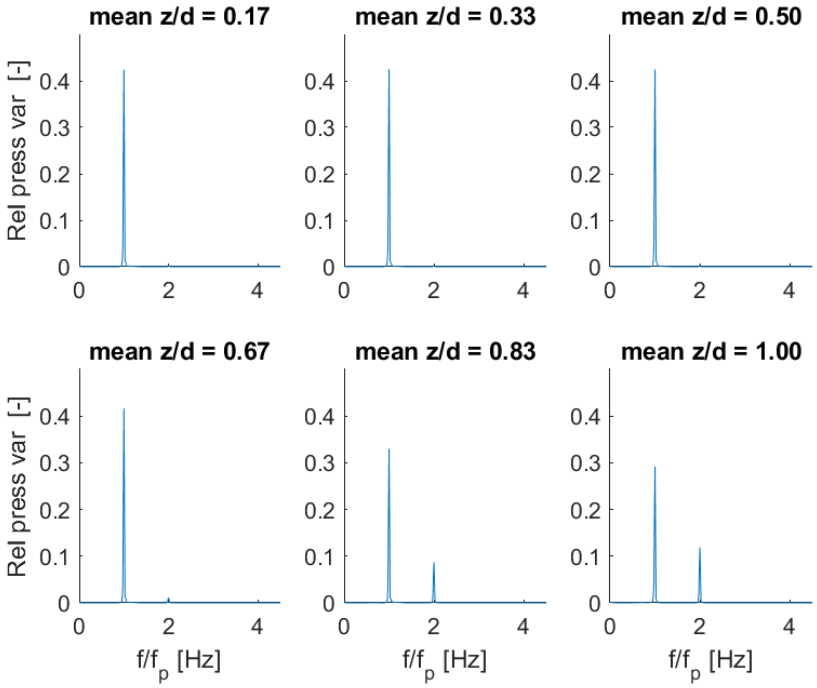


Figure C.9: Origin of a multi-dimensional bimodal wave spectrum in front of the coast of the Netherlands, based on: Holthuijsen (2007)

In a partial depth of 0.83 and 1, a second order component is recognized. The effect of a second order element on the surface elevation is know. Waves crests get steeper and wave troughs get smoother. This concept is showed in the top plot in figure C.10. Here, the maximum of the second order component coincidence with the first order component. For the pressure $p_0$ however, we recognize a smaller maximum pressure and a greater negative pressure. This could be explained by a phase difference of the second order component of $\pi$. In addition, the amplitude of the second order pressure component seems relatively high with the result of a double peaked pressure profile in the time domain. This concept is showed in the lower plot of figure C.10.
In a closer analysis on steep waves, even a third order component of the pressure can be recognized. This causes an additional wiggle when the minimum pressure for $p_0(t)$ is reached. This is recognized in the $p_0(t)$

for steep waves in a visual analysis. It is therefore expected that this higher order component is the origin for the phase difference. Where the maximum pressure induced on each depth $z$ approximates the value indicated by the LWT, the maximum force indicated by LWT overestimates the actual wave force. The influence of wave steepness, relative depth, wall porosity and location should be investigated further to deduct certain aspects. After that, more investigation should be done in the field of comparison between the progressive wave and standing wave.

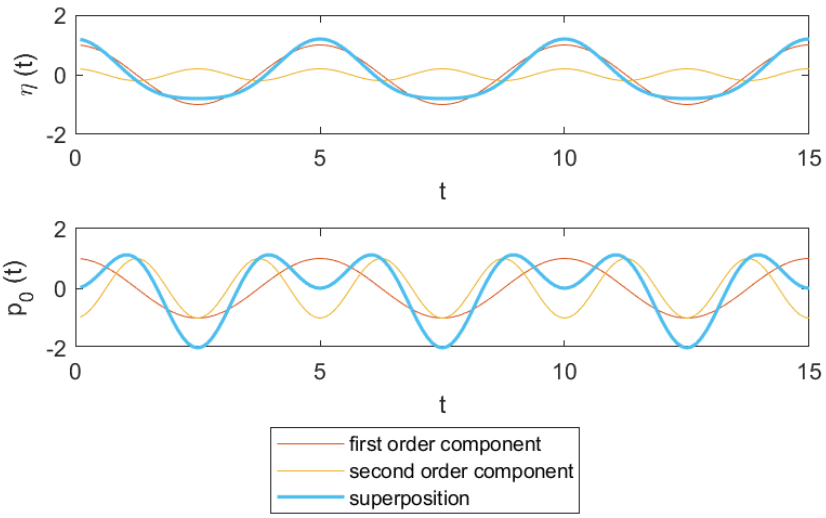


Figure C.10: Theory on the origin of the phase difference in the pressure distribution in greater depths.

The figure shows the wave force in the negative direction becomes larger than the wave force in the positive direction. This agrees with the theoretical consideration by Goda and Kakizai (1967). In Figure C.11, it is seen that waves in water deeper than $d/L = 0.25$ the wave force is in general larger in the direction from the wall than in the direction on the wall.

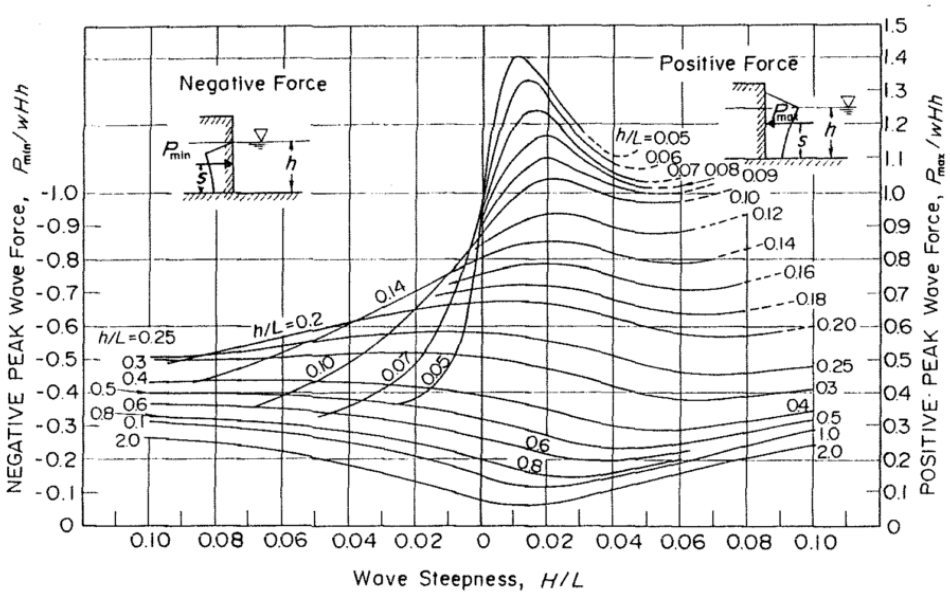


Figure C.11: Forces generated by a nonlinear standing wave based on:Goda and Kakizai (1967)

## C.4. Input parameters

The simulations carried out in this thesis were distinguished in four parts. For the simulation of the bimodal spectrum, two large ranges of simulations were addressed. This section gives an overview of the input parameters for simulation of the:

- Regular waves, see Table C.5.
- Uni-modal spectrum, see Table C.6.
- Bimodal spectrum part 1, see Table C.7
- Bimodal spectrum part 2, see Table C.8
- Probability distribution, see Table C.8

Table C.5: Input parameters for the simulation of regular waves.

| Run | $H$ [m] | $f_p$ [Hz] |
|---|---|---|
| 1 | 0.5 | 0.05 |
| 2 | 1 | 0.05 |
| 3 | 1.5 | 0.05 |
| 4 | 2 | 0.05 |
| 5 | 2.5 | 0.05 |
| 6 | 3 | 0.05 |
| 7 | 0.5 | 0.1 |
| 8 | 1 | 0.1 |
| 9 | 1.5 | 0.1 |
| 10 | 2 | 0.1 |
| 11 | 2.5 | 0.1 |
| 12 | 3 | 0.1 |
| 13 | 0.5 | 0.15 |
| 14 | 1 | 0.15 |
| 15 | 1.5 | 0.15 |
| 16 | 2 | 0.15 |
| 17 | 2.5 | 0.15 |
| 18 | 3 | 0.15 |
| 19 | 0.5 | 0.2 |
| 20 | 1 | 0.2 |
| 21 | 1.5 | 0.2 |
| 22 | 2 | 0.2 |
| 23 | 2.5 | 0.2 |
| 24 | 3 | 0.2 |
| 25 | 0.5 | 0.25 |
| 26 | 1 | 0.25 |
| 27 | 1.5 | 0.25 |
| 28 | 2 | 0.25 |
| 29 | 2.5 | 0.25 |
| 30 | 3 | 0.25 |
| 31 | 0.5 | 0.3 |
| 32 | 1 | 0.3 |
| 33 | 1.5 | 0.3 |
| 34 | 2 | 0.3 |
| 35 | 2.5 | 0.3 |
| 36 | 3 | 0.3 |

Table C.6: Input parameters for the simulation of uni-modal wave spectra

| Run | $H_{m0}$ [m] | $f_p$ [Hz] |
|---|---|---|
| 1 | 0.25 | 0.1 |
| 2 | 0.5 | 0.1 |
| 3 | 0.75 | 0.1 |
| 4 | 1 | 0.1 |
| 5 | 1.5 | 0.1 |
| 6 | 2 | 0.1 |
| 7 | 2.5 | 0.1 |
| 8 | 3 | 0.1 |
| 9 | 0.25 | 0.15 |
| 10 | 0.5 | 0.15 |
| 11 | 0.75 | 0.15 |
| 12 | 1 | 0.15 |
| 13 | 1.5 | 0.15 |
| 14 | 2 | 0.15 |
| 15 | 2.5 | 0.15 |
| 16 | 3 | 0.15 |
| 17 | 0.25 | 0.2 |
| 18 | 0.5 | 0.2 |
| 19 | 0.75 | 0.2 |
| 20 | 1 | 0.2 |
| 21 | 1.5 | 0.2 |
| 22 | 2 | 0.2 |
| 23 | 2.5 | 0.2 |
| 24 (fail) | 3 | 0.2 |
| 25 | 0.25 | 0.25 |
| 26 | 0.5 | 0.25 |
| 27 | 0.75 | 0.25 |
| 28 | 1 | 0.25 |
| 29 | 1.5 | 0.25 |
| 30 | 2 | 0.25 |
| 31 (fail) | 2.5 | 0.25 |
| 32 (fail) | 3 | 0.25 |

Table C.7: Input parameters for the simulation of bimodal wave spectra with the addition of the swell peak.

| Run | $H_{m01}$ [m] | $f_{p1}$ [Hz] | $H_{m01}$ [m] | $f_{p2}$ [Hz] |
|---|---|---|---|---|
| 1 (base case) | 0 | 0.05 | 1.5 | 0.2 |
| 2 | 0.05 | 0.05 | 1.5 | 0.2 |
| 3 | 0.075 | 0.05 | 1.5 | 0.2 |
| 4 | 0.1 | 0.05 | 1.5 | 0.2 |
| 5 | 0.15 | 0.05 | 1.5 | 0.2 |
| 6 | 0.2 | 0.05 | 1.5 | 0.2 |
| 7 | 0.3 | 0.05 | 1.5 | 0.2 |
| 8 | 0.4 | 0.05 | 1.5 | 0.2 |
| 9 | 0.5 | 0.05 | 1.5 | 0.2 |
| 10 | 0.6 | 0.05 | 1.5 | 0.2 |
| 11 | 0.75 | 0.05 | 1.5 | 0.2 |
| 12 | 0.05 | 0.05 | 1.5 | 0.2 |
| 13 | 0.075 | 0.05 | 1.5 | 0.2 |
| 14 | 0.1 | 0.05 | 1.5 | 0.2 |
| 15 | 0.15 | 0.05 | 1.5 | 0.2 |
| 16 | 0.2 | 0.05 | 1.5 | 0.2 |
| 17 | 0.3 | 0.05 | 1.5 | 0.2 |
| 18 | 0.4 | 0.05 | 1.5 | 0.2 |
| 19 | 0.5 | 0.05 | 1.5 | 0.2 |
| 20 | 0.6 | 0.05 | 1.5 | 0.2 |
| 21 | 0.75 | 0.05 | 1.5 | 0.2 |
| 22 | 0.05 | 0.05 | 1.5 | 0.2 |
| 23 | 0.075 | 0.05 | 1.5 | 0.2 |
| 24 | 0.1 | 0.05 | 1.5 | 0.2 |
| 25 | 0.15 | 0.05 | 1.5 | 0.2 |
| 26 | 0.2 | 0.05 | 1.5 | 0.2 |
| 27 | 0.3 | 0.05 | 1.5 | 0.2 |
| 28 | 0.4 | 0.05 | 1.5 | 0.2 |
| 29 | 0.5 | 0.05 | 1.5 | 0.2 |
| 30 (fail) | 0.6 | 0.05 | 1.5 | 0.2 |
| 31 (fail) | 0.75 | 0.05 | 1.5 | 0.2 |

Table C.8: Input parameters for the simulation of bimodal wave spectra. * These runs are also carried out for simulations for 12 hours. ** These runs failed in the 12 hour simulation.

| run [-] | $H_{m01}$ [m] | $f_{p1}$ [Hz] | $H_{m02}$ [m] | $f_{p2}$ [Hz] |
|---|---|---|---|---|
| 1* | 0.00 | 0.052 | 0.75 | 0.130 |
| 2 | 0.17 | 0.053 | 0.73 | 0.133 |
| 3* | 0.24 | 0.054 | 0.71 | 0.136 |
| 4 | 0.29 | 0.054 | 0.69 | 0.136 |
| 5* | 0.34 | 0.059 | 0.68 | 0.147 |
| 6* | 0.38 | 0.058 | 0.66 | 0.146 |
| 7* | 0.00 | 0.052 | 1.46 | 0.130 |
| 8 | 0.33 | 0.053 | 1.43 | 0.134 |
| 9* | 0.47 | 0.055 | 1.40 | 0.138 |
| 10 | 0.57 | 0.056 | 1.36 | 0.139 |
| 11* | 0.66 | 0.058 | 1.33 | 0.145 |
| 12* | 0.75 | 0.061 | 1.29 | 0.152 |
| 13* | 0.00 | 0.064 | 0.52 | 0.160 |
| 14 | 0.12 | 0.065 | 0.51 | 0.163 |
| 15* | 0.17 | 0.067 | 0.50 | 0.167 |
| 16 | 0.20 | 0.068 | 0.48 | 0.170 |
| 17* | 0.23 | 0.070 | 0.47 | 0.176 |
| 18* | 0.26 | 0.074 | 0.46 | 0.184 |
| 19* | 0.00 | 0.064 | 1.05 | 0.160 |
| 20 | 0.24 | 0.065 | 1.02 | 0.161 |
| 21* | 0.33 | 0.066 | 1.00 | 0.165 |
| 22 | 0.41 | 0.068 | 0.98 | 0.169 |
| 23* | 0.47 | 0.070 | 0.95 | 0.175 |
| 24* | 0.53 | 0.074 | 0.93 | 0.185 |
| 25* | 0.00 | 0.064 | 1.55 | 0.160 |
| 26 | 0.35 | 0.066 | 1.52 | 0.164 |
| 27* | 0.49 | 0.066 | 1.48 | 0.165 |
| 28 | 0.61 | 0.069 | 1.45 | 0.172 |
| 29** | 0.71 | 0.071 | 1.41 | 0.178 |
| 30** | 0.79 | 0.075 | 1.37 | 0.186 |
| 31* | 0.00 | 0.076 | 0.37 | 0.190 |
| 32 | 0.08 | 0.077 | 0.36 | 0.193 |
| 33* | 0.12 | 0.080 | 0.35 | 0.200 |
| 34 | 0.15 | 0.082 | 0.35 | 0.204 |
| 35* | 0.17 | 0.083 | 0.34 | 0.208 |
| 36* | 0.19 | 0.087 | 0.33 | 0.218 |
| 37* | 0.00 | 0.076 | 0.74 | 0.190 |
| 38 | 0.17 | 0.078 | 0.72 | 0.194 |
| 39* | 0.24 | 0.080 | 0.71 | 0.200 |
| 40 | 0.29 | 0.081 | 0.69 | 0.201 |
| 41* | 0.34 | 0.086 | 0.67 | 0.216 |
| 42* | 0.38 | 0.088 | 0.65 | 0.220 |
| 43* | 0.00 | 0.076 | 1.12 | 0.190 |
| 44 | 0.25 | 0.077 | 1.09 | 0.192 |
| 45* | 0.36 | 0.081 | 1.07 | 0.202 |
| 46 | 0.44 | 0.081 | 1.04 | 0.204 |
| 47* | 0.51 | 0.085 | 1.01 | 0.211 |
| 48* | 0.57 | 0.089 | 0.99 | 0.223 |

## C.5. SWASH input file

This section shows the input files used for the SWASH calculation. The basic input parameters are:

- Wall porosity = 0.1
- Computational time step = 0.0001 sec
- Lower limit courant number = 0.1
- Upper limit courant number = 0.5
- Length sponge layer = 30 m
- $\Delta x$ = 0.25 m
- Depth = 20 m
- Computation time regular waves = 20 minutes
- Computation time irregular waves = 2 hours
- Computation time irregular waves for extreme values = 12 hours
- Vertical layers = 6

An example of the used SWASH input file is presented in figure C.12. The settings in this input file account for nearly all the simulations carried out in the main part of this thesis. In the figure, few parameters are indicated with squared brackets, which give the location of the input parameters that vary over the different simulations:

- `OPTIONWAVETYPREG`
  If regular wave type is considered this value is empty [ ], otherwise it is [$] to neglect regular wave input.
- `HSINPUT`
  Specific input wave height in regular wave field.
- `TINPUT`
  Specific input wave period in regular wave field.
- `OPTIONWAVETYPIRR`
  If irregular wave type is considered this value is empty [ ], otherwise it is [$] to neglect irregular wave input.
- `SPECINPUTFILE`
  Imports a spectrum input file, including the discretized frequency range and variance spectrum.

In the input file, also several names of input and output files are given, indicated by quotation marks. The relation to these files is further explained in appendix C.6.

```
PROJECT  'WLOVW' '1' 'Regular'                          $Project name
$
SET DEPMIN 0.01                                         $Minimum waterdepth 0.01 m
$
MODE NONstationary  ONEDimensional                      $Non stationary, 1D mode
SET RHOWAT=1025                                         $Salt water density*
SET SEED=12345678                                       $Input for random generator (=default)
$
SET LEVEL=0                                             $Set SWL = 0 (=default)
COORDinates  CARTesian                                  $Cartesian Co-ordinate system
$
CGRID REGular  0. 0. 0.  240 0 960 0                    $discretization horizontal grid
$
VERT 6                                                  $6 vertical layers
$
INPgrid BOTTOM REG 0. 0. 0. 960 0 0.25 0                $Address bottom input grid
READinp BOTTOM 1. 'BOB_01_example.bot' 1 0 FREE         $Reads bottom input file
PORO 0.1                                                $Indicates char. grain size of por. str.
INPgrid PORO REG 0. 0. 0. 960 0 0.25 0                  $Address porosity input grid
READinp PORO 1. 'BOB_01_example.por' 1 0 FREE           $Reads porosity input file
$INPgrid HSTRUC REG 0. 0. 0. 960 0 0.25 0               $Inserting a hydraulic structure set off
$READinp HSTRUC 1. 'BOB_01_example.hst' 1 0 FREE        $Inserting a hydraulic structure set off
$INPgrid PSIZE REG 0. 0. 0. 960 0 0.25 0                $Inserting grain size set off
$READinp PSIZE 1. 'BOB_01_example.siz' 1 0 FREE         $Inserting grain size set off
$
INITial ZERO                                            $Initial conditions (u & zeta) set to zero
$
SPON E 30                                               $30m of spong layer on east b.c.
$
$              Definition of the boundary conditions:
[OPTIONWAVETYPREG] BOUND SIDE W BTYPE WEAK CON REG [HSINPUT] [TINPUT]
[OPTIONWAVETYPIRR] BOUND SIDE W BTYPE WEAK CON SPECFILE [SPECINPUTFILE] 30 MIN
$
$NONHYDrostatic BOX PREC ILU                            $Box-keller scheme set off
NONHYDrostatic STA                                      $Apply central differencing method**
$
DISCRET UPW MOM                                         $Space discretization
DISCRET UPW WMOM H BDF                                  $Space discretization**
BOTCEL MIN                                              $Definition of bottom cell
$                                                          (min. of surrounding cells)
TIMEI METH 0.1 0.5                                      $Time integration and upper and
$                                                           lower boudary of CFL cond.
$
POINTS 'punten' FILE 'BOB_01_example.pnt'                   $Read measurement locations
TABle 'punten' HEAD 'BOB_01_example.tbl' TSEC XP DEPTH WATL PRESS PRESSK &
  ZK HK OUTPUT 000000.000 0.1 SEC                       $Define measurement output
$
BLOCK 'COMPGRID' NOHEAD 'BOB_01_example.mat'  XP WATL OUTPUT 000000.000 0.2 SEC
                                                        $Measurement output over x-axis
$
COMPUTE 000000.000 0.0001 SEC 020000.000                $Computational timestep and total duration
STOP                                                    $Command to indicate end of input file
$    * = PRT file gives value of 1023, which is applied throughout report
$    ** = Suggestion by Marcel Zijlema
```

Figure C.12: Input file of SWASH

## C.6. Matlab scripts

Table C.9 presents an overview of the main scripts used, their copyright and function.

Table C.9: Overview of MATLAB scripts used for the post-processing of data. * Indicates that modifications have been made by Bob van Maris for specific purposes in this thesis

| Name script | Written by | Function |
|---|---|---|
| `Convert_swash_table` | Gerbrant van Vledder* | Convert SWASH output file to a Matlab struct |
| `Create_bot_por_hstruc` | Gerbrant van Vledder* | Generates input files for SWASH |
| `Decomp` | Henk Jan Bakkenes | Calculates the coefficient of reflection |
| `Dispersion` | Gabriel Ruiz Martinez | Applies dispersion formula |
| `find_results` | Bob van Maris | Carries out overall analysis of SWASH output |
| `fjonswap` | Gerbrant van Vledder* | Generates JONSWAP spectrum |
| `get_letters` | Gerbrant van Vledder | Replaces number by alphabetic letter |
| `get_words` | Gerbrant van Vledder | Reads the words in a string |
| `goda` | Bob van Maris | Applies simplified Goda formula |
| `lwt` | Bob van Maris | Applies LWT formula |
| `make_1d_spectrum` | Gerbrant van Vledder | Createsl uni-modal or bimodal wave spectrum |
| `make_movie_gif` | Gerbrant van Vledder | Function to save animated gif |
| `make_spectrumfile` | Gerbrant van Vledder | Writes wave variance to input spectrum file |
| `make_taper` | Gerbrant van Vledder | Constructs taper based on a series of N points |
| `making_gif_pressure` | Bob van Maris | Makes a gif of the vertical pressure distribution |
| `making_gif_surface` | Bob van Maris | Makes a gif of the surface elevation |
| `master_swash_runs` | Gerbrant van Vledder* | Generates input data for SWASH |
| `P1` | Bob van Maris | Extracting the maxi pressures at SWL |
| *various plot scripts* | Bob van Maris | Generating figures for report |
| `read_textfile` | Gerbrant van Vledder | Reads text file in cell array |
| `sainflou` | Bob van Maris | Employs the Sainflou formula (TAW, 2003) |
| `spectral analysis` | Gerbrant van Vledder* | Obtain spectral characteristics of time series |
| `spectral calculation` | Bob van Maris | Carries out spectral calculation |
| `time_domain_analysis` | Gerbrant van Vledder | Obtains time domain characteristics |
| `z_smooth1d` | Gerbrant van Vledder | Smoothens a time series |
| `zero_crossing` | Gerbrant van Vledder* | Excecutes zero down crossing in time series |

# D

# Additional results

**Increase in mean water level (irregular wave field)**
Figure D.1 presents the increase in mean water level at the wall for various wave steepness. The expression by Sainflou is applied with the significant wave height $H_{1/3}$.

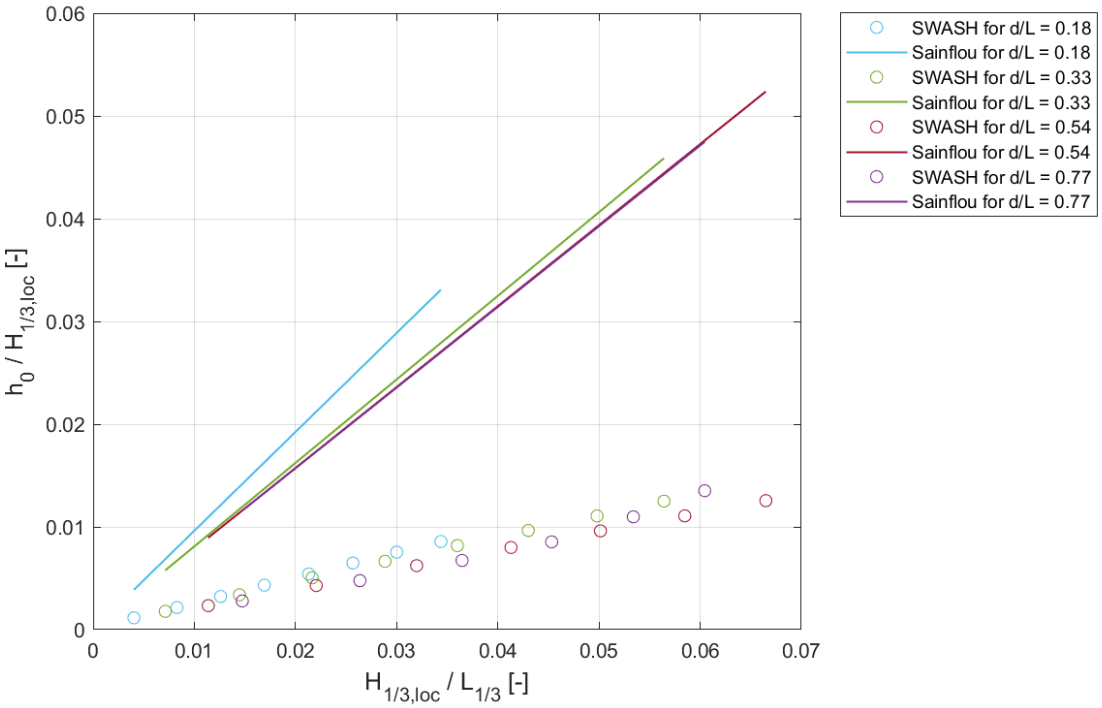


Figure D.1: Non dimensional force for an increasing wave steepness, plotted for various relative depths. Numerical results are indicated by dots and the continuous lines presents the analytical solutions of design guidelines.

**Different design periods**

Figure D.2 presents the relative force of the spectral calculation method and Goda for increasing swell component. Goda is applied with $H_{1/3}$ and $T_p$.

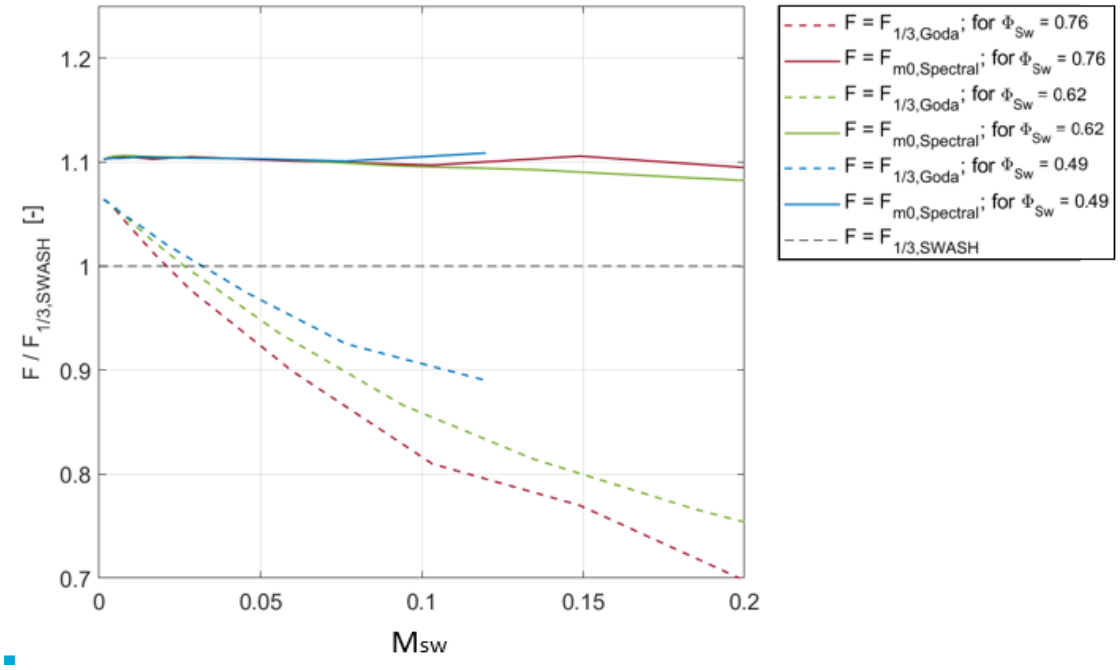


Figure D.2: Relative force of the spectral calculation method and Goda for different bimodal wave spectra (linear interpolated). Goda is applied with $H_{1/3}$ and $T_p$

Figure D.3 presents the relative force of the spectral calculation method and Goda for increasing swell component. Goda is applied with $H_{1/3}$ and $T_{-1,0}$.

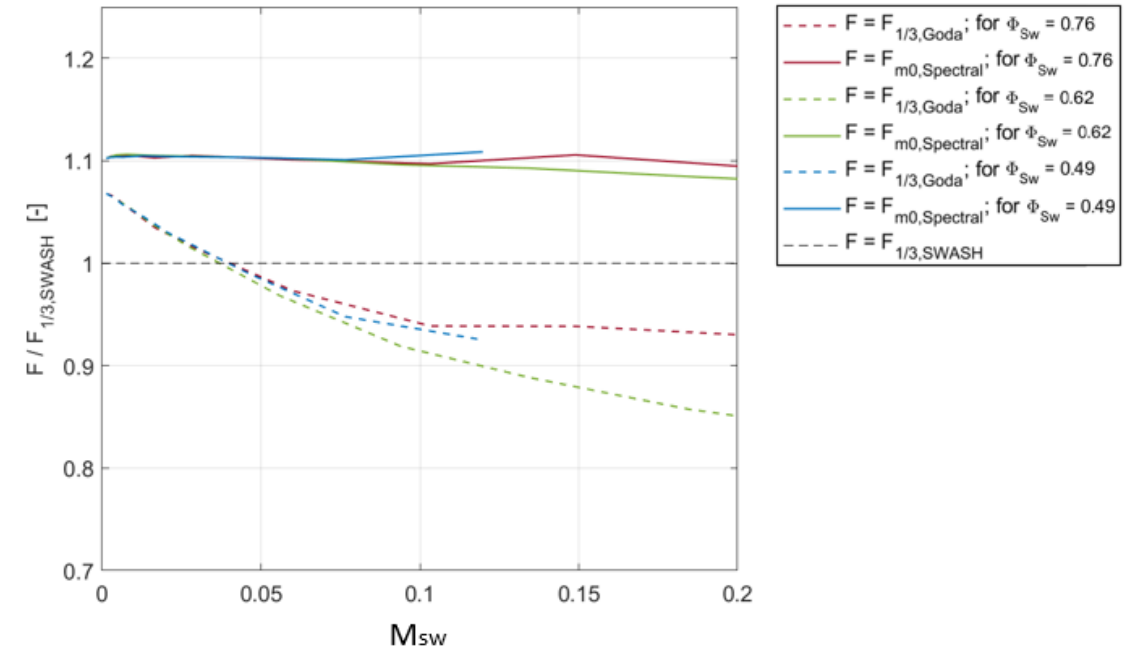


Figure D.3: Relative force of the spectral calculation method and Goda for different bimodal wave spectra (linear interpolated). Goda is applied with $H_{1/3}$ and $T_{m-1,0}$

**Probability distribution**

Figure D.4, D.5, D.6 and D.7 present the deviation from the Rayleigh distribution for a probability of exceedance of 5%, 2%, 1% and 0.5% respectively. On the horizontal axis is the relative swell parameter located. The different colours indicate the relative depth. The marker type indicates the wave steepness.

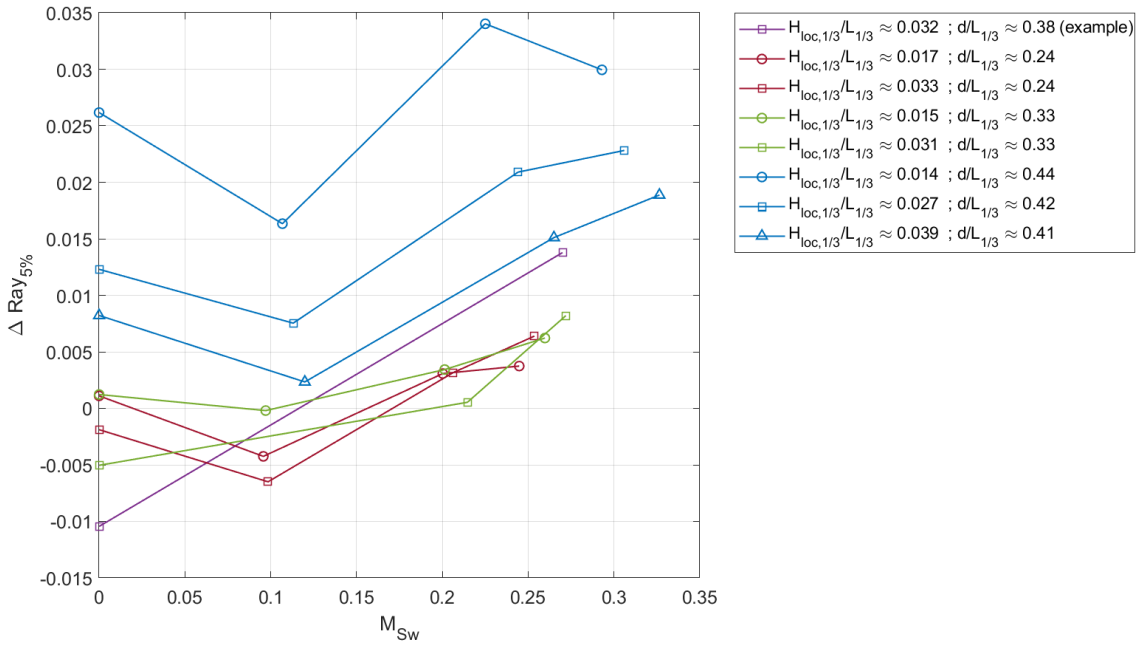


Figure D.4: Relative deviation from the Rayleigh distribution for the 5% probality of exceedance.

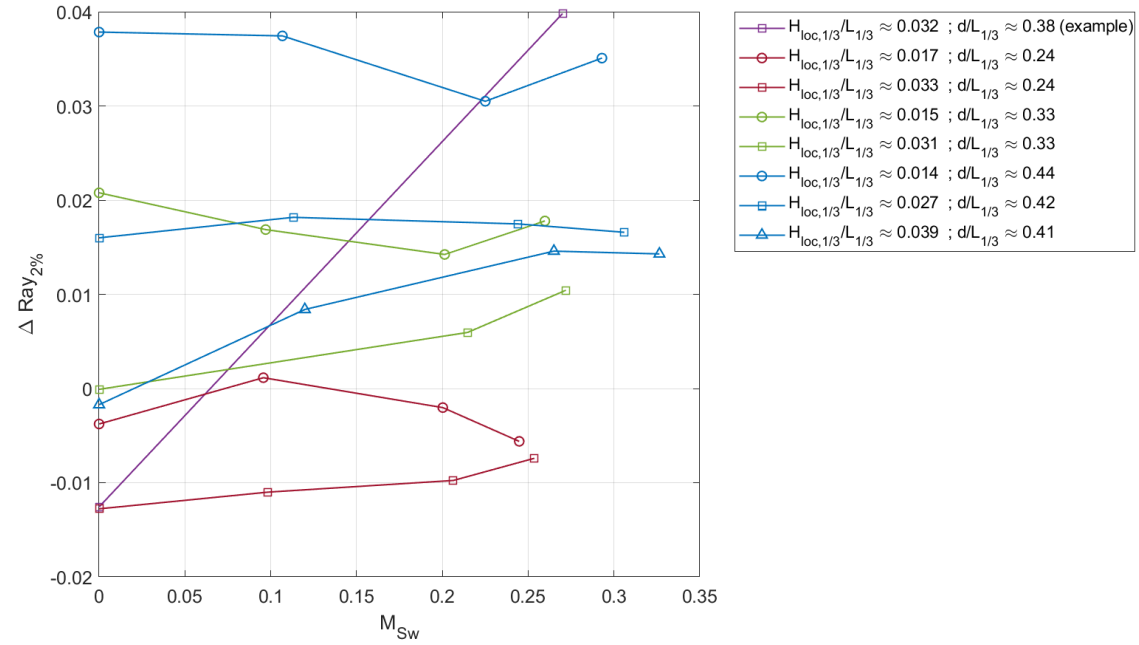


Figure D.5: Relative deviation from the Rayleigh distribution for the 2% probality of exceedance.

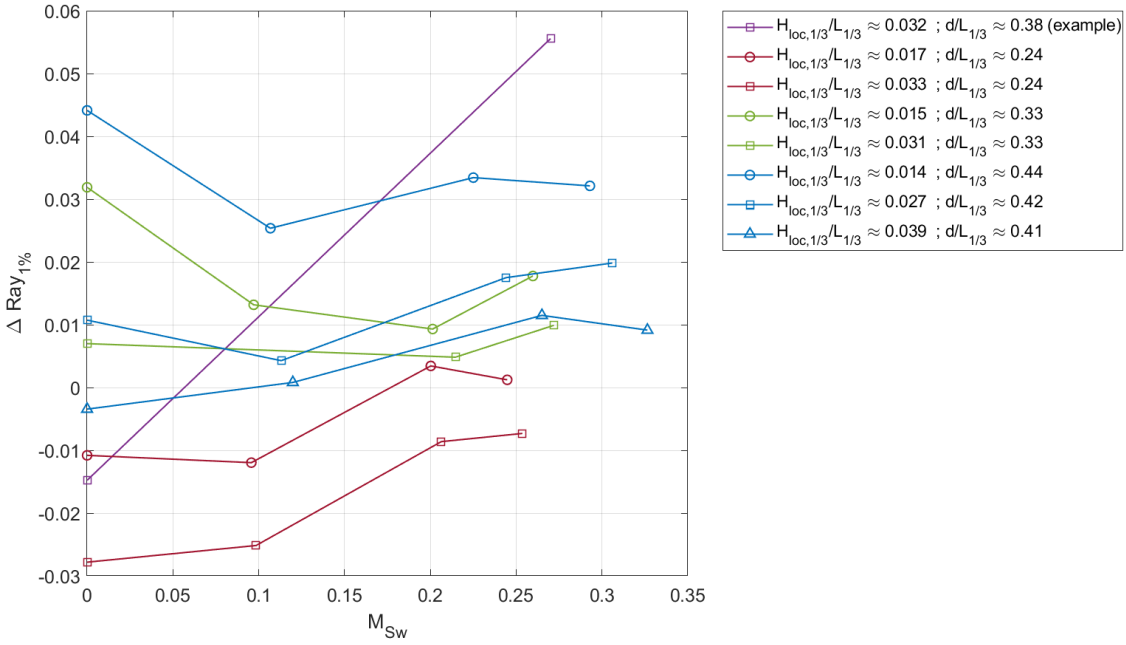


Figure D.6: Relative deviation from the Rayleigh distribution for the 1% probality of exceedance.

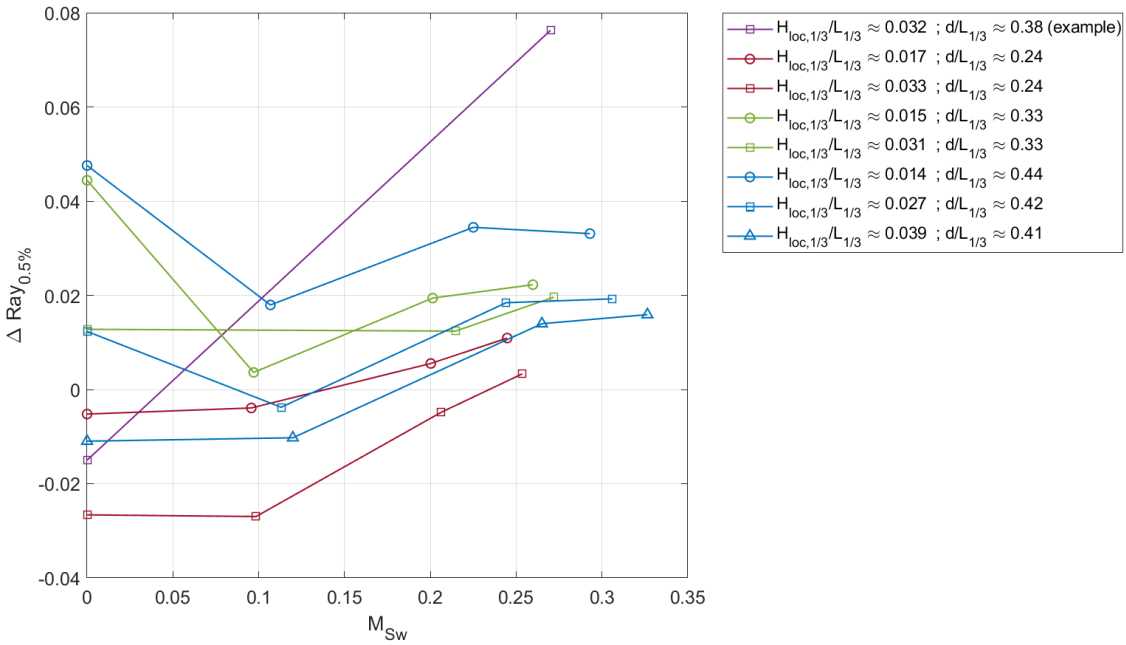


Figure D.7: Relative deviation from the Rayleigh distribution for the 0.5% probality of exceedance.

# E

# Superposition of wave forces

In the elaboration of the spectral calculation method it was seen that the force $F_{m_0}$ is a function of the square root of the wave force variance. Likewise, the significant wave height $H_{m_0}$ is a function of the square root of the wave variance. The hypoto Furthermore, wave variance was linear translated to the wave force variance. The hypothetis is therefore that quadratic superposition of the wave heights can be applied on the wave force as well.

From wave heights it is known:

$$H_{m_0} = 4\sqrt{m_0} \tag{E.1}$$

$$H_{m_0} = 4\sqrt{m_{0,swell} + m_{0,wind}} \tag{E.2}$$

$$H_{m_0} = \sqrt{16(m_{0,swell} + m_{0,wind})} \tag{E.3}$$

$$H_{m_0} = \sqrt{16m_{0,swell} + 16m_{0,wind}} \tag{E.4}$$

$$H_{m_0} = \sqrt{(4\sqrt{m_{0,swell}})^2 + (4\sqrt{m_{0,F_{wind}}})^2} \tag{E.5}$$

$$H_{m_0} = \sqrt{(H_{m0,swell})^2 + (H_{m0,wind})^2} \tag{E.6}$$

In the same fashion, this is derived for the wave force with the assumption that $m_{0,F} \equiv m_0$

$$F_{m_0} = 2\sqrt{m_{0,F}} \tag{E.7}$$

$$F_{m_0} = 2\sqrt{m_{0,F_{swell}} + m_{0,F_{wind}}} \tag{E.8}$$

$$F_{m_0} = \sqrt{4(m_{0,F_{swell}} + m_{0,F_{wind}})} \tag{E.9}$$

$$F_{m_0} = \sqrt{4m_{0,F_{swell}} + 4m_{0,F_{wind}}} \tag{E.10}$$

$$F_{m_0} = \sqrt{(2\sqrt{m_{0,F_{swell}}})^2 + (2\sqrt{m_{0,F_{wind}}})^2} \tag{E.11}$$

$$F_{m_0} = \sqrt{(F_{swell})^2 + (F_{wind})^2} \tag{E.12}$$

For the decomposed bimodal spectrum, an example is given with the LWT and the Goda formula, based on the data of Table 4.1. For Goda, the horizontal wave force becomes:

$$F_{1/3,sum,Goda} = \sqrt{(F_{1/3,swell,Goda})^2 + (F_{1/3,wind,Goda})^2} = \sqrt{27.23^2 + 81.22^2} = 85.66 \text{ kN/m} \tag{E.13}$$

And for the LWT:

$$F_{1/3,sum,LWT} = \sqrt{(F_{1/3,swell,LWT})^2 + (F_{1/3,wind,LWT})^2} = \sqrt{30.78^2 + 78.27^2} = 84.10 \text{kN/m} \tag{E.14}$$

Both estimations give a close estimation of the bimodal spectrum: $F_{1/3,SWASH} = 78.91$ kN/m